

RECENT MAFIC ERUPTIONS AT NEWBERRY VOLCANO AND IN THE
CENTRAL OREGON CASCADES: PHYSICAL VOLCANOLOGY
AND IMPLICATIONS FOR HAZARDS

by

DANIELE MCKAY

A DISSERTATION

Presented to the Department of Geological Sciences
and the Graduate School of the University of Oregon
in partial fulfillment of the requirements
for the degree of
Doctor of Philosophy

September 2012

DISSERTATION APPROVAL PAGE

Student: Daniele McKay

Title: Recent Mafic Eruptions at Newberry Volcano and in the Central Oregon Cascades:
Physical Volcanology and Implications for Hazards

This dissertation has been accepted and approved in partial fulfillment of the requirements for the Doctor of Philosophy degree in the Department of Geological Sciences by:

Dr. Katharine V. Cashman	Chair
Dr. Paul J. Wallace	Member
Dr. Eugene D. Humphreys	Member
Dr. Daniel G. Gavin	Outside Member

and

Kimberly Andrews Espy	Vice President for Research & Innovation/Dean of the Graduate School
-----------------------	---

Original approval signatures are on file with the University of Oregon Graduate School.

Degree awarded September 2012

© 2012 Daniele McKay

DISSERTATION ABSTRACT

Daniele McKay

Doctor of Philosophy

Department of Geological Sciences

September 2012

Title: Recent Mafic Eruptions at Newberry Volcano and in the Central Oregon Cascades: Physical Volcanology and Implications for Hazards

Mafic eruptions have been the dominant form of volcanic activity in central Oregon throughout the Holocene. These eruptions have produced cinder cones, extensive lava flows, and tephra blankets. In most cases, the extent and volume of the tephra blankets has not been determined, despite the fact that future tephra production would pose considerable hazards to transportation, infrastructure, and public health. The economy of the region, which is largely based in tourism, would also be negatively impacted. For this reason, developing a better understanding of the extent and dynamics of tephra production at recent mafic vents is critical, both in terms of mitigating the hazards associated with future eruptions and in improving our scientific understanding of explosive mafic activity.

Here I present detailed field and laboratory studies of tephra from recent mafic vents at Newberry Volcano and in the central Oregon High Cascades. Studies of Newberry vents show that eruption style is strongly correlated with eruptive volume, that extensive magma storage and assimilation occurred prior to the eruption of these vents, and that minimum pre-magmatic water content as recorded by plagioclase was 2.5 wt.%. Detailed mapping and physical studies of tephra deposits from High Cascades vents show

that several recent eruptions produced extensive tephra deposits. These deposits are physically similar to well-documented historic eruptions that have been characterized as violent strombolian. At least one Cascade cinder cone (Sand Mountain) produced a tephra deposit that is unusually large in volume and characterized by uniformly fine-grained clasts, which is interpreted as evidence for syn-eruptive interaction with external water. Microtextural characteristics of tephra, along with an evaluation of possible water sources, support this interpretation.

These investigations demonstrate that magma storage and eruption style at mafic vents is both variable and complex. Additionally, these studies show that cinder cones in central Oregon have the potential to erupt much more explosively than previously assumed. The results of this study will be an important tool for developing comprehensive regional hazard assessments.

This dissertation includes previously published and unpublished co-authored material.

CURRICULUM VITAE

NAME OF AUTHOR: Daniele McKay

GRADUATE AND UNDERGRADUATE SCHOOLS ATTENDED:

University of Oregon, Eugene

DEGREES AWARDED:

Doctor of Philosophy, Geological Sciences, 2012, University of Oregon
Bachelor of Science, General Social Science with a Minor in Geological Sciences,
2005, University of Oregon

AREAS OF SPECIAL INTEREST:

Physical Volcanology
Igneous Petrology and Geochemistry
Science Education

PROFESSIONAL EXPERIENCE:

Adjunct instructor, Oregon State University-Cascade Campus, Bend, Oregon,
2011-12

Program coordinator, Undergraduate Catalytic Outreach & Research Experiences
(UCORE), Department of Physics, University of Oregon, 2011-12

Teaching assistant, Department of Geological Sciences, University of Oregon,
Eugene, 2005-2011

GRANTS, AWARDS, AND HONORS:

Travel Grant, Legacy Teaching Workshop, Center for Astronomy Education,
2011

Travel and Research Grant, American Scandinavian Society, 2011

Outstanding Student Paper Award, American Geophysical Union, 2010

Public Impact Fellowship, University of Oregon Graduate School, 2010

“Good Citizen” Award, Department of Geological Sciences, University of Oregon, 2009

Miller Family Graduate Award in Technology and Science, College of Arts and Sciences, University of Oregon, 2009

Harris Lectureship to Advance Understanding of the Scientific Process, Department of Chemistry, University of Oregon, 2008

Kleinman Grant for Volcano Research, United States Geological Survey, 2008

Travel Grant, National Science Foundation, 2008

Baldwin Research Grant, Department of Geological Sciences, University of Oregon, 2008

Lloyd Staples Award, Department of Geological Sciences, University of Oregon, 2006-08

Lipman Research Award, Geological Society of America, 2007

General University Scholarship, University of Oregon, 2005

Marguerite Award, Oregon State Chapter PEO Sisterhood, 2005

Central Oregon Scholarship, University of Oregon, 2004

Science Scholarship, Central Oregon Community College, 2004

Bend Women’s Scholarship Fund, 2004

PEO Program for Continuing Education, International Chapter PEO Sisterhood, 2004

Marguerite Award, Oregon State Chapter PEO Sisterhood, 2004

PUBLICATIONS:

McKay, D., Donnelly-Nolan, J.M., Jensen, R.A., & Champion, D.E. (2009). The post-Mazama northwest rift zone eruption at Newberry Volcano, Oregon. *In O’Connor, J.E., Dorsey, R.J., and Madin. I.P., eds. Volcanoes to Vineyards: Geologic Field Trips through the Dynamic Landscape of the Pacific Northwest.* Geological Society of America, Field Guide 15.

Jensen, R.A., Donnelly-Nolan, J.M., & McKay, D. (2009). A field guide to Newberry Volcano, Oregon. In *O'Connor, J.E., Dorsey, R.J., and Madin, I.P., eds. Volcanoes to Vineyards: Geologic Field Trips through the Dynamic Landscape of the Pacific Northwest*. Geological Society of America, Field Guide 15.

ACKNOWLEDGEMENTS

I would like to thank my advisor, Kathy Cashman, for encouraging me to develop projects in central Oregon and for providing constant discussion, guidance, and support. Kathy's enthusiasm for multidisciplinary projects and her constant quest for knowledge have been inspirational. It has been both a pleasure and a privilege to work with her. I would also like to thank Paul Wallace, my secondary advisor, who was always available for advice and thoughtful feedback on many aspects of my projects. Dan Gavin, my outside committee member, also acted as an advisor and provided generous access to his lab facilities and field equipment. Without Dan's help, I would probably still be trying to figure out how to assemble and operate the lake coring equipment! Finally, I want to thank Gene Humphreys, my committee chair, for his guidance, both scientific and logistical, during annual committee meetings and at my dissertation defense.

There have been many people who have helped me throughout my graduate career and to whom I am deeply thankful. The outstanding faculty and administrative staff in the Department of Geological Sciences at the U.O. has been instrumental in shaping my career as a scientist and as a teacher. In particular, I would like to thank David Blackwell and Jack Rice for being exceptional teachers and for encouraging me to pursue a graduate degree in geology. Julie Donnelly-Nolan at the U.S. Geological Survey provided generous guidance, feedback, access to data, and numerous opportunities for collaboration and professional development throughout my graduate career. Larry Chitwood and Bob Jensen, both formerly with the U.S. Forest Service, shared their considerable knowledge of the geology of central Oregon and inspired me to become a geologist. I would like to thank all my fellow graduate students at the U.O. for

contributing to a collegiate, supportive (and always fun!) network; in particular, Isolde Belien, Nick Deardorff, Natalia Deligne, Lisa Emerson, Emily Gottesfeld, Emily Johnson, Dan Ruscitto, and Beth Wisely all collaborated on field and lab projects. Thanks to Laura Pioli for teaching me how to dig a proper sample pit and for many helpful scientific discussions. Thanks also to Jen Erskine, Patricia MacQueen, and Tracy Terrall, who provided considerable help in the field and lab. Thanks to Rick Conrey for providing whole-rock XRF and ICP-MS data, John Donovan for assistance on the electron microprobe and SEM, and Colin Long, Shaun Marcott, and Marco Pistoiesi for sharing tephra samples they collected. Thanks also to Hoodoo Ski Resort and the U.S. Forest Service Sisters and McKenzie Ranger Districts for help with field logistics, and to Bob Bonine and his tireless team of mules for hauling equipment, camping supplies, and many pounds of rock and tephra samples. I would also like to thank Ross and Judy Hart, who generously took me into their home during my first few months in Eugene.

Finally, I want to thank my extended family and friends for their constant support and for keeping me grounded throughout this endeavor. My immediate family - John McKay, Barbara Tyler, Michele McKay, Bry Robey, Justin McKay, Rachel Horodner, Allyson McKay, and Erin McKay - were always ready with encouragement, love, and distractions when they were needed most. My in-laws - Bob and Marguerite Nangle, Liz Ryan, Rob Nangle, and their families - have been a second family to me and I am so appreciative of their love and support. Most importantly, I want to thank my husband, John Nangle, who makes every aspect of my life better and whose steadfast love has seen me through the rewards and challenges of graduate school.

This dissertation is dedicated in loving memory to two great men:

my uncle, Tony Qamar, who led me on many adventures and inspired my interest in volcanoes;

and my dad, John McKay, who gave me a deep appreciation for alpine meadows, rocky peaks, and snow.

TABLE OF CONTENTS

Chapter	Page
I. INTRODUCTION.....	1
II. MAGMA STORAGE AND ERUPTION OF THE CA. 7000 YR B.P. NORTHWEST RIFT ZONE ERUPTION, NEWBERRY VOLCANO, OREGON	5
2.1. Introduction.....	5
2.2. Geologic Setting of Newberry Volcano and the Northwest Rift Zone.....	8
2.2.1. The Northwest Rift Zone	11
2.3. Methods.....	15
2.4. Results.....	17
2.4.1. Physical Characteristics of Tephra.....	17
2.4.1.1. Stratigraphy of the Lava Cascade Tephra Deposit	20
2.4.1.2. Stratigraphy of the South Sugarpine Tephra Deposit	21
2.4.1.3. Stratigraphy of the Lava Butte Tephra Deposit	22
2.4.1.4. Stratigraphy of the Mokst Butte Tephra Deposit.....	23
2.4.2. Juvenile Components of Tephra	24
2.4.3. Microtextural Characteristics of Tephra	27
2.4.4. Tephra Compositions	29
2.5. Discussion.....	32
2.5.1. Calculation of Magma H ₂ O Contents	33
2.5.2. Geochemical Evolution of NWRZ Magmas.....	41
2.5.3. Geophysical Evidence for Magma Storage and Assimilation	45
2.5.4. Interpretation of Eruption Styles.....	49
2.5.5. Controls on Explosive Mafic Eruptions.....	52
2.5.6. Implications for Hazards.....	55
2.6. Conclusions.....	57
2.7. Bridge Between Chapter II and Chapter III.....	59

Chapter	Page
III. PHYSICAL VOLCANOLOGY OF TEPHRA DEPOSITS FROM THREE RECENT CINDER CONE ERUPTIONS IN THE CENTRAL OREGON HIGH CASCADES.....	60
3.1. Introduction.....	60
3.2. Geologic Setting.....	62
3.2.1. Four-in-One Cone.....	64
3.2.2. Collier Cone.....	65
3.2.3. Sand Mountain.....	66
3.3. Methods.....	67
3.3.1. Field Methods.....	67
3.3.2. Sample Preparation and Analytical Methods.....	68
3.4. Results.....	69
3.4.1. Isopach Maps.....	70
3.4.1.1. Four-in-One Cone.....	70
3.4.1.2. Collier Cone.....	72
3.4.1.3. Sand Mountain.....	73
3.4.2. Stratigraphy of the Tephra Deposits.....	74
3.4.2.1. Four-in-One Cone.....	74
3.4.2.2. Collier Cone.....	75
3.4.2.3. Sand Mountain.....	79
3.4.3. Stratigraphy of Lake Sediments.....	81
3.4.3.1. Big Lake.....	82
3.4.3.2. Lost Lake.....	82
3.4.3.3. Patjens Lakes.....	83
3.4.3.4. Round Lake.....	84
3.4.3.5. Mafic Tephra in Other Lake Sediments.....	88
3.4.4. Juvenile Components of the Tephra Deposits.....	90
3.4.5. Microtextural Characteristics of Tephra.....	93
3.4.6. Tephra Compositions.....	94
3.5. Discussion.....	99

Chapter	Page
3.5.1. Volume Estimates of the Tephra Deposits.....	100
3.5.2. Interpretation of Eruption Styles.....	105
3.5.3. Implications for Hazards.....	109
3.6. Conclusions.....	111
3.7. Bridge Between Chapter III and Chapter IV.....	112
IV. EVIDENCE FOR WATER-MAGMA INTERACTION DURING THE SAND MOUNTAIN CINDER CONE ERUPTION, CENTRAL OREGON CASCADES.....	113
4.1. Introduction.....	113
4.2. Background.....	114
4.3. Methods and Results.....	116
4.3.1. Typical Cascade Cinder Cone Deposits.....	117
4.3.2. Sand Mountain – An Unusual Tephra Deposit.....	118
4.3.3. Microtextural Characteristics of Tephra.....	120
4.4. Discussion.....	122
4.4.1. Glacial Ice and Snow in the Central Oregon High Cascades.....	123
4.4.2. Surface and Groundwater Patterns in the Central Oregon High Cascades.....	125
4.5. Conclusions.....	128
V. CONCLUSIONS.....	129
REFERENCES CITED.....	134

LIST OF FIGURES

Figure	Page
Chapter II	
2.1. Map showing the location of Newberry Volcano	9
2.2. Map of Newberry Volcano and the northwest rift zone	13
2.3. Representative stratigraphic columns	18
2.4. Grain size distributions	19
2.5. Inman sorting coefficients and median grain sizes	20
2.6. Photo of juvenile tephra components	25
2.7. Componentry of juvenile tephra	26
2.8. SEM images of tephra clasts	28
2.9. MgO and SiO ₂ contents of bulk NWRZ lava and tephra	32
2.10. Calculated liquidus temperatures and modeled H ₂ O contents	38
2.11. H ₂ O contents calculated from plagioclase and glass compositions	39
2.12. Experimentally derived phase diagram	39
2.13. TiO ₂ and K ₂ O contents of bulk NWRZ lava and tephra	42
2.14. Modeled assimilation trends	44
2.15. Schematic cartoons illustrating the inferred magma storage network	47
2.16. Relationships between eruption intensity and H ₂ O and SiO ₂ contents	54
Chapter III	
3.1. Map showing the location of the central Oregon High Cascades	64
3.2. Isopach maps	71
3.3. Representative stratigraphic column of the Four-in-One Cone deposit	76
3.4. Inman sorting coefficients and median grain sizes	77
3.5. Representative stratigraphic columns of the Collier Cone deposit	78
3.6. Representative stratigraphic column of the Sand Mountain deposit	80
3.7. Representative stratigraphic column of Patjents Lakes sediments	85
3.8. Representative stratigraphic column of Round Lake sediments	86
3.9. Photo of juvenile tephra clasts from the Collier Cone deposit	90

Figure	Page
3.10. Componentry of juvenile tephra.....	91
3.11. SEM images of tephra clasts	93
3.12. Trace element data for tephra from lake sediments and known vents	99
3.13. Estimated isopachs for trace deposits from Collier Cone	102
3.14. Thickness versus dispersal area for Cascade tephra deposits.....	102
3.15. Isopach maps for Sand Mountain and Paricutin, Mexico	103
Chapter IV	
4.1. Map of the 2010 eruption of Eyjafjallajökull, Iceland	117
4.2. Inman sorting coefficients and median grain sizes	119
4.3. SEM images of tephra clasts	121
4.4. Historic and Neoglacial snowpack and temperatures.....	124

LIST OF TABLES

Table	Page
Chapter II	
2.1. Volumes of eruptive products from NWRZ vents.	14
2.2. Bulk chemical analyses of NWRZ tephra samples	30
2.3. Average compositions of plagioclase microphenocrysts	35
2.4. Average glass compositions	37
2.5. Physical controls on eruption style.....	52
Chapter III	
3.1. Volumes of eruptive products	72
3.2. Mafic tephra layers preserved in lake sediments.....	82
3.3. Loss on ignition results for tephra from the Round Lake core.....	87
3.4. Bulk chemical analyses of tephra samples	95
3.5. Bulk chemical analyses of tephra samples from lake cores	97
3.6. Minimum and maximum volumes estimates for tephra deposits.....	103

CHAPTER I

INTRODUCTION

Mafic volcanoes are the most common volcanic landform on Earth and in many regions they occur in close proximity to highly populated areas. They are equally common in convergent, extensional, and intraplate tectonic settings, where they can occur as isolated volcanic features, part of extensive volcanic fields, or in association with long-lived stratovolcanoes and calderas. Because mafic activity is so common, mafic eruptions – and in particular cinder cone eruptions – represent the most likely volcanic hazard in many of these tectonic settings. Despite this, cinder cones have received relatively little attention in terms of hazard assessments and evaluations of eruption dynamics as compared to longer-lived silicic vents. In this dissertation I present detailed studies of the eruption dynamics of several recent (Holocene) mafic vents in the central Oregon Cascades. These vents produced a variety of volcanic landforms, including large and small cinder cones, spatter ramparts, and fissure vents. I use these studies to draw attention to the complex chemical evolution and range in eruptive styles that can occur in mafic volcanic fields. Additionally, I use the results of these studies to highlight the need for comprehensive hazard assessments in regions where mafic activity is common.

The central Oregon Cascades make up the central section of the Cascade volcanic arc. Although volcanism along much of the arc is focused at major central volcanoes, the dominant form of Holocene activity in the central section of the arc has been the production of large and small cinder cones (e.g. Sherrod and Smith, 1990; Sherrod et al.,

2004; Hildreth, 2007). These vents occur in a broad region that encompasses both the Cascade arc and back-arc. Regional extension of both the arc and back-arc (e.g. Wells, 1990; Priest, 1990; Taylor, 1990; Conrey et al., 2000) has promoted the eruption of voluminous mafic lavas, forming extensive volcanic fields that occur both in association with longer-lived mafic to silicic volcanoes and as isolated clusters of vents (e.g. Wells, 1990; Priest, 1990; Taylor, 1990; Scott and Gardner, 1992; Conrey et al., 2000). The vents in this study occur in a variety of settings ranging from flank eruptions associated with a large caldera volcano (Newberry Volcano) to chains of mafic vents that occur in relative isolation (i.e. they are not associated with a larger stratovolcano or caldera). In each setting, I focus in detail on the tephra deposits that were produced at each vent.

Tephra production represents the most explosive phases of volcanic activity, thus it is an important indicator of eruption style. Additionally, tephra deposits preserve information about both deep and shallow magmatic processes (e.g. Johnson et al., 2008; Erlund et al., 2009; Ruscitto et al., 2010), thus detailed tephra studies give insight into the pre-eruptive storage regions, chemical evolution, and eruptive dynamics of mafic vents. Finally, only a few of the tephra deposits produced by mafic vents in the central Oregon Cascades have been mapped, despite the fact that establishing the extent and volume of these deposits is necessary in determining the hazards associated with past activity. Urban areas in central Oregon overlap with multiple volcanic fields and future activity in these fields is likely. Thus, regional hazard assessments need address the variety of eruption styles that could occur.

The central Oregon Cascades is an ideal location for detailed mafic tephra studies because mafic vents and lava fields are young, numerous, and easily accessible. This

dissertation integrates field-based observations and mapping of multiple tephra deposits with detailed physical and geochemical analyses of the tephra. In Chapter II, I present detailed textural characteristics, chemical compositions, and pre-eruptive magmatic H₂O contents of tephra from recent mafic vents at Newberry Volcano. I use these data to infer eruption styles at individual vents and to show that the most recent mafic activity at Newberry Volcano was not a simple monogenetic eruption. This work expands our understanding of explosive mafic activity in central Oregon and draws attention to the hazards that mafic eruptions pose to nearby communities.

In Chapter III, I expand my investigation of explosive mafic eruptions to three recent vents in the central Oregon High Cascades. I present detailed maps of the tephra deposits from each of these vents, along with chemical compositions and detailed textural characteristics of the tephra. As in Chapter II, I use these data to infer the eruption styles at each vent and to expand our understanding of recent mafic activity in central Oregon. In particular, I focus on estimating the extent of trace tephra deposits from mafic vents because even very small amounts of tephra deposition from future eruptions would pose significant hazards to the region.

In Chapter IV, I focus in detail on one of the Cascade vents described in Chapter III (Sand Mountain), which produced an unusually large, fine-grained tephra deposit. I investigate the role of syn-eruptive interaction with water and make comparisons to the 2010 eruption of Eyjafjallajökull, Iceland, which interacted with glacial melt water during eruptive activity and produced a very fine-grained tephra deposit that posed significant hazards to air travel. As in Chapters II and III, the investigation of the Sand Mountain eruption in Chapter IV is used to draw attention to the range of activity that can

occur at mafic vents and the importance of addressing the hazards of future mafic eruptions in the Cascades.

Chapter II of this dissertation is in preparation for publication in the *Geological Society of America Bulletin* with coauthors Dr. K.V. Cashman and Dr. P.J. Wallace. Portions of this chapter have been previously published as coauthored material in *McKay, D., Donnelly-Nolan, J.M., Jensen, R.A., and Champion, D.E., 2009, The post-Mazama northwest rift zone eruption at Newberry Volcano, Oregon, in O'Connor, J.E., Dorsey, R.J., and Madin. I.P., eds., Volcanoes to Vineyards: Geologic Trips through the Dynamic Landscape of the Pacific Northwest: Geological Society of America Field Guide 15, p. 91-110*. In addition to the field and analytical work described in the published paper, new work is included in this chapter. In particular, detailed physical descriptions of the northwest rift zone tephra deposits, as well as calculations of pre-eruptive magmatic H₂O contents, are presented here. This work has resulted in new interpretations of the magma storage system and eruption of the northwest rift zone eruptive event. The work presented here was performed entirely by me and the writing is entirely mine. Drs. Cashman and Wallace provided guidance during analytical work, as well as editorial assistance.

Chapter III of this dissertation includes coauthored material with Dr. K.V. Cashman, Dr. P.J. Wallace, Dr. D.M. Ruscitto, and Dr. D.G. Gavin. The analytical work was performed entirely by me and the writing is entirely mine. Drs. Cashman, Wallace, and Gavin provided guidance during field and analytical work, as well as editorial assistance. Chapter IV is in preparation for publication in *Geology*. Coauthor Dr. K.V. Cashman provided editorial assistance and guidance during analytical work. I performed the field and laboratory work and was the primary author.

CHAPTER II

MAGMA STORAGE AND ERUPTION OF THE CA. 7000 YR B.P. NORTHWEST RIFT ZONE ERUPTION, NEWBERRY VOLCANO, OREGON

This chapter is in preparation for publication in the *Geological Society of America Bulletin* with coauthors Dr. K.V. Cashman and Dr. P.J. Wallace. Portions of this chapter have been previously published as coauthored material in *McKay, D., Donnelly-Nolan, J.M., Jensen, R.A., and Champion, D.E., 2009, The post-Mazama northwest rift zone eruption at Newberry Volcano, Oregon, in O'Connor, J.E., Dorsey, R.J., and Madin. I.P., eds., Volcanoes to Vineyards: Geologic Trips through the Dynamic Landscape of the Pacific Northwest: Geological Society of America Field Guide 15, p. 91-110*. In addition to the field and analytical work described in the published paper, new work is included in this chapter. In particular, detailed physical descriptions of the northwest rift zone tephra deposits, as well as calculations of pre-eruptive magmatic H₂O contents, are presented here. This work has resulted in new interpretations of the magma storage system and eruption of the northwest rift zone eruptive event. The work presented in this chapter was performed entirely by me and the writing is entirely mine. Drs. Cashman and Wallace provided guidance during analytical work, as well as editorial assistance.

2.1. Introduction

Cinder cone eruptions range from effusive to explosive and can produce a variety of eruptive products including the cones themselves, lava flows, and tephra blankets.

They are the most common volcanic landform on Earth, yet we have a limited understanding of the plumbing systems feeding these eruptions or the controls on eruption dynamics and styles. Cinder cones are often classified as monogenetic, but many cinder cone fields are characterized by chemically distinct magmas that range in bulk composition from basalt to andesite and feed eruptions from multiple vents (e.g. Strong and Wolff, 2003; Brenna et al., 2011), thereby requiring complex modes of magma evolution and ascent through the crust. Volatile content, chemical composition, and magma temperature are commonly assumed to be the most important controls on the explosivity of cinder cone eruptions. However, abrupt transitions from explosive to effusive behavior can occur without corresponding changes in these variables (e.g. Erlund et al., 2009). Thus in at least some circumstances, mass eruption rate may provide the dominant control on eruption style, particularly in low viscosity mafic magmas where the rate of magma ascent controls the efficiency of pre- and syn-eruptive gas segregation (Pioli et al., 2009).

The ca. 7000 yr B.P. eruption of the northwest rift zone (NWRZ) of Newberry Volcano, Oregon, provides an excellent opportunity to examine eruption conditions within a recent cinder cone field. Although both the eruption ages and the spatial distribution of mafic vents along the NWRZ suggest that this eruption was a single magma injection event, other aspects of the eruption tell a more complex story. First, the eruptive activity was distributed over multiple cinder cone, spatter, and fissure vents that are not aligned along a single radial fissure. Second, the vents erupted lavas with a range of chemical compositions from basalt to andesite. Third, the vents exhibited a range of eruptive styles, producing volcanic deposits that include large and small cinder cones,

tephra blankets, and extensive lava flows (McKay et al., 2009). Moreover, there is no apparent correlation between magma composition and eruption style. Variations in magma temperature, as well as pre-eruptive magmatic H₂O content, may have contributed to this observed range of eruption styles (e.g. Roggensack et al., 1997; Luhr, 2001; Cervantes and Wallace, 2003; Johnson et al., 2008; Erlund et al., 2009). However, neither of these parameters is known for NWRZ magmas. Thus the primary goals of this paper are to: 1) constrain the genetic relationship between magma batches erupted at different vents; 2) determine pre-eruptive storage conditions of individual magma batches; and 3) assess the possible controls on eruptive style, particularly from the perspective of volcanic hazard assessment.

I address these questions by examining the physical characteristics of NWRZ tephra deposits and use the volumes of fragmented material (in cinder cones and tephra blankets) produced at each vent to describe eruption style. I then estimate pre-eruptive magmatic H₂O contents of tephra from individual vents using an application of the plagioclase-melt hygrometer (Lange et al., 2009). Finally I examine the geochemical evolution of the magma that fed these vents. This work shows that: 1) eruption style at individual vents is strongly correlated to eruptive volume and not to chemical composition or magmatic H₂O content; 2) the pre-eruptive magmatic H₂O contents of NWRZ lavas are similar to those measured from other recent mafic lavas in the central Oregon Cascades; and 3) magma storage and assimilation occurred in a complex network of shallow dikes or sills prior to eruption rather than in a single, integrated magma chamber.

Importantly, by focusing on tephra, I am expanding on the record that is preserved in lava flows (e.g. Pioli et al., 2009). It has been demonstrated that tephra deposits preserve information about both deep and shallow magmatic processes and storage regions (e.g. Johnson et al., 2008; Erlund et al., 2009; Ruscitto et al., 2010). The tephra studies presented here build upon geochemical data already collected for NWRZ lavas (McKay et al., 2009), thus extending our range of understanding to the entire eruption sequence. Additionally, since tephra production represents the most explosive phases of activity, determining the nature and extent of NWRZ tephra deposits is important for volcanic hazard assessment.

2.2. Geologic Setting of Newberry Volcano and the Northwest Rift Zone

Newberry Volcano is located in central Oregon, ~60 km east of the Cascade Range (Figure 2.1). The regional tectonic regime is dominated by three extensional fault systems that converge near or below Newberry Volcano (e.g. Higgins, 1973; MacLeod and Sherrod, 1988; Figure 2.1). Offsets of early Newberry lavas by two of these, the Walker Rim and Sisters fault zones, suggest that strata below the volcano are considerably faulted (e.g. MacLeod and Sherrod, 1988). Magmatic pathways are likely controlled by these fault systems, resulting in a netlike distribution of dikes and magma pods below the volcano (Higgins, 1973). Magmatism at Newberry has been variously attributed to the migration of volcanism across the High Lava Plains (e.g. Walker, 1974; MacLeod et al., 1975; McKee et al., 1976; MacLeod and Sherrod, 1988; Jordan et al., 2004), back-arc extension coupled with volcanism of the High Lava Plains (e.g. Hildreth, 2007), and arc volcanism of the Cascades (e.g. Donnelly-Nolan, 2008, Donnelly-Nolan et

al., 2008). Isotopic and petrological studies indicate that Newberry lavas are not related to High Lava Plains lavas, but include inputs of subduction fluids (Carlson et al., 2008; Graham et al., 2009; Grove et al., 2009; Rowe et al., 2009). Recent geologic work at Newberry Volcano reinforces these studies and indicates that Newberry is a rear-arc Cascade volcano (Donnelly-Nolan, 2009; Donnelly-Nolan et al., 2010). Regional extension is likely enhancing volcanism by providing strong magmatic focus below the volcano (e.g. MacLeod and Sherrod, 1988; Hildreth, 2007; Donnelly-Nolan, 2009), but subduction fluids and shallow hot mantle also play essential roles in Newberry volcanism (Donnelly-Nolan, 2009).

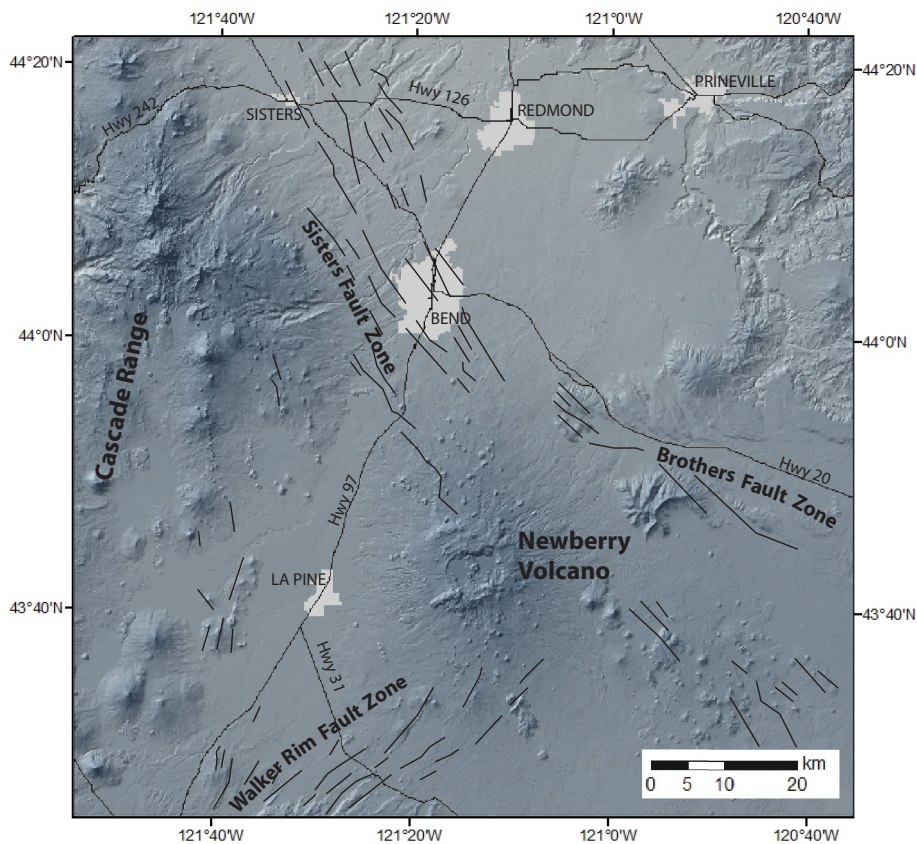


Figure 2.1. Map showing the location of Newberry Volcano, the Cascade Range, and densely populated areas in central Oregon. Black lines represent regional fault systems (after Weldon et al., 2003). The Walker Rim, Sisters, and Brothers fault zones (after MacLeod and Sherrod, 1988) are labeled. Numerous cinder cone vents cover the flanks of Newberry Volcano, especially the north and south flanks (visible as small dots).

Unlike most other large Cascade volcanoes, Newberry has a broad shield shape topped by a 45-km² summit caldera. Erupted compositions range from basalt to rhyolite, with mafic volcanism dominating the flanks and silicic volcanism restricted to the caldera and upper sections of the volcano; lavas of intermediate compositions are relatively rare (MacLeod and Sherrod, 1988; Jensen et al., 2009). The oldest known Newberry lavas form a ca. 400 ka rhyolite dome (Donnelly-Nolan et al., 2010); the youngest is the ca. 1300 yr B.P. intracaldera Big Obsidian Flow and associated rhyolitic tephra (MacLeod and Sherrod, 1988; MacLeod et al., 1995; Jensen et al., 2009). Large-volume flows of basalt occur on the flanks and extend well beyond the main edifice (e.g. Champion et al., 2004; Donnelly-Nolan et al., 2010). Hundreds of mafic cinder cones and fissure vents also cover the flanks of Newberry (Figure 2.1), many of which are located on the north and south flanks and are aligned north-northwest to north-northeast, reflecting a strong tectonic influence on magmatic pathways (Donnelly-Nolan, 2009; Donnelly-Nolan et al., 2010). The most recent caldera-forming eruption occurred at ~75 ka and produced a compositionally zoned rhyolitic to andesitic ash flow tuff informally called the tuff of Paulina Creek Falls (Donnelly-Nolan et al., 2010). There are at least two older ash flow tuffs (MacLeod et al., 1995), the rhyodacitic tuff of Tepee Draw and a dacitic tuff informally called the tuff of Brooks Draw, that are ~300 ka in age and may be associated with previous caldera-forming eruptions (Donnelly-Nolan, 2009; Jensen et al., 2009; Donnelly-Nolan et al., 2010). Recent silicic activity has been limited to the caldera, where multiple high-SiO₂ obsidian flows have erupted over the past 10 ka (MacLeod and Sherrod, 1988; MacLeod et al., 1995).

Electrical studies (Fitterman et al., 1988), seismic refraction (Catchings and Mooney, 1988), and gravity data (Gettings and Griscom, 1988) suggest that a large intrusive complex lies ~3-6 km below the summit caldera. This zone is interpreted to be composed of numerous solidified dikes, sills, and pod-shaped bodies of various compositions, as well as at least one rhyolitic magma body (Achauer et al., 1988; Fitterman, 1988; MacLeod and Sherrod, 1988; Beachly, 2011). Repeated mafic inputs have probably contributed to the intrusive zone throughout the ~0.4 Ma history of the volcano (Fitterman, 1988). Mafic lavas exposed at the surface suggest that the parent magmas are a combination of calc-alkaline basalts, low-K tholeiites, and enriched intraplate basalts (Rowe et al., 2009). Although these primitive magmas have fed very large flank eruptions, geophysical evidence for a complex intrusive zone indicates that some magma batches do not make it to the surface. Rather, they stall in the shallow crust where they interact with previously intruded dikes and sills of varying compositions. Evidence for this process is provided by mafic inclusions in the 1300 yr B.P. Big Obsidian Flow, which have been interpreted as the result of up to 30% assimilation of basaltic andesite intrusions by liquid rhyolite (e.g. Linneman and Myers, 1990).

2.2.1. The Northwest Rift Zone

The most recent mafic activity at Newberry occurred ~7000 years ago from multiple vents located on the northwest flank, the north caldera wall, and the upper southwest flank (Figure 2.2). These vents are informally called “the northwest rift zone” after Peterson and Groh (1965). MacLeod and Sherrod (1988) describe the NWRZ eruption as Episode 4 of Holocene volcanism at Newberry. This episode was

immediately preceded (within ~100 years) by obsidian flows (73.96-74.21 wt.% SiO₂) that erupted from several intracaldera vents (Episode 3, the East Lake tephra, Central Pumice Cone obsidian flow, and Interlake obsidian flow; MacLeod and Sherrod, 1988). NWRZ tephra and lavas from East Lake Fissure vent, on the north wall of the caldera (Figure 2.2), immediately overlie unweathered pumice interpreted to be from Episode 3 (MacLeod and Sherrod, 1988). Tephra and lavas from other NWRZ vents immediately overlie tephra from the 7478-7620 cal yr B.P. eruption of Mt. Mazama (Hallett et al., 1997). Multiple radiocarbon ages have been obtained from NWRZ lava flows and are reported in MacLeod et al. (1995). Calibrated ages range from 6610 to 7240 yr B.P. (errors range from ±60 to ±210 years) with an average of 6927 yr B.P. (MacLeod et al., 1995). Paleomagnetic data indicate that NWRZ vents can be divided into a north group and a south group (Figure 2.2) and that several decades to a century elapsed between the eruptions of these two groups, suggesting that the resolution of radiocarbon data is too low to record the true duration of activity (McKay et al., 2009). Although several of the vents are located close to each other, few of the lava flows and tephra deposits overlap, making it difficult to constrain the relative timing of eruptive activity at individual vents.

The NWRZ eruptions produced cinder cones, spatter ramparts, and extensive lava flows that cover a total area of ~70 km². Several vents produced tephra blankets, which have been mapped by MacLeod et al. (1995) and Jensen (2006). Table 2.1 lists vent types and the volumes of vent material (cinder cones or spatter ramparts), tephra blankets, and lava flows erupted from individual vents. The Lava Butte and Mokst Butte vents produced much larger volumes of both tephra and lava than other NWRZ vents; they are also the only vents with large cinder cones. South Sugarpine, South Kelsey, and

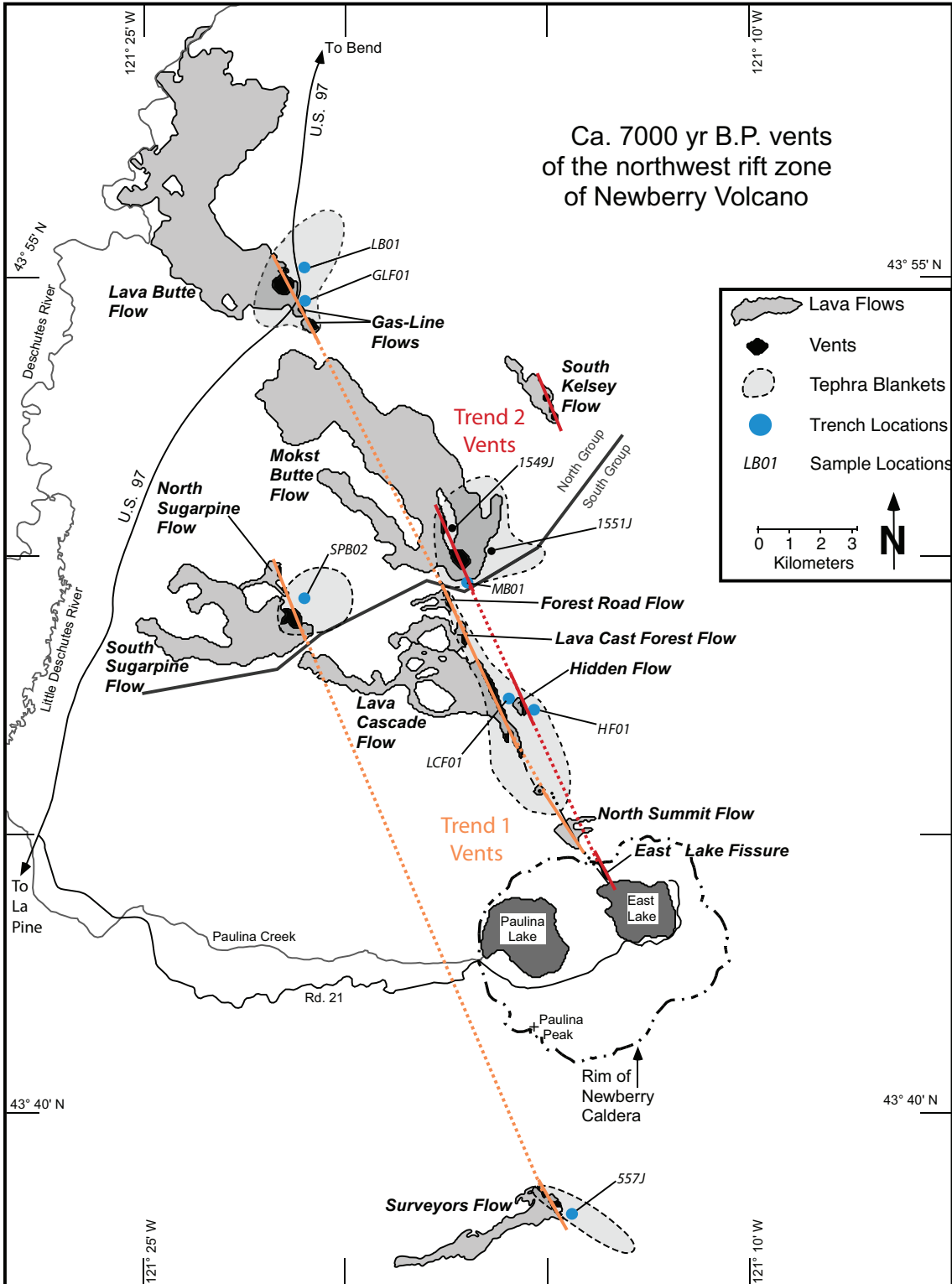


Figure 2.2. Map of Newberry Volcano showing the vents, lava flows, and tephra blankets of the northwest rift zone (after Jensen, 2006). Paved roads are indicated with solid black lines, rivers and streams with solid gray lines. North and south group vents, as defined by paleomagnetic data, are separated by a heavy black line. Trend 1 and Trend 2 vents, as defined by K_2O - TiO_2 content, are indicated with red and orange lines.

Surveyors vents produced small cinder cones, while the rest of the vents produced spatter ramparts but no cones. This observed range in eruptive products, particularly in the volume of pyroclastic material, indicates that eruption style varied considerably from vent to vent. Chemical compositions of NWRZ vents range from basalt at 51.7 wt% SiO₂ to andesite at 58.4 wt% SiO₂ (McKay et al., 2009). This range in composition does not appear to be correlated with the types of eruptive products listed in Table 2.1, suggesting that the production of cinder cones and tephra blankets was not directly related to SiO₂ content, but might be controlled by other variables such as volatile content, magma temperature, or mass eruption rate. Since understanding the range in volcanic deposits produced by mafic vents has significant implications for hazards, it is important to determine the extent to which these variables controlled activity during the NWRZ eruption.

Table 2.1. Volumes of eruptive products from NWRZ vents.

Vent name	Vent type	Eruptive volumes (10 ⁶ m ³)			
		Vent (DRE)	Tephra (DRE)	Lava	Total
Lava Butte	Large cinder cone	24.6	2.6	282.0	309.2
Gas Line	Spatter	0.1	0.03	1.0	1.13
Mokst Butte	Large cinder cone	20.4	2.1	359.4	381.9
South Kelsey	Small cinder cone	0.5	?	10.7	11.2
North Sugarpine	Spatter	0.02	?	1.0	1.02
South Sugarpine	Small cinder cone	7.6	1.1	92.9	101.6
Forest Road	Spatter	0.02	0.003	1.2	1.223
Lava Cast Forest	Spatter	0.1	0.2	4.0	4.3
Lava Cascade	Spatter	2.5	1.6	34.6	38.7
Hidden	Spatter	0.03	0.002	0.4	0.432
Unnamed	Spatter	0.02	?	0.1	0.12
North Summit	Spatter	0.06	?	0.8	0.86
East Lake Fissure	Spatter	0.2	?	0.0	0.2
Surveyors	Small cinder cone	0.8	0.9	8.7	10.4

All volumes are from McKay et al. (2009).

Activity at the NWRZ appears to be typical of other recent (late Pleistocene and Holocene) mafic eruptions at Newberry in that it involved multiple vents, was apparently active intermittently over decades to a century, and produced multiple lava flows. The north and south flanks of the volcano are covered by numerous, relatively low-volume basalt and basaltic andesite flows that erupted from late Pleistocene and Holocene cinder cones and fissure vents (e.g. Jensen et al., 2009). Recent mapping (Jensen et al., 2009; Donnelly-Nolan et al., 2010) indicates that many of these eruptions involved multiple vents, although few are as extensive in area as the ca. 7000 ybp NWRZ vents. If similar multi-vent eruptive episodes occur in the future, they will present multiple hazards to populated areas near Newberry Volcano (Sherrod et al., 1997; McKay et al., 2009).

2.3. Methods

Tephra samples were collected by digging trenches in the proximal deposits (<1 km from the vent) of seven NWRZ vents, shown in Figure 2.2. These locations were chosen based on tephra thickness and representative deposit descriptions from Jensen (2006). Samples were collected from the lower and upper units of each tephra deposit. In addition, samples of complete stratigraphic sequences were collected from Lava Butte, South Sugarpine, and Lava Cascade vents. These vents represent endmembers in morphologies (large cinder cones vs. small or no cinder cones), as well as in tephra stratigraphies (alternating layers of fine and coarse grained material vs. massive layers of lapilli or bombs) observed in the field. Grain size analyses of these sample suites were done by dry sieving at one-phi intervals from -6 to 3 ϕ . After sieving, each suite of samples was separated into three juvenile components that differ in vesicularity: 1) tan,

highly vesicular scoria (sideromelane), 2) black, less vesicular scoria (tachylite), and 3) dense fragmented lava (e.g. Heiken, 1978; Valentine et al., 2005; Pioli et al., 2008). Componentry was determined for all grain size fractions from -6 to 0 ϕ . Textural and chemical examinations presented here focus on the sideromelane component because it is least affected by late-stage degassing and crystallization (e.g. Erlund et al., 2009). Clasts from the bottom and top of each stratigraphic sequence were examined in backscattered imaging mode on a FEI Quanta 200 FEG Environmental SEM at the University of Oregon.

Bulk tephra analyses were performed by X-ray fluorescence (XRF) at the GeoAnalytical Laboratory at Washington State University, courtesy of J.D. Nolan at the U.S. Geological Survey as part of a larger Newberry mapping project. Analyses of matrix glass and plagioclase from representative sideromelane clasts from Lava Cascade, South Sugarpine, Lava Butte, Gas Line, and Mokst Butte were analyzed by electron microprobe at the University of Oregon. The first three vents were chosen because they span the range of inferred NWRZ eruptive styles; Gas Line was included because it represents the first phase of the Lava Butte eruption (McKay et al., 2009); and Mokst Butte was included because it appears to be the result of a distinct assimilation history and, in addition to Lava Butte, is the only vent that produced a large cinder cone and a relatively large tephra blanket. Glass and plagioclase compositions were used to calculate minimum pre-eruptive H₂O contents using the plagioclase-liquid hygrometer/thermometer described by Lange et al. (2009). A complete discussion of these calculations is given in Section 2.5.1. All glass and mineral compositions were measured using a Cameca SX-100 electron microprobe operating at a 15 kV accelerating voltage, 10 nA beam current,

and a 10 μm beam diameter. A combination of natural and artificial glass and mineral standards was used for these analyses. Plagioclase compositions were measured in transects parallel to the short dimension of individual microphenocrysts and on groundmass crystals. All analyses were performed on euhedral normally zoned crystals that did not exhibit resorption textures.

2.4. Results

2.4.1. Physical Characteristics of Tephra

NWRZ tephra deposits can be characterized by three end members: 1) thin proximal deposits (<2 m) of massive, poorly-sorted blocks and lapilli from vents that produced spatter ramparts; 2) thin proximal deposits (<2 m) of massive, well-sorted lapilli layers from vents that produced very small cinder cones; and 3) and thick proximal deposits (>2 m) of alternating ash and lapilli layers from vents that produced large cinder cones. Lava Cascade, South Sugarpine, and Lava Butte, respectively, represent these three endmembers. In the following sections, I describe the stratigraphy of each of these deposits in detail. Representative stratigraphic columns and grain size distributions from each major layer of the deposits are shown in Figures 2.3 and 2.4. All of the deposits immediately overlie rhyodacitic ash from the 7478-7620 cal yr B.P. (Hallett et al., 1997) eruption of Mt. Mazama (MacLeod et al., 1995; Jensen, 2006). Contacts between the base of each deposit and Mazama ash are sharply defined by the dramatic color contrast from white to black. Inman Graphical Standard Deviation (IGSD) sorting coefficients (σ_s) and median grain sizes (M_d) are plotted for each vent in Figure 2.5, along with fields defining different eruption styles.

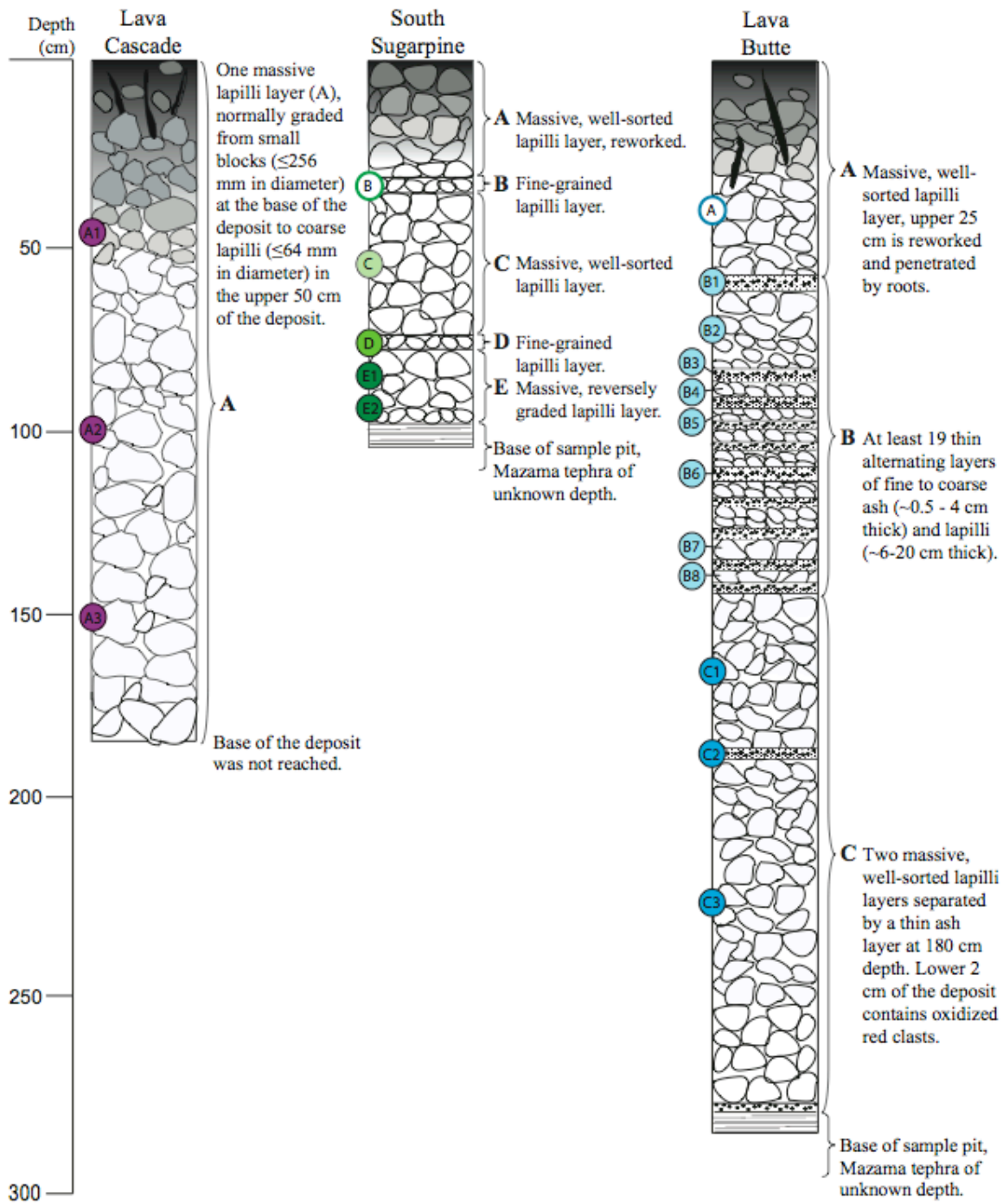


Figure 2.3. Representative stratigraphic columns of the Lava Cascade, South Sugarpine, and Lava Butte tephra deposits. Sample trench locations are shown in Figure 2.2 (labeled *LCF01*, *SPB02*, and *LB01*, respectively). Stratigraphic units are labeled and described to the right of each column. Colored circles represent locations where samples were collected for grain size, componentry, and chemical analyses.

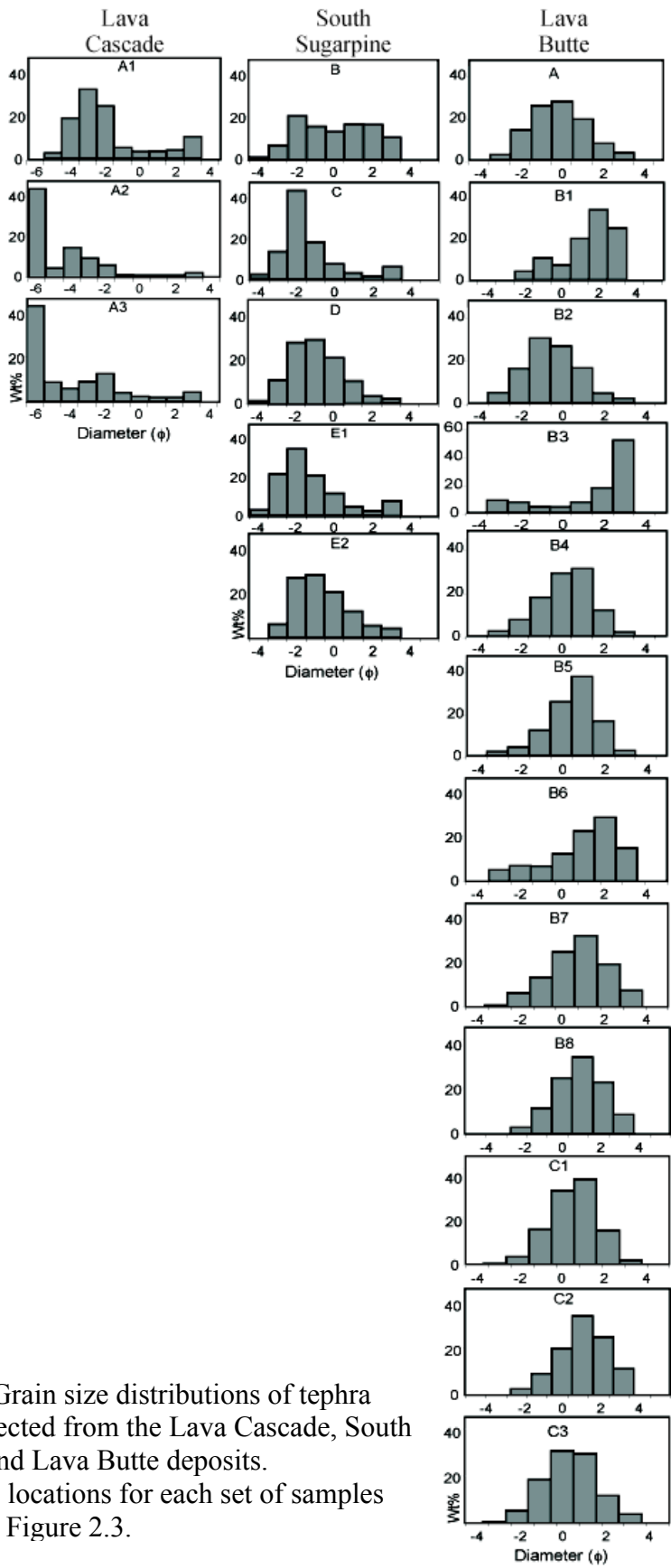


Figure 2.4. Grain size distributions of tephra samples collected from the Lava Cascade, South Sugarpine, and Lava Butte deposits. Stratigraphic locations for each set of samples are shown in Figure 2.3.

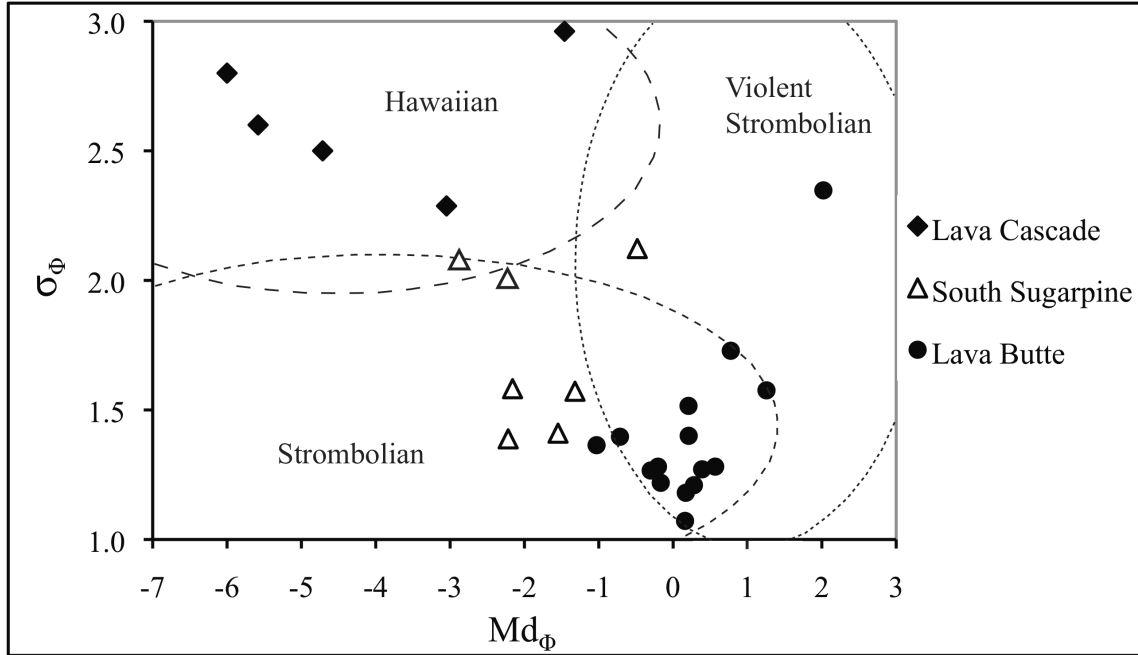


Figure 2.5. Inman sorting coefficients (σ_ϕ) and median grain sizes (Md_ϕ) for the Lava Cascade, South Sugarpine, and Lava Butte tephra deposits. Fields defining eruption styles are after Walker and Croasdale (1972), Parfitt (1998), Houghton and Gonnermann, (2008), and Pioli et al. (2008).

2.4.1.1. Stratigraphy of the Lava Cascade Tephra Deposit

The Lava Cascade deposit consists of one massive layer that is normally graded from small blocks (≤ 256 mm in diameter) at the base of the deposit to coarse lapilli (≤ 64 mm in diameter) in the upper 50 cm of the deposit. The lower 130 cm consists of unaltered black clasts with brown weathered clasts scattered throughout. The upper 30 cm contains brown weathered clasts that grade into 20 cm of tephra-rich soil (Figure 2.3). The entire deposit is poorly sorted ($\sigma = 2.29$ to 2.96 ; Figure 2.5), shows no internal stratification, and is characterized by very fragile, angular clasts with ragged edges; they are highly vesicular and glassy in appearance. Vesicles sizes in hand samples vary from >10 cm to <1 mm in diameter. There is no evidence of Lava Cascade tephra on lava

flows from the same vent, indicating that the more explosive phases of tephra production occurred prior to effusive activity.

2.4.1.2. *Stratigraphy of the South Sugarpine Tephra Deposit*

The South Sugarpine eruption likely began as a small fissure eruption that produced spatter and small lava flows from the North Sugarpine vent. As the eruption progressed, activity migrated to the southeast and became focused at the South Sugarpine vent, where it produced a small cinder cone and tephra blanket. In contrast to the abundance of block-sized clasts in the Lava Cascade deposit, the South Sugarpine deposit is dominated by fine-grained lapilli (2-4 mm) with occasional medium to coarse clasts (>4 mm but ≤ 32 mm). There are three massive well-sorted ($\sigma = 1.39$ to 2.12) lapilli layers separated by two thin layers (2-5 cm) of slightly finer grained lapilli located at depths of 73 and 34 cm. Contacts between these slightly finer grained layers and the massive lapilli layers above and below are gradational. The lower ~10 cm of the bottom lapilli layer is reversely graded to slightly smaller clasts (≤ 16 mm). The lower 68 cm of the deposit consists of unaltered black tephra overlain by 24 cm of weathered brown tephra that is penetrated by roots. The upper 8 cm of the deposit grades into tephra-rich soil. Lapilli clasts in all layers are angular and highly vesicular, similar to clasts in the Lava Cascade deposit but smaller in size. Vesicle sizes in hand samples show less size variation than in clasts from the Lava Cascade deposit and range from ~1 cm to <1 mm in diameter.

Pockets of tephra cover the proximal region of the South Sugarpine lava flow, indicating that some tephra production occurred after effusive activity. However,

breaching of the South Sugarpine cinder cone in the direction of the lava flow shows that the cone was rafted apart by lava during or after construction; subsequent phases of explosive activity did not rebuild the cone. This, along with the limited amount of tephra on the lava flow, indicates that the most explosive phases of activity occurred prior to effusive activity.

2.4.1.3. *Stratigraphy of the Lava Butte Tephra Deposit*

In sharp contrast to both the Lava Cascade and South Sugarpine deposits, the Lava Butte deposit shows much more variability in grain size from bottom to top. The deposit can be divided into three sections based on the distribution and thickness of alternating layers of ash and lapilli. The lower section, from the base of the deposit to 140 cm depth, consists of two massive, well-sorted ($\sigma = 1.22$ and 1.07) lapilli layers separated by a thin (3-4 cm) ash layer at 180 cm depth. Both lapilli layers show crude internal stratification. The middle section of the deposit, from 140-60 cm depth, is marked by a striking change from massive lapilli layers to thin, alternating layers of fine to coarse ash and lapilli. Ash layers vary in thickness from ~ 0.5 -4 cm and are separated by sharp contacts from the lapilli layers above and below, which vary in thickness from ~ 6 -20 cm. Individual ash and lapilli layers are well-sorted and show crude internal stratification; several lapilli layers are reversely graded. The upper 60 cm of the deposit consists of one massive, well-sorted ($\sigma = 1.4$) lapilli layer. There is a thin (~ 2 cm) layer of oxidized red clasts at the base of the deposit; the rest of the deposit consists of unaltered black tephra to ~ 85 cm depth where it grades into brown weathered tephra. The upper 25 cm of the deposit appears reworked and is penetrated by roots. Tephra clasts throughout the entire

deposit are highly vesicular, but are less glassy and more rounded than clasts from the Lava Cascade and South Sugarpine deposits. Vesicles sizes in hand samples are much more uniform than Lava Cascade and South Sugarpine clasts; the majority of all visible vesicles in Lava Butte clasts are ≤ 2 mm in diameter.

The Lava Butte eruption began as a fissure eruption that produced small spatter cones, a limited tephra blanket, and lava flows of the Gas Line vent (McKay et al., 2009). Stratigraphy of the Gas Line tephra deposit, which is exposed in a quarry shown in Figure 2.2, resembles that of the Lava Cascade tephra deposit. Tephra clasts range from small blocks to large lapilli and are angular with ragged edges, highly vesicular and glassy in appearance. As the eruption progressed, activity was focused into a single vent that produced the Lava Butte cinder cone, tephra blanket, and lava flows (McKay et al., 2009). Lava Butte tephra covers lava flows of the Gas Line vent, but does not cover lava flows of the Lava Butte vent, indicating that explosive activity at Lava Butte occurred after the Gas Line fissure eruption but prior to effusive phases of the Lava Butte eruption.

2.4.1.4. Stratigraphy of the Mokst Butte Tephra Deposit

Since Mokst Butte is the only other NWRZ vent that produced a large cinder cone and a relatively large tephra blanket, a brief description of the tephra deposit produced by this vent is given here. Detailed sampling, sieving, and separation of juvenile components was not done for the entire stratigraphy of the Moskt Butte deposit. However, a sample trench in the proximal section of the tephra deposit (Figure 2.2) exposed alternating layers of ash and lapilli with similar stratigraphy to the Lava Butte deposit. Mokst Butte differs from other NWRZ vents in that it is the only location where a significant amount

of tephra was deposited on the lava flows (Jensen, 2006). Detailed LIDAR imagery shows that there may have been an earlier cinder cone at the Mokst Butte vent location that erupted lavas to the north (R.A. Jensen, personal communication). The Mokst Butte cone was built on top of this earlier cone and tephra from the more recent cone covers both the older cone and the southern portion of the older lava flows (R.A. Jensen, personal communication). The younger Mokst Butte cone erupted lavas to the southwest and the cone is breached in that direction. There are large sections of rafted cone material incorporated into these lava flows, indicating that the last phases of activity were effusive.

2.4.2. Juvenile Components of Tephra

Three juvenile components were identified in NWRZ tephra deposits: 1) tan, highly vesicular scoria (sideromelane), 2) black, less vesicular scoria (tachylite), and 3) dense fragmented lava. Representative examples of each component are shown in Figure 2.6. Tephra deposits from vents that produced spatter ramparts or small cinder cones (e.g. Lava Cascade and South Sugarpine) contain just one juvenile component: tan, highly vesicular sideromelane clasts. Tephra deposits from vents that produced large cinder cones (e.g. Lava Butte and Mokst Butte) contain all three types of juvenile components. Here I provide quantitative analyses of the juvenile components from the Lava Cascade, South Sugarpine, and Lava Butte deposits. Relative proportions of each component throughout the stratigraphies of the deposits are shown in Figure 2.7.

The Lava Cascade deposit contains sideromelane clasts with angular shapes, ragged edges, glassy appearance, and a broad range in vesicle sizes (>10 cm to <1 mm);

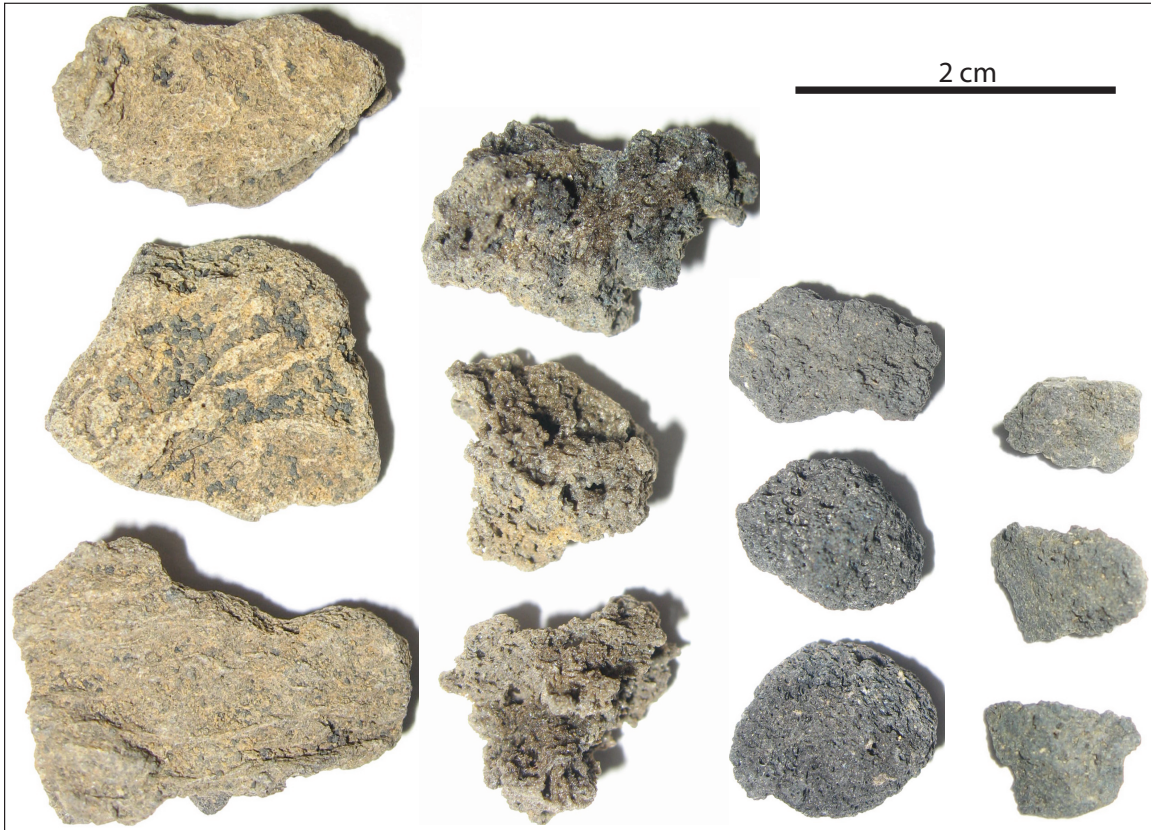


Figure 2.6. Photo of juvenile tephra components identified in NWRZ deposits. Dense lava fragments are pictured in the far right column. Black, less vesicular scoria clasts (tachylite), which are more rounded than the lava fragments, are pictured in the middle right column. Tan, highly vesicular scoria clasts (sideromelane) are pictured in the middle left column. Clasts in the left column resemble tan scoria but have flattened shapes and relatively smooth surfaces.

all characteristics of pyroclasts produced during hawaiian-style eruptions (e.g. Parfitt, 2004; Parfitt, 1998). Sideromelane clasts of the South Sugarpine deposit are very similar, but with less variation in vesicle sizes (~1 cm to <1 mm). Tephra from both the Lava Cascade and South Sugarpine vents are crystal poor, but some clasts contain tabular plagioclase phenocrysts ≤ 2 mm in diameter. Loose crystals are not present in either deposit.

The Lava Butte deposit contains all three juvenile components (Figure 2.6). Tan sideromelane clasts differ from those in the Lava Cascade and South Sugarpine deposits

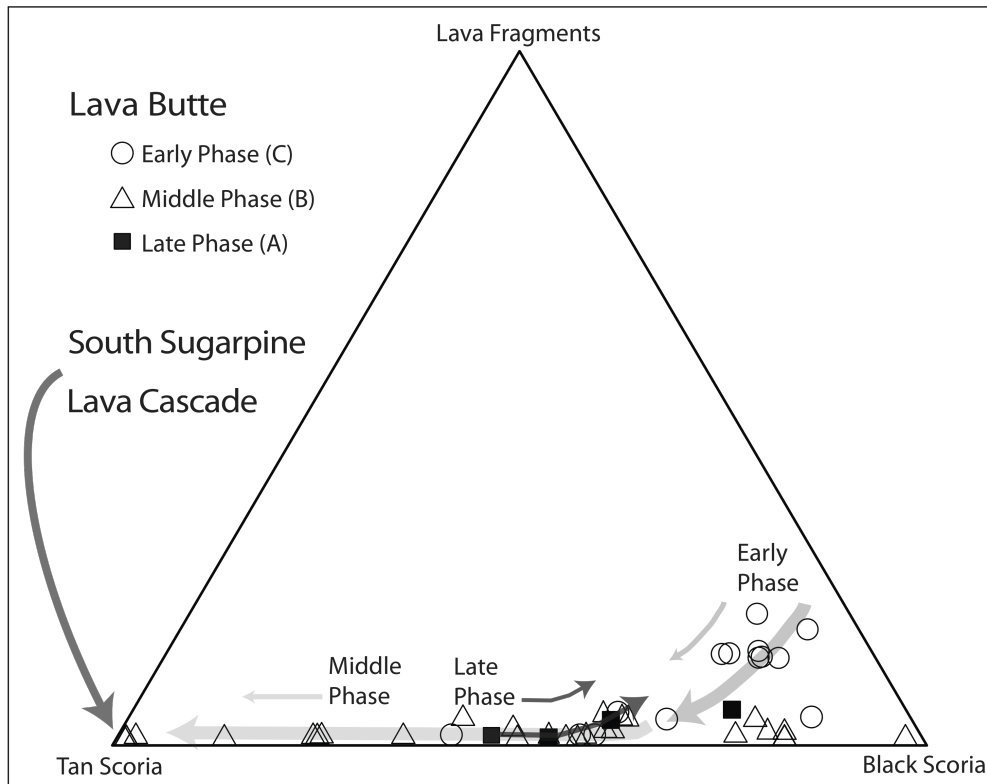


Figure 2.7. Componentry of juvenile tephra from the Lava Cascade, South Sugarpine, and Lava Butte deposits. All stratigraphic horizons of the Lava Cascade and South Sugarpine deposits contain 100% tan scoria (indicated with arrow). Stratigraphic horizons A-C of the Lava Butte tephra deposit (Figure 2.3) are shown by symbols. Early phase: black scoria dominates. Middle phase: light gray arrows indicate decreasing proportions of dense lava fragments and black scoria, and increasing proportions of tan scoria; some layers within these horizons are entirely dominated by tan scoria. Late phase: dark gray arrows indicate that black scoria again becomes more dominant and proportions of dense lava fragments increase slightly.

in having smooth outer edges and smaller vesicles (≤ 2 mm) that are more uniform in size.

They resemble pyroclasts from strombolian to violent strombolian eruptions described by

Heiken (1978) and Pioli et al. (2008). All three components are crystal poor, although

some clasts contain tabular plagioclase phenocrysts ≤ 2 mm in diameter. Loose crystals

are very rare. The relative abundance of the three components varies from the bottom to

the top of the deposit (Figure 2.7). Black, moderately dense tachylite clasts dominate the

massive lapilli layers produced early in the eruption. Dense, angular lava fragments are

also present in these layers. The middle of the deposit, characterized by alternating layers of lapilli and ash, contains markedly fewer lava fragments and shows increasing proportions of tan sideromelane clasts. The largest grain size fractions (-3ϕ) in this section are composed entirely of tan clasts. Several of the layers in this section also contain lapilli clasts that resemble the tan scoria but have flattened shapes and relatively smooth surfaces (Figure 2.6). Similar clasts have been observed in the tephra deposit from Paricutin, Mexico and are associated with violent strombolian phases of activity (Pioli et al., 2008). The trend toward higher proportions of tan clasts in the middle of the deposit reverses in the upper massive lapilli layer, where black clasts again become dominant. The proportion of lava fragments in this layer is lower than in the two massive lapilli layers at the base of the deposit.

2.4.3. Microtextural Characteristics of Tephra

Tan scoria clasts from Lava Cascade, South Sugarpine, and Lava Butte are all moderately crystalline and characterized by abundant plagioclase microphenocrysts and microlites (Figure 2.8A-C). Plagioclase crystals are elongate in cross-section, tabular in three dimensions, and are often aligned. Less abundant olivine and pyroxene are also present, both as euhedral microphenocrysts and as microlites. Tan scoria clasts from all three vents are characterized by round microvesicles that vary in size from $\sim 1\text{mm}$ to $\sim 25 \mu\text{m}$ in cross sectional diameter. In some cases, vesicles appear to have deformed around individual crystals (e.g. Figure 2.8A).

Black scoria clasts from Lava Butte have a much more crystalline groundmass than tan scoria (Figure 2.8D). As in tan scoria, plagioclase microphenocrysts and

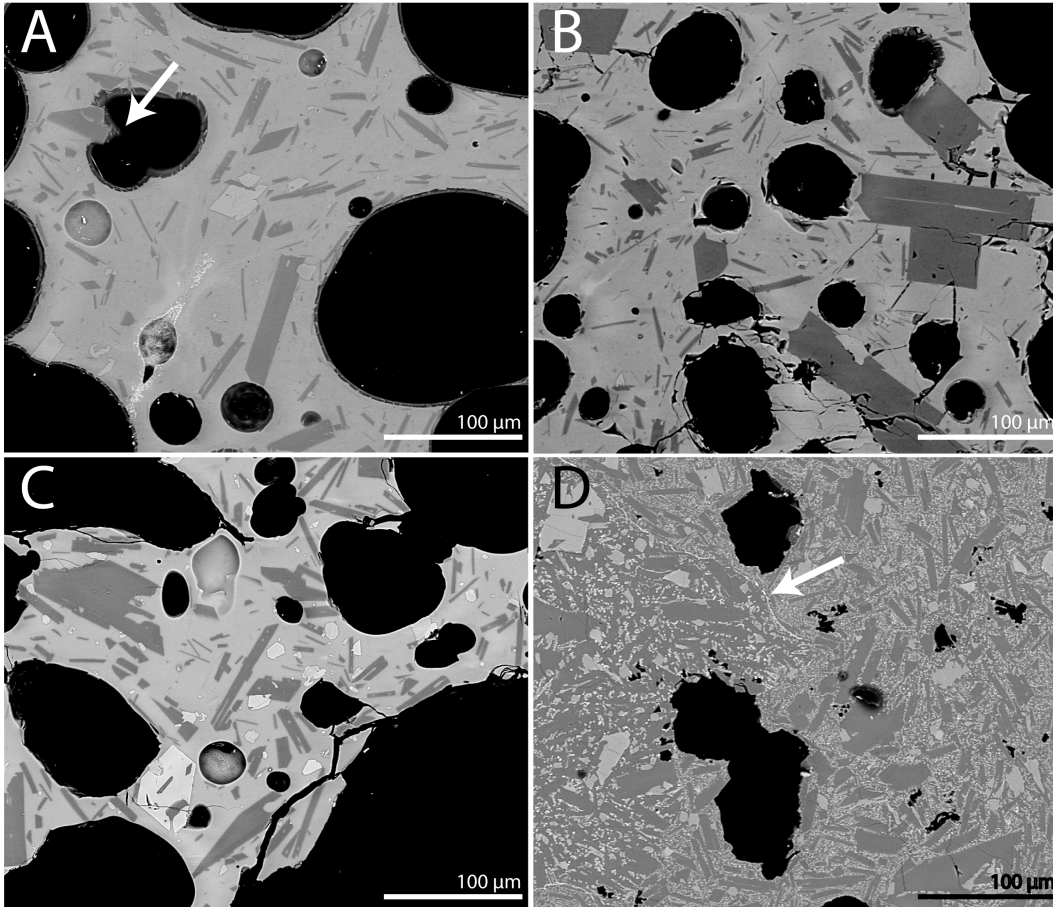


Figure 2.8. SEM images of tephra clasts from the Lava Cascade, South Sugarpine, and Lava Butte deposits. Images A-C are of tan scoria from Lava Cascade (A), South Sugarpine (B), and Lava Butte (C). Black scoria from Lava Butte (D) is also shown. Arrows indicate examples of a vesicle deformed around crystals (A) and the boundary between recycling textures (D).

microlites are abundant. Again, less abundant olivine and pyroxene are also present, both as microphenocrysts and as microlites. Microvesicles in black scoria clasts are less abundant than in tan scoria, smaller in size (typically ~ 0.5 mm to < 25 μm), and many appear to be deformed and often have ragged edges. Black scoria clasts are also characterized by intermingling of two different textures: 1) areas that are very densely populated with interlocking plagioclase crystals; and 2) areas where plagioclase crystals are separated by abundant groundmass crystals (Figure 2.8D). Boundaries between these two textures are lined with very tiny late-stage oxides.

2.4.4. Tephra Compositions

Bulk compositions of juvenile tephra are listed in Table 2.2 and are plotted along with bulk lava compositions from McKay et al. (2009) in Figure 2.9. Tephra compositions range from 51.3 to 57.2 wt.% SiO₂ (Table 2.2 and Figure 2.9). Although the tephra data do not extend the compositional range recorded by lavas for the entire NWRZ eruptive episode, they do significantly extend the compositional range erupted from individual vents. At each vent, bulk tephra compositions are lower in both SiO₂ and MgO than bulk lava compositions (Figure 2.9). Because stratigraphic relationships between the tephra and lavas show that explosive phases of activity occurred prior to effusive phases, this pattern of compositional changes shows that at each vent, the erupted magma became more silicic with time.

Vents of the NWRZ can be divided into two groups based on SiO₂ content, shown in Figure 2.9 with orange and red symbols and designated as Trend 1 and Trend 2 vents. Interestingly, many of the vents with lower SiO₂ contents (orange symbols) are located along the same fissure system (the Lava Cascade, Lava Cast Forest, and Forest Road vents; Figure 2.2). As shown in Figure 2.2, the North Summit, Gas Line, and Lava Butte vents are aligned along this same trend. The Surveyors vents and North and South Sugarpine vents are each aligned along similar, but smaller, trends to the south and west (Figure 2.2). Vents with higher SiO₂ contents are aligned along yet another trend, located to the east of Trend 1 vents (Figure 2.2). These include the East Lake Fissure, Hidden, and Mokst Butte vents (Trend 2 vents in Figures 2.2 and 2.9). The South Kelsey vents are also aligned along a similar, smaller trend to the east and are included in Trend 2 vents based on spatial distribution and relatively high SiO₂ contents (Figures 2.2 and 2.9).

Table 2.2. Bulk chemical analyses of NWRZ tephra samples.

Vent	Lava Butte LB01				Gas Line GLF01	Mokst Butte						
	43° 55.363					1549J ¹ 45° 50.59			1551J ¹ 43° 50.33			
Lat (N)	121° 21.015				121° 20.934	121° 16.99			121° 16.13			
Long (W)												
wt. %												
SiO ₂	55.66	56.65	56.10	55.71	55.24	55.01	54.94	55.29	56.76	57.21	56.96	
Al ₂ O ₃	17.66	17.19	17.28	17.60	17.59	19.67	19.03	18.32	18.17	17.30	17.07	
FeO*	7.40	6.90	7.05	7.34	7.33	8.96	9.04	8.79	8.25	8.05	8.07	
MgO	4.80	4.81	5.01	4.98	5.26	3.73	3.96	4.15	3.62	3.89	4.11	
CaO	7.94	7.81	8.09	8.05	8.33	6.21	6.62	6.88	6.36	6.62	6.94	
Na ₂ O	3.80	3.86	3.76	3.62	3.61	3.17	3.23	3.39	3.54	3.64	3.61	
K ₂ O	1.22	1.41	1.30	1.24	1.17	1.40	1.33	1.35	1.56	1.63	1.55	
TiO ₂	1.14	1.04	1.05	1.10	1.11	1.44	1.46	1.44	1.34	1.30	1.32	
P ₂ O ₅	0.24	0.22	0.22	0.22	0.23	0.26	0.24	0.23	0.24	0.21	0.22	
MnO	0.14	0.13	0.13	0.14	0.14	0.16	0.17	0.16	0.15	0.15	0.15	
ppm												
Rb	29	35	32	30	27	35	34	35	41	43	41	
Sr	487	380	391	386	399	241	256	280	261	262	275	
Y	27	27	26	26	25	36	37	36	33	34	33	
Zr	161	160	149	152	141	213	199	190	207	195	182	
Nb	11	10	10	10	10	13	13	12	14	13	12	
Ba	375	388	353	372	343	380	381	382	404	410	405	
Ni	47	48	48	49	53	18	20	24	16	17	18	
Cu	63	57	63	63	69	56	64	69	52	56	60	
Zn	74	71	71	69	73	62	65	85	71	70	74	
Cr	99	102	108	108	112	47	48	48	43	43	47	
Ce	34	35	29	32	27	39	37	38	42	39	38	
Ga	19	19	17	17	18	20	20	20	20	19	19	
La	12	15	15	9	13	18	19	17	16	18	19	
Nd	19	19	18	18	17	22	21	23	22	21	20	
V	164	162	170	166	172	191	197	194	186	183	190	

Table 2.2. Continued.

Vent	South Sugarpine SPB02			Lava Cascade LCF01			Hidden HF01		Surveyors 5575J ¹
Lat (N)	43° 49.617			43° 47.195			43° 47.357		43° 38.21
Long (W)	121°20.710			121° 15.856			121° 15.449		121° 14.49
wt. %									
SiO ₂	51.33	53.18	52.81	52.97	53.77	54.21	52.24	55.97	54.00
Al ₂ O ₃	19.34	17.94	17.52	19.53	18.40	17.45	20.72	17.37	19.12
FeO*	9.79	9.07	9.19	9.29	8.89	8.47	9.66	8.47	8.52
MgO	5.17	5.06	5.25	4.21	4.58	5.04	4.00	4.26	4.72
CaO	8.62	8.62	9.19	7.80	8.26	8.47	6.98	7.11	7.45
Na ₂ O	3.12	3.39	3.36	3.37	3.35	3.64	3.31	3.60	3.28
K ₂ O	0.62	0.82	0.73	0.88	0.91	0.97	1.06	1.48	1.07
TiO ₂	1.53	1.47	1.50	1.47	1.39	1.32	1.52	1.36	1.37
P ₂ O ₅	0.29	0.29	0.28	0.32	0.29	0.28	0.32	0.23	0.33
MnO	0.18	0.17	0.17	0.16	0.16	0.15	0.18	0.16	0.16
ppm									
Rb	11	17	13	18	20	20	24	38	25
Sr	382	395	399	391	407	409	312	281	346
Y	28	28	26	29	27	26	33	34	36
Zr	130	137	129	159	147	138	181	188	180
Nb	10	11	11	11	10	10	12	12	14
Ba	287	299	269	373	366	340	300	372	394
Ni	42	33	28	35	34	32	28	21	37
Cu	89	81	79	77	73	68	74	63	79
Zn	78	83	81	89	89	83	69	77	91
Cr	134	109	107	102	100	96	90	46	107
Ce	28	29	29	35	30	28	41	41	33
Ga	19	18	17	19	19	18	21	19	19
La	15	14	13	17	12	14	19	17	14
Nd	19	17	17	19	20	17	25	21	14
V	213	205	223	193	198	201	206	197	162

¹Samples collected by J.D. Nolan. Sample locations are shown in Figure 2.2. Chemical analyses were performed by X-ray fluorescence (XRF) at the GeoAnalytical Laboratory at Washington State University, courtesy of J.D. Nolan. Major element analyses are normalized to 100% volatile-free with iron calculated as FeO and indicated as FeO*.

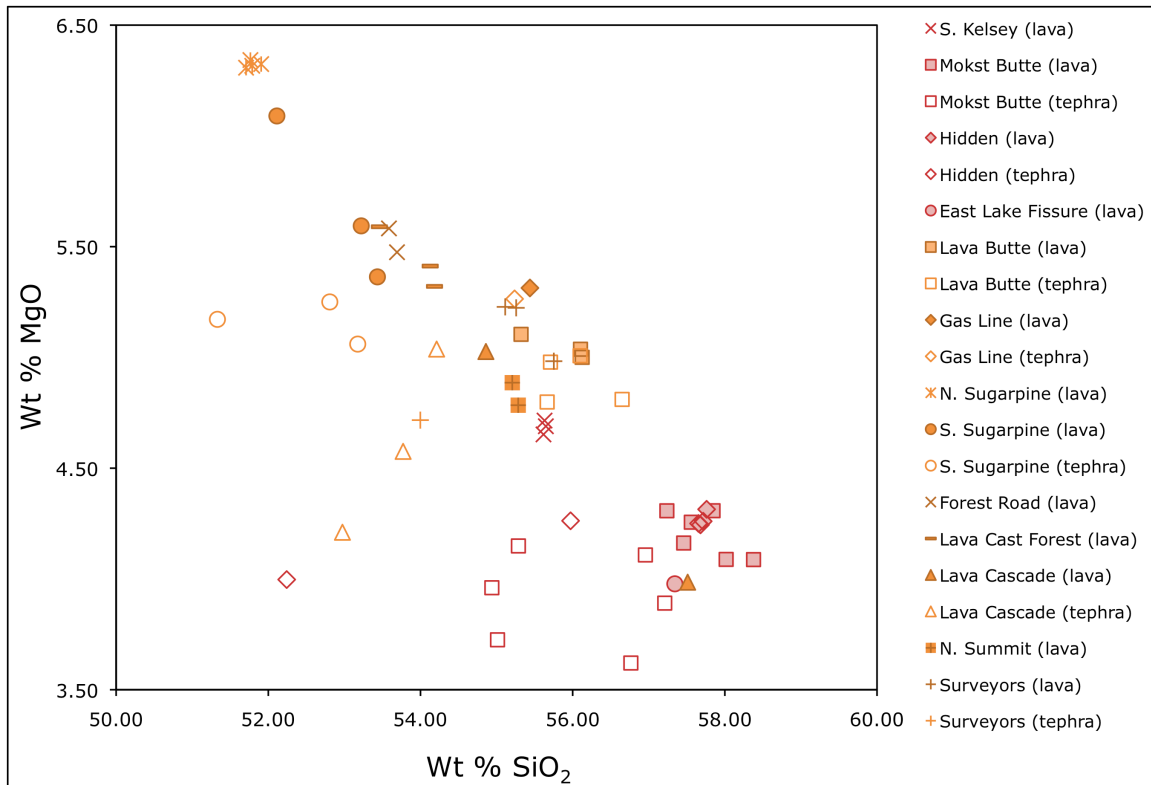


Figure 2.9. MgO and SiO₂ contents of bulk NWRZ lava (McKay et al., 2009) and tephra (Table 2.2) show the variability of chemical compositions among vents. Tephra compositions show that at each vent, erupted magma became higher in both SiO₂ and MgO with time. Orange symbols represent Trend 1 vents and red symbols represent Trend 2 vents, as shown in Figure 2.2.

2.5. Discussion

Determining the pre-eruptive volatile contents of magmas is an important aspect of understanding the role volatiles play in controlling eruption style. Initial pre-eruptive volatile contents can be measured from olivine-hosted melt inclusions (e.g. Luhr, 2001; Cervantes and Wallace, 2003; Johnson et al., 2008; Ruscitto et al., 2010), but NWRZ vents do not contain sufficiently large olivine for these analyses. For this reason, I estimated pre-eruptive H₂O contents using plagioclase phenocryst compositions; the results are used to evaluate the effects of H₂O on the various eruption styles of NWRZ vents. In the following sections, I also examine the role that crustal assimilation played in

magma evolution and what this process can tell us about the pre-eruptive storage system of Newberry Volcano. I evaluate the various eruption styles that occurred during the NWRZ eruption and investigate possible controls on eruption style. Finally, I discuss the implications for hazards if future activity at Newberry Volcano is similar to that of the NWRZ eruption.

2.5.1. Calculation of Magma H₂O Contents

Several thermodynamic models have been constructed based on the equilibrium exchange of albite and anorthite between plagioclase and hydrous silicate melts (e.g. Housh and Luhr, 1991; Putirka, 2005; Lange et al., 2009). These models have been used as either a hygrometer (e.g. Housh and Luhr, 1991; Putirka, 2005) a thermometer/geobarometer (e.g. Putirka, 2005), or a hygrometer/thermometer (Lange et al., 2009). The model presented by Lange et al. (2009) allows the effect of temperature and pressure on the plagioclase exchange reaction to be calculated independently from the effect of melt composition, resulting in more accurate estimates of the effect of composition on the reaction. This model was calibrated on hydrous and anhydrous plagioclase-liquid experiments and is applicable to all lava compositions in equilibrium with An₉₅-An₃₅ plagioclase (Lange et al., 2009).

When the Lange et al. (2009) model is used as a hygrometer, temperature must be determined independently. In the applications presented in Lange et al. (2009), lava temperatures were either known or were calculated from Fe-Ti oxide thermometry. Since NWRZ tephra lacks sufficient Fe-Ti oxides for temperature determination, I estimated lava temperatures from the thermodynamic model MELTS (Ghiorso and Sack, 1995;

Asimow and Ghiorso, 1998). A constant pressure of 1 kbar was assumed for all modeling calculations. For each vent, MELTS was used to calculate a range of liquidus temperatures using average bulk chemical compositions of tephra (Table 2.2), the nickel-nickel oxide (NNO) buffer, and H₂O contents that varied by increments of 0.25 wt% (Figure 2.10). The plagioclase hygrometer was used to model a range of H₂O contents using liquidus temperatures that varied in each run according to the outputs from MELTS, the most An-rich plagioclase compositions measured from phenocrysts (Table 2.3), and average glass compositions of tephra (Table 2.4). The estimated error for temperature outputs from MELTS is ± 10 °C (Ghiorso and Sack, 1995; Asimow and Ghiorso, 1998); the estimated error for H₂O outputs from the plagioclase hygrometer is ± 0.32 wt.% (Lange et al., 2009). Because liquidus temperatures from MELTS were used, H₂O estimates are most accurate for phenocrysts. The intersections of the modeled temperature - H₂O curves were used to estimate magma temperature and maximum H₂O content at initial plagioclase crystallization for each vent (Figure 2.10).

To test this method of estimating magmatic H₂O, I applied the same technique to a vent with similar lava compositions where H₂O contents are known from melt inclusion analyses. Four-in-One Cone is a Holocene cinder cone located in the central Oregon Cascades ~65 km northwest of Newberry Volcano (see Chapter III for a complete description of Four-in-One Cone). Olivine-hosted melt inclusions in tephra erupted from Four-in-One Cone record H₂O contents ranging from 1.8 to 3.1 wt.% over pressures of 1 to 2 kbar (Ruscitto, 2011). The application of MELTS and the plagioclase-liquid hygrometer for Four-in-One Cone yields a maximum of 1.3 wt.% H₂O (Figure 2.11), which is lower than the values recorded by olivine-hosted melt inclusions. An

Table 2.3. Average compositions of plagioclase microphenocrysts.

		Lava Butte					Gas Line						
	Average n=6	8	5	3	9	4	3	3	3	3	3	3	3
SiO ₂	51.14	51.01	53.72	54.38	53.53	51.04	53.46	53.36	51.30	53.33	52.80	50.74	52.98
Al ₂ O ₃	29.95	29.88	27.67	26.95	27.83	28.73	27.49	28.42	29.40	27.94	28.52	30.41	28.31
FeO	0.58	0.63	0.83	1.07	0.81	0.53	0.89	0.58	0.66	0.73	0.68	0.63	0.74
MgO	0.15	0.16	0.17	0.26	0.26	0.18	0.35	0.18	0.18	0.20	0.16	0.16	0.20
CaO	13.12	12.97	10.81	10.41	11.33	13.18	11.01	11.18	12.63	11.09	11.58	13.24	11.64
Na ₂ O	3.78	3.88	5.02	4.94	4.70	3.77	4.78	4.85	4.14	4.80	4.63	3.80	4.73
K ₂ O	0.14	0.15	0.28	0.34	0.23	0.13	0.30	0.27	0.17	0.27	0.23	0.15	0.25
TiO ₂	0.05	0.06	0.09	0.13	0.09	0.05	0.13	0.09	0.08	0.09	0.06	0.06	0.09
Total	99.06	98.90	98.73	98.66	98.93	97.81	98.45	98.94	98.57	98.45	98.69	99.21	98.96
		Gas Line			Mokst Butte			South Sugarpine					
	Average n=3	3	3	6	3	3	4	4	4	4	4	3	6
SiO ₂	53.27	52.43	50.92	54.12	55.39	56.44	43.39	53.04	50.74	52.68	52.52	50.93	51.12
Al ₂ O ₃	28.03	28.57	29.31	28.43	26.97	26.56	22.12	28.51	31.01	29.44	29.99	30.90	30.85
FeO	0.69	0.65	0.68	0.76	0.89	1.11	2.14	0.95	0.63	0.83	0.79	0.62	0.62
MgO	0.20	0.17	0.19	0.13	0.14	0.30	1.58	0.38	0.16	0.18	0.16	0.15	0.15
CaO	11.04	11.60	12.57	11.53	10.35	9.94	8.94	11.86	13.57	12.35	12.52	13.54	13.41
Na ₂ O	4.89	4.59	4.17	4.83	5.26	5.57	5.66	4.69	3.76	4.58	4.42	3.66	3.87
K ₂ O	0.26	0.22	0.17	0.24	0.34	0.39	1.71	0.17	0.10	0.15	0.14	0.11	0.11
TiO ₂	0.07	0.08	0.07	0.08	0.10	0.16	1.53	0.14	0.06	0.08	0.07	0.06	0.07
Total	98.48	98.34	98.09	100.14	99.47	100.49	100.75	100.86	101.15	101.43	101.73	101.12	101.32
		South Sugarpine				Lava Cascade							
	Average n=8	3	3	4	6	3	6	6	3	3	3	3	3
SiO ₂	51.42	51.52	51.01	52.32	52.97	52.90	52.50	47.40	52.09	52.06	53.53	51.95	52.81
Al ₂ O ₃	30.85	30.57	30.76	29.65	28.25	28.60	28.19	32.25	29.21	27.89	26.36	28.81	28.40
FeO	0.69	0.64	0.73	0.86	0.93	1.18	0.92	0.56	0.80	0.91	1.49	0.77	1.03
MgO	0.18	0.14	0.16	0.18	0.36	0.46	0.34	0.12	0.22	0.29	0.65	0.19	0.40

Table 2.3. Continued.

CaO	13.13	13.25	13.57	12.67	11.79	11.94	12.07	15.76	12.22	11.66	11.27	12.37	11.91
Na ₂ O	4.11	4.05	3.91	4.33	4.63	4.39	4.35	2.46	4.38	4.51	4.78	4.28	4.54
K ₂ O	0.11	0.10	0.10	0.14	0.23	0.22	0.18	0.06	0.17	0.18	0.27	0.17	0.20
TiO ₂	0.07	0.06	0.07	0.10	0.14	0.17	0.11	0.03	0.09	0.10	0.25	0.08	0.14
Total	101.68	101.47	101.43	101.35	99.32	99.87	98.69	98.66	99.19	97.67	98.68	98.64	99.47
Four-in-One Cone													
	Average												
	n=5	2	3	3	4	4	2	3	4				
SiO ₂	52.91	53.36	53.12	54.26	50.32	50.21	52.61	52.16	53.01				
Al ₂ O ₃	29.56	29.10	29.28	28.70	31.13	31.28	29.60	29.49	29.43				
FeO	0.58	0.82	0.73	0.78	0.55	0.49	0.73	0.69	0.76				
MgO	0.06	0.10	0.11	0.09	0.12	0.11	0.12	0.09	0.13				
CaO	12.16	11.95	12.08	11.30	14.29	13.95	12.57	12.48	12.23				
Na ₂ O	4.59	4.83	4.66	4.96	3.38	3.41	4.38	4.22	4.43				
K ₂ O	0.11	0.15	0.14	0.16	0.07	0.08	0.13	0.11	0.14				
TiO ₂	0.05	0.08	0.06	0.09	0.05	0.04	0.07	0.06	0.08				
Total	100.05	100.38	100.16	100.34	99.90	99.59	100.22	99.33	100.20				

Sample locations for Lava Butte, Gas Line, Mokst Butte, South Sugarpine, and Lava Cascade are listed in Table 2.2 and shown in Figure 2.2. Four-in-One Cone samples are described in Chapter III. Plagioclase compositions were measured at the University of Oregon using a Cameca SX-100 electron microprobe operating at a 15 kV accelerating voltage, 10 nA beam current, and a 10 μm beam diameter.

Table 2.4. Average glass compositions.

	Lava Butte	Gas Line	Mokst Butte	South Sugarpine	Lava Cascade	Four-in-One
Average n=9		18	56	50	9	45
SiO ₂	56.26	55.92	60.85	52.36	55.00	60.03
Al ₂ O ₃	14.45	14.72	16.21	15.53	15.21	13.75
FeO	9.25	8.52	7.13	9.88	9.19	9.42
MgO	3.91	4.17	2.38	5.26	5.09	2.48
CaO	6.53	7.23	5.69	8.74	7.45	5.27
Na ₂ O	3.14	3.82	3.50	4.15	2.80	2.86
K ₂ O	1.73	1.64	1.22	0.94	1.16	1.65
TiO ₂	1.62	1.47	1.40	1.61	1.56	2.04
P ₂ O ₅	0.39	0.31	0.24	0.35	0.33	0.40
MnO	0.17	0.16	0.14	0.18	0.18	0.18
Total	97.45	97.97	98.75	100.16	97.98	98.20

Sample locations for Lava Butte, Gas Line, Mokst Butte, South Sugarpine, and Lava Cascade are listed in Table 2.2 and shown in Figure 2.2. Four-in-One Cone samples are described in Chapter III. Glass compositions were measured at the University of Oregon using a Cameca SX-100 electron microprobe operating at a 15 kV accelerating voltage, 10 nA beam current, and a 10 μm beam diameter.

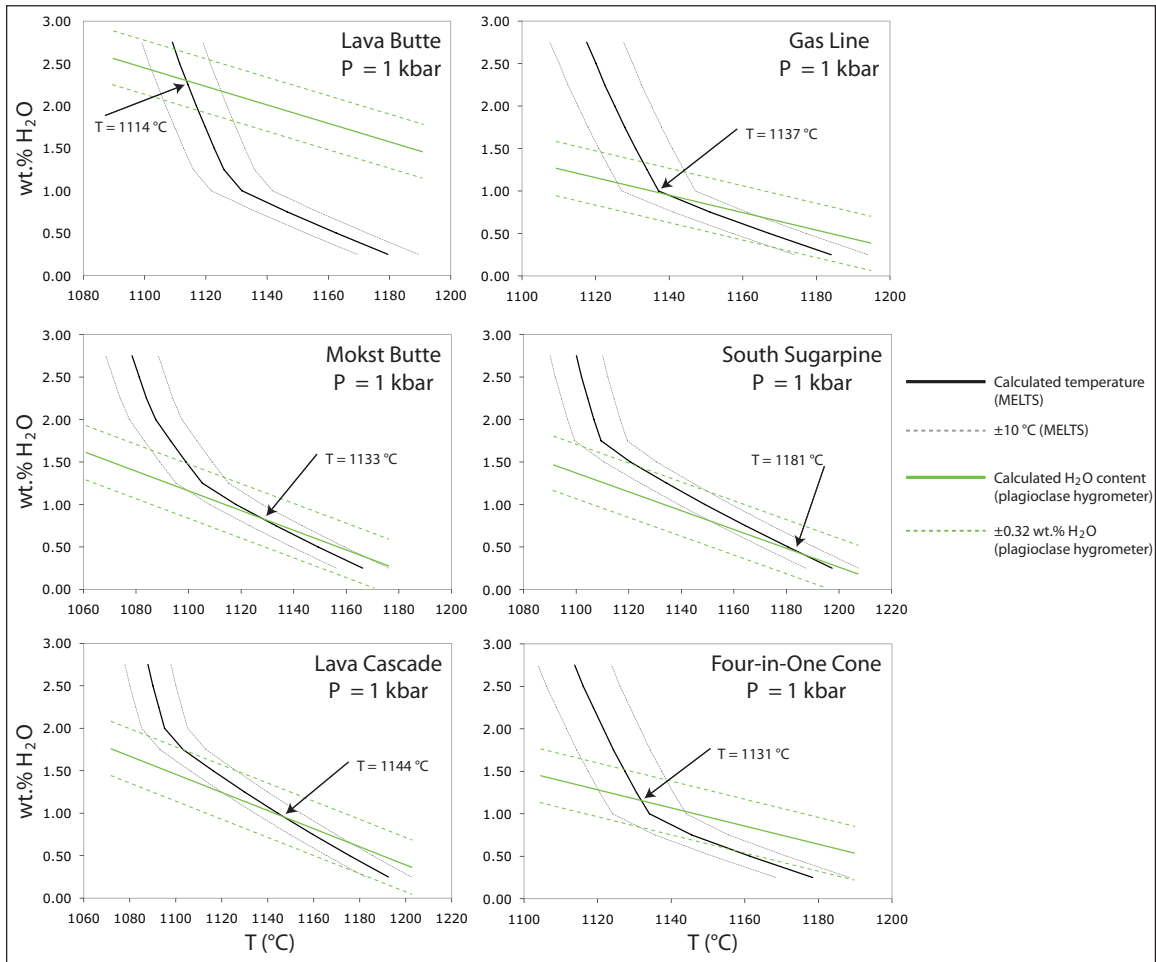


Figure 2.10. Calculated range of liquidus temperatures from MELTS (Ghiorso and Sack, 1995; Asimow and Ghiorso, 1998) and modeled H₂O contents from the plagioclase-liquid hygrometer (Lange et al., 2009) for NWRZ vents and Four-in-One Cone in the central Oregon Cascades.

experimentally derived phase diagram for a mafic arc magma of similar composition to Four-in-One Cone (Figure 2.12) predicts that at the calculated magma temperature (1131 °C) and at H₂O contents of ~3 wt.%, olivine crystallization occurs at ~1 kbar and plagioclase crystallization begins at lower pressures (~0.75 kbar) and at lower H₂O contents (starting at ~2.5 wt.% and continuing as late-stage degassing occurs). These H₂O values are consistent with both the values measured from olivine-hosted melt inclusions

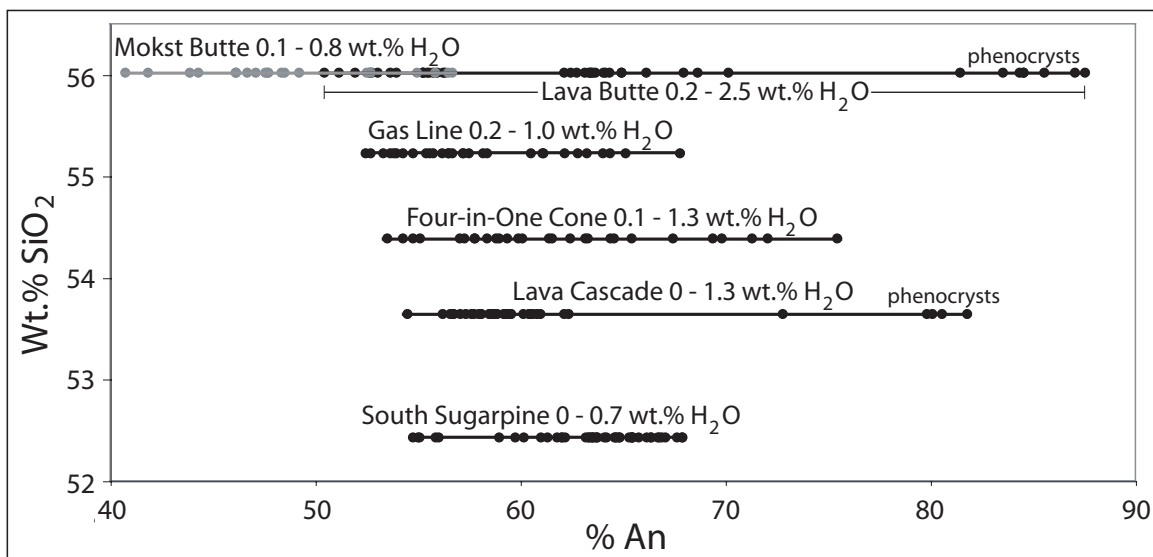


Figure 2.11. H₂O contents calculated from plagioclase and average glass compositions from NWRZ and Four-in-One Cone tephra. Each point represents analysis for a single plagioclase crystal. H₂O calculations were made using a single temperature estimate for each vent, shown in Figure 2.10.

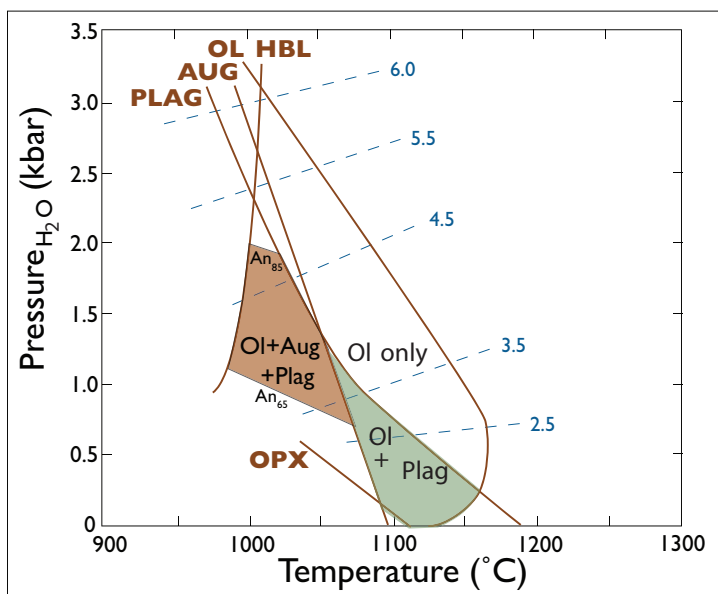


Figure 2.12. Experimentally derived phase diagram for a mafic arc magma of similar composition to Four-in-One Cone (after Moore et al., 1998). Phase relationships predict that at the calculated magma temperature for Four-in-One Cone (1131 °C) and at H₂O contents of ~3 wt.% (Ruscitto, 2011), olivine crystallization occurs at ~1 kbar; plagioclase crystallization begins at lower pressures (~0.75 kbar) and lower H₂O contents (starting at ~2.5 wt.% and continuing as late-stage degassing occurs).

and the values modeled by a combination of MELTS and the plagioclase-liquid

hygrometer. Thus, H₂O contents calculated for NWRZ vents are assumed to represent

minimum magmatic H₂O contents. This application of the plagioclase-liquid hygrometer provides a useful way to estimate minimum H₂O contents for vents where tephra clasts contain insufficient phenocrysts (particularly olivine) for melt inclusion analysis.

To calculate H₂O contents for the complete observed range of plagioclase phenocrysts and microphenocrysts, the plagioclase-liquid hygrometer was used with average glass compositions for each vent (Table 2.4), individual measured plagioclase compositions (Table 2.3), and temperature values determined by the intersection of the modeled temperature - H₂O curves (Figure 2.10). Pre-eruptive NWRZ H₂O contents as recorded by plagioclase range from 0 to 2.5 wt.% (Figure 2.11). The estimates for Lava Butte extend to the highest H₂O contents (2.5 wt.%), followed by Lava Cascade and Gas Line tephra (1.3 and 1.0 wt.% respectively). Mokst Butte and South Sugarpine tephra record the lowest H₂O contents (0.7 and 0.8 wt.% respectively). The highest H₂O values are recorded by plagioclase phenocrysts; microphenocrysts record H₂O contents as low as 0 wt.%, suggesting that at each vent late-stage degassing and plagioclase crystallization occurred just prior to eruption. This is consistent with the experimentally derived phase diagram from Moore et al. (1998; Figure 2.12). By comparison with data from Ruscitto et al., 2010, H₂O contents \geq 1-2.5 wt.% suggest that NWRZ magmas are subduction-related, supporting the interpretation of Newberry as a rear-arc Cascade volcano (e.g. Carlson et al., 2008; Donnelly-Nolan, 2008; Donnelly-Nolan et al., 2008; Donnelly-Nolan, 2009; Graham et al., 2009; Grove et al., 2009; Rowe et al., 2009; Donnelly-Nolan, 2010).

2.5.2. Geochemical Evolution of NWRZ Magmas

The range in chemical compositions of NWRZ vents, along with the spatial distribution of vents, suggests an eruptive history that is more complex than a single batch of magma ascending directly from a mantle source. The range in erupted lavas from basalt to andesite indicates that either fractional crystallization or assimilation of crustal material occurred prior to the NWRZ eruption. Similar compositional ranges have been observed at other mafic vents, notably at the Giant Crater Lava Field and the Callahan lava flows at Medicine Lake Volcano, California (e.g. Donnelly-Nolan, 1991; Kinzler et al., 2000), to which Newberry Volcano has often been compared (e.g. Donnelly-Nolan, 2008; Donnelly-Nolan et al., 2008), and at Paricutin, Mexico (e.g. Wilcox, 1954; McBirney et al., 1987; Erlund et al., 2009). Chemical variations in the Giant Crater and Callahan lavas are interpreted to result from both fractional crystallization and assimilation of crustal material (Donnelly-Nolan, 1991; Kinzler et al., 2000), as are variations in lavas from Phase 3 (mid-1947) of the Paricutin eruption (Wilcox, 1954; McBirney et al., 1987).

The compositional effects of fractional crystallization and crustal assimilation can be distinguished using relations between K_2O and TiO_2 , which show positive correlation with fractional crystallization and negative correlation with assimilation of a high K_2O - low TiO_2 crustal contaminant (Luhr, 2001; Erlund et al., 2009). NWRZ compositions show a negative correlation between K_2O and TiO_2 (Figure 2.13), suggesting that crustal assimilation, rather than simple fractionation of a parent magma, could explain much of the chemical variation between NWRZ vents. Intriguingly, the NWRZ compositions define two separate K_2O - TiO_2 trends in Figure 2.13. The geographical distribution of

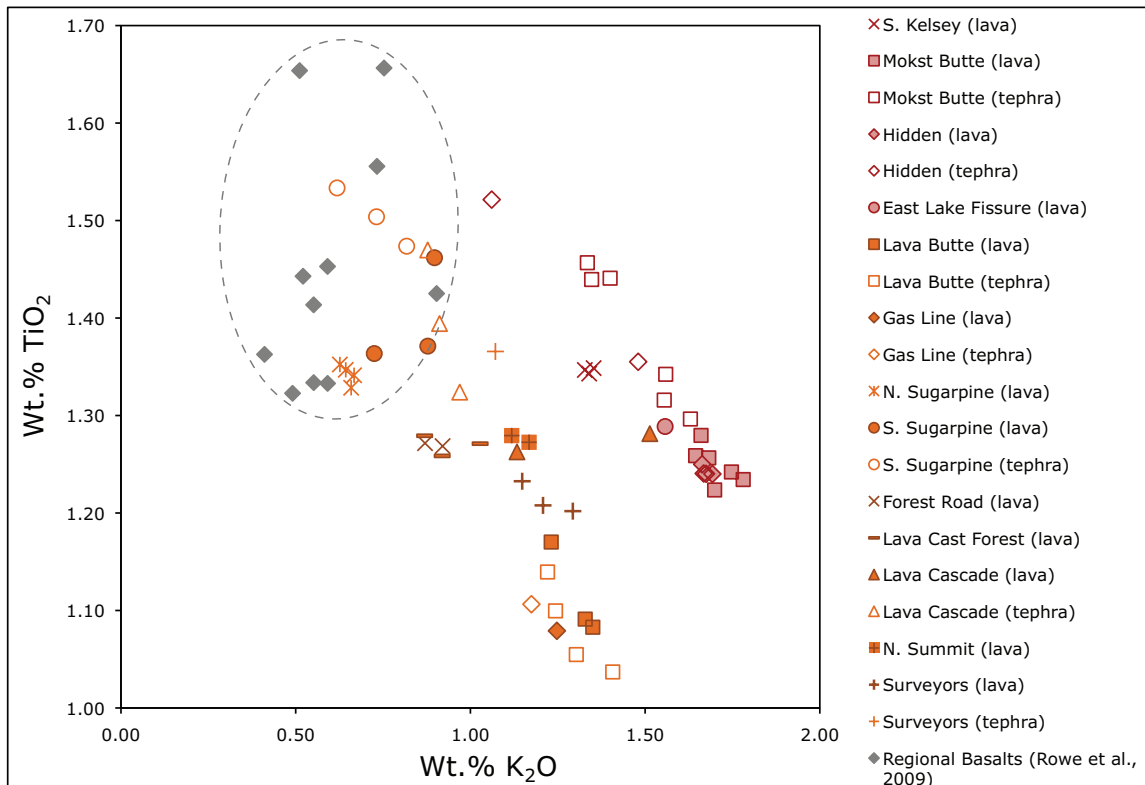


Figure 2.13. TiO₂ and K₂O contents of bulk NWRZ lava (McKay et al., 2009) and tephra (Table 2.2). Trend 1 vents are shown with orange symbols and Trend 2 vents with red symbols. Regional basalts (Rowe et al., 2009) are shown with gray symbols.

these trends is shown in Figure 2.2. Interestingly, the two trends do not conform to the north and south groups identified by paleomagnetic data (McKay et al., 2009), but instead appear to lie on several different parallel fissure systems (Figure 2.2). Most of the NWRZ vents plot along Trend 1 (Figures 2.2 and 2.13), but the South Kelsey, Mokst Butte, Hidden, and East Lake Fissure vents all plot along Trend 2 (Figures 2.2 and 2.13). With the exception of the South Kelsey vent, these vents are all aligned along the same fissure system, which begins in the north caldera wall at the East Lake Fissure vent and extends to the Mokst Butte vent (Figure 2.2). Here I explore possible reasons for this spatial distribution of chemically distinct lavas by modeling crustal assimilation by a primitive NWRZ parent magma. The original parent magma was likely similar in composition to

NWRZ parent magma. The original parent magma was likely similar in composition to the lavas of North and South Sugarpine vents, which represent the most primitive endmembers of NWRZ magmas and have compositions similar to other regional primitive basalts (Rowe et al., 2009; Figure 2.13).

To model crustal assimilation, I use observed trends of increasing K_2O/P_2O_5 (both incompatible elements) with decreasing MgO (Figure 2.14). Likely sources of contamination are intrusions below the summit caldera of Newberry Volcano, which may have compositions that range from basalt to rhyolite (e.g. Fitterman, 1988). Intermediate and silicic lavas and tuffs exposed at the surface of Newberry can be used as proxies for these intrusions. Chemical compositions of several exposed lavas are documented in the literature; these include the ca. 7000 yr B.P. (but pre-NWRZ) Interlake and Central Pumice Cone obsidian flows exposed in the caldera (Episode 3 from MacLeod and Sherrod, 1988), the ca. 8000 to ca. 10,000 yr B.P. South obsidian flow also exposed in the caldera (MacLeod and Sherrod, 1988), the ca. 75 ka Tuff of Paulina Creek Falls exposed on the west flank (Jensen et al., 2009; Donnelly-Nolan et al., 2010), the ca. 83 ka rhyolite of Paulina Peak exposed on the summit (Jensen et al., 2009), and the ca. 300 ka Tuff of Tepee Draw and Tuff of Brooks Draw, both exposed on the east flank (Jensen et al., 2009). For the mixing calculations shown in Figure 2.14, these compositions are used as proxies for intrusions below the summit of the caldera; the highest MgO composition of North Sugarpine lava is used as the mafic endmember.

To account for the observed range of NWRZ magma compositions through contamination, more than one crustal contaminant is required. For example, assimilation curves shown in Figure 2.14 require $\leq \sim 33\%$ assimilation of material similar to Holocene

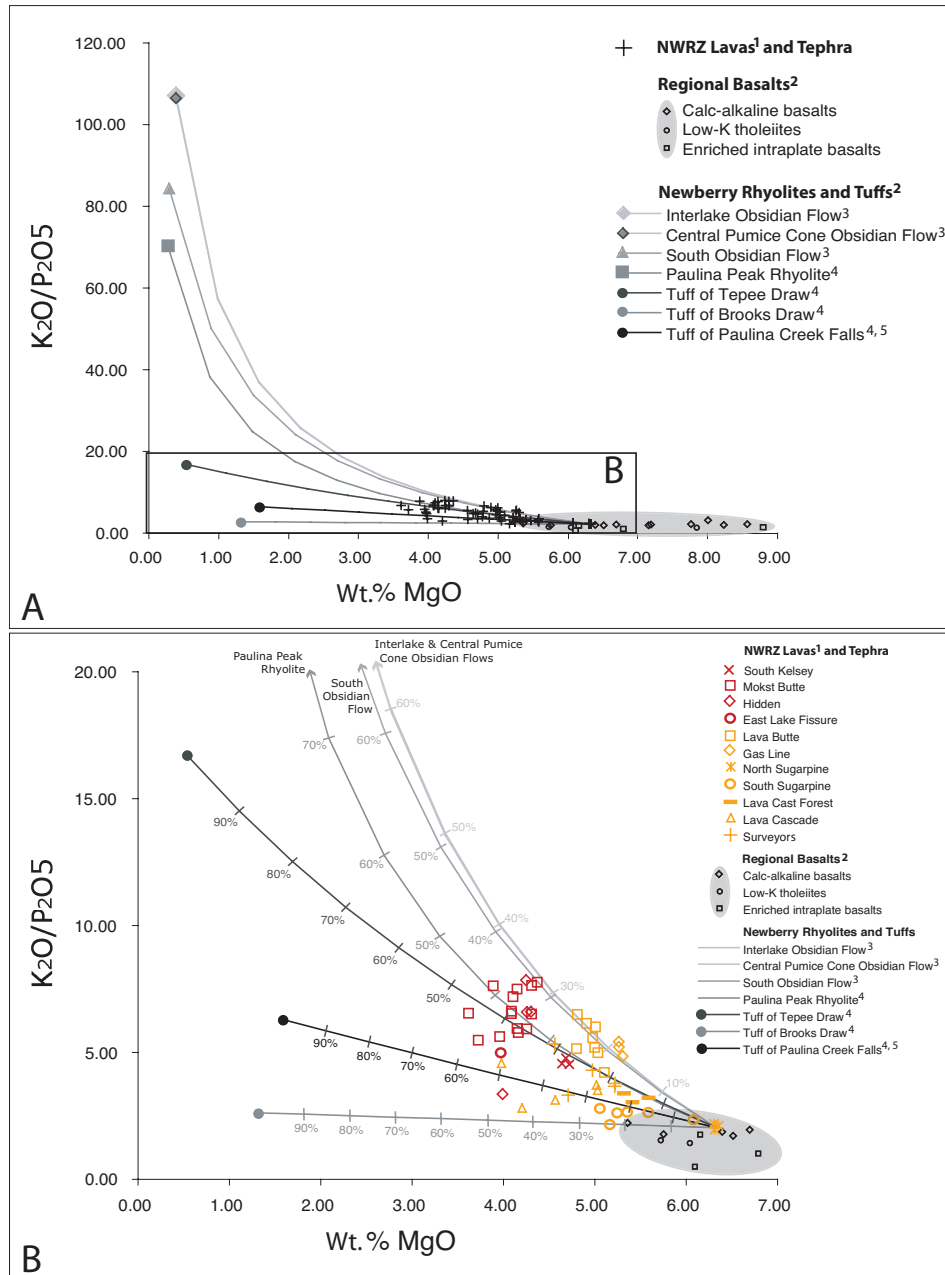


Figure 2.14. Modeled assimilation trends for NWRZ parent lavas and crustal contaminants. (A) shows regional basalts (open symbols in shaded region), which are likely similar to the original parent magma that fed NWRZ vents. The increasing K_2O/P_2O_5 with decreasing MgO trend of NWRZ lavas and tephra are shown as cross symbols. Intermediate and silicic lavas exposed at the surface of Newberry are shown in closed symbols. Assimilation curves between parent magma and intermediate to silicic crustal material are shown as shaded lines. Inset (B) shows detailed assimilation curves and compositional data for individual NWRZ vents. Trend 1 vents are shown with orange symbols and Trend 2 vents with red symbols. Data are from this study and from: ¹McKay et al. (2009), ²Rowe et al. (2009), ³MacLeod and Sherrod, (1988), ⁴Jensen et al. (2009) and ⁵Donnelly-Nolan et al. (2010).

intracaldera obsidians, $\leq \sim 41\%$ assimilation of material similar to the rhyolite of Paulina Peak, $\leq \sim 45\%$ assimilation of material similar to the Tuff of Tepee Draw, $\leq \sim 50\%$ assimilation of material similar to the Tuff of Paulina Creek Falls, and $\leq \sim 42\%$ assimilation of material similar to the Tuff of Brooks Draw. Most of the NWRZ vents cluster along the assimilation trends defined by the Tuff of Tepee Draw, the Paulina Peak rhyolite, and the intracaldera obsidians, suggesting that intrusions with similar compositions are the most likely sources of contamination.

2.5.3. Geophysical Evidence for Magma Storage and Assimilation

Geophysical evidence for an intrusive zone and at least one magma reservoir suggests that a complex magma storage network currently exists below the summit caldera of Newberry Volcano (e.g. Achauer et al., 1988; Fitterman, 1988; Beachly, 2011). Geologic evidence shows that the volcano has been fed by episodic inputs of mafic magma throughout its history (e.g. Fitterman, 1988; Linneman and Myers, 1990). Moreover, evidence for silicic eruptions within a few hundred years of the NWRZ eruption (Episode 3; MacLeod and Sherrod, 1988) indicates that an active magma storage area existed in the summit region just prior to NWRZ activity. A complex magma storage network below the volcano is consistent with the model presented here for crustal assimilation, as it explains both the geochemical evolution of NWRZ lavas and the spatial distribution of vents.

I envision a scenario similar to that described in Fitterman (1988), where mafic magma ascends to the shallow crust, either as a single large batch or as several smaller batches, and then stalls beneath silicic magma that has accumulated immediately below

the caldera (Figure 2.15). Formation of a network of pods, dikes, and sills at a depth of ~2.5 to 7 km (Fitterman, 1988; Beachly, 2011) would allow the mafic magma to come into contact with previous intrusions of intermediate to silicic compositions and possibly with a magma reservoir. In fact, the large amounts of contamination indicated by Figure 2.14 may require mafic magma to have come into direct contact with intrusions that were still hot, or even with supersolidus magma. The magma reservoir that fed Episode 3 vents (the Central Pumice Cone and Interlake obsidian flows; MacLeod and Sherrod, 1988) is a good candidate for contamination. The degree of assimilation that occurred prior to the eruption of any given NWRZ magma batch would then depend on the relative volumes, temperatures, and duration of contact of the original parent magma and the intrusions. Previous work by Linneman and Myers (1990) suggests that up to 30% assimilation of basaltic andesite by liquid rhyolite could account for mafic inclusions in the 1300 yr B.P. intracaldera Big Obsidian Flow. Estimates of up to 33% assimilation of material similar in composition to the Central Pumice Cone and Interlake obsidian flows by NWRZ parent magma (Figure 2.14) are consistent with this estimate.

Eruption from the shallow crustal storage areas as shown in Figure 2.15 probably requires a triggering event such as a new influx of mafic magma or a tectonic event. The width of the active zone during the NWRZ eruptive event suggests that faulted and fractured strata along regional fault zones likely distributed magma along several broad vertical planes trending NW across both the north and west flanks of the volcano (Trends 1 and 2, Figure 2.2). Additionally, it seems likely that the NWRZ eruption occurred in response to the same triggering event that initiated eruptions from a highly evolved magma reservoir that fed the silicic vents of Episode 3 (the Central Pumice Cone and

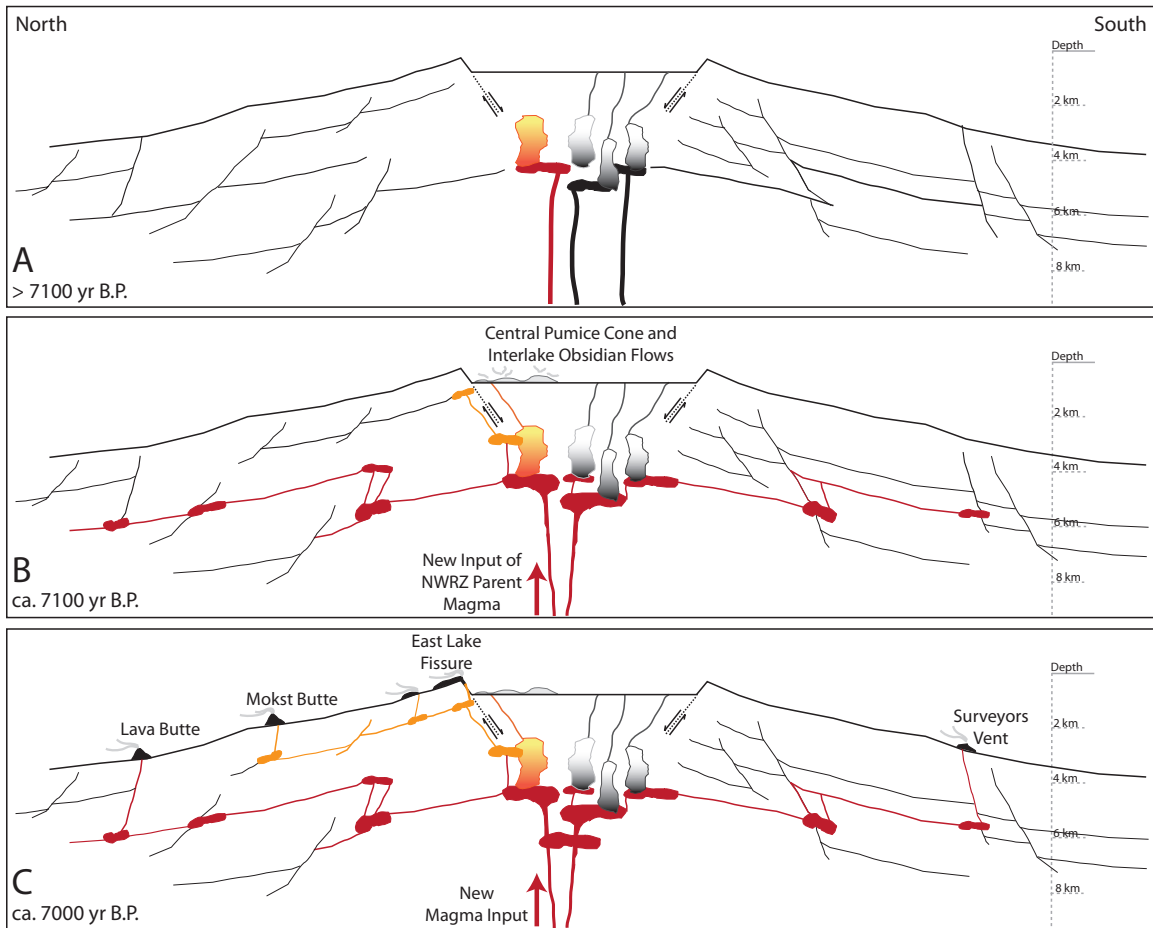


Figure 2.15. Schematic cartoons illustrating the inferred magma storage network below Newberry Volcano. (A) shows a simplified version of the pre-NWRZ intrusive complex below the caldera (after Fitterman, 1988). Gray shaded bodies represent solidified intrusions of various compositions; the orange shaded body represents a highly evolved liquid magma reservoir. The depth of the intrusive complex is estimated after Fitterman, (1988) and Beachly (2011). Black lines represent faulted strata below the volcano (e.g. Higgins, 1973; MacLeod and Sherrod, 1988). (B) Input of mafic NWRZ parent magma, which may have triggered the eruption of the ca. 7100 yr B.P. Central Pumice Cone and Interlake obsidian flows (Episode 3; MacLeod and Sherrod, 1988). In this scenario, most of the magma either stalled beneath the intrusive complex or migrated along faulted strata below the volcano, where it formed a complex network of dikes, sills and pods shown in red. Some of the magma may have migrated up along ring fractures associated with the north caldera wall, where it formed a storage network that could interact with several different intrusions and with the supersolidus magma reservoir that fed vents of Episode 3. This more highly contaminated magma storage network is shown in orange. (C) A second magma input triggers the ca. 7000 yr B.P. NWRZ eruption. Vents of Trend 1 were fed by the more extensive storage network shown in red; vents of Trend 2 by the more highly contaminated storage network shown in orange.

Interlake obsidian flows; MacLeod and Sherrod, 1988). This inferred linkage is supported by the close temporal association of the two eruptive episodes and by the assimilation trends in Figure 2.14, which show compositions similar to the Interlake and Central Pumice Cone obsidians as likely crustal contaminants for NWRZ lavas.

The two K_2O - TiO_2 trends in Figure 2.13 suggest that varying degrees of assimilation could explain the range in chemistry at NWRZ vents. Additionally, the spatial distribution of vents defining Trend 1 and 2 (Figure 2.2) suggests these vents may have been supplied from different storage regions. Lavas and tephra from the vents of Trend 2 (Figure 2.13) show the highest degrees of assimilation in Figure 2.14, suggesting that storage regions supplying these vents interacted longer, or with more crustal contaminants, than storage regions supplying vents of Trend 1. This can be interpreted as evidence that the storage network for Trend 2 vents was located directly below the caldera, where interaction could occur with several different intrusions as well as the silicic magma reservoir that fed Episode 3 (Figure 2.15). This is consistent with the spatial distribution of Trend 2 vents, which are directly aligned with the East Lake Fissure vent. The East Lake Fissure cuts through the entire exposed section of the north caldera wall (Figure 2.2), suggesting that magma feeding this vent came from a shallow storage system below the caldera, migrated up along ring fractures associated with the north caldera wall, then was directed northwest along regional fault systems. Magma from other nearby storage areas below the caldera could have followed this same path, but traveled farther to the northwest along the same fault system. Intriguingly, all of the Trend 2 vents are located on the east side of the NWRZ (Figure 2.2), suggesting that although there are a number of parallel fault systems trending northwest across the flanks

of the volcano, magma supplying the Trend 2 vents only migrated along the eastern fault systems.

In contrast to Trend 2 vents, lavas and tephra of Trend 1 (Figure 2.13) show less assimilation (Figure 2.14), suggesting that the storage regions supplying these vents interacted for less time, or with fewer crustal contaminants, than storage regions supplying vents of Trend 2. This can be interpreted as evidence that the storage networks supplying Trend 1 vents may have been located farther away from the central intrusive complex and interacted with fewer contaminants (Figure 2.15). The intrusive zone may have acted as a physical barrier by preventing most of the original input of mafic magma from rising vertically. A limited network of storage regions was apparently established directly below the caldera and later fed Trend 2 vents, but most of the original input of mafic magma was forced up around the edges of the intrusive zone and stored along shallow northwest and southwest trending fault zones (Figure 2.15). A complex network of faulted strata below the volcano would allow for this distribution of shallow magma storage areas (e.g. MacLeod and Sherrod, 1988; Higgins, 1973). Different contamination histories for Trend 1 and 2 vents based on spatial distribution of magma storage areas as shown in Figure 2.15 could explain the chemical range of NWRZ vents. This interpretation also suggests that shallow crustal storage networks extended over a broad area below the volcano.

2.5.4. Interpretation of Eruption Styles

The pyroclastic deposits produced by NWRZ vents indicate that eruptive activity ranged from hawaiian, to low-energy strombolian, to energetic strombolian and violent

strombolian activity. These interpretations are made based on the eruptive products of individual vents, the physical characteristics of tephra clasts, and interpretations of various mafic eruption styles from the literature (e.g. Walker, 1973; McGetchin et al., 1974; Heiken, 1978; Parfitt, 1998; Arrighi et al., 2001; Parfitt, 2004; Francis and Oppenheimer, 2004; Pioli et al., 2008; Valentine and Gregg, 2008).

The Lava Cascade vent can be used to represent NWRZ eruptions that occurred along fissure systems and produced spatter ramparts, lava flows, and limited tephra blankets. These characteristics are typically associated with hawaiian activity. Detailed analyses of the Lava Cascade tephra support this classification. The mean clast size (M_d) and sorting coefficients (σ_s) for each layer in the deposit are similar to those of hawaiian eruptions (Figure 2.5). Inefficient fragmentation during hawaiian activity not only produces large clasts, but also a wide range in clast sizes, resulting in poorly sorted tephra deposits. Additionally, juvenile components of the Lava Cascade tephra consist entirely of glassy, highly vesicular, angular clasts with ragged edges, all indicative of fire-fountaining activity (e.g. Parfitt, 1998; Parfitt, 2004; Francis and Oppenheimer, 2004; Valentine and Gregg, 2008; Stovall et al., 2011). Together, the grain size distribution, sorting, and componentry of the Lava Cascade deposit are all consistent with tephra produced during bursts of fire-fountaining activity in what was otherwise an effusive hawaiian-style eruption.

The South Sugarpine vent represents NWRZ eruptions that produced small cinder cones and limited tephra deposits. Like the Lava Cascade tephra, the South Sugarpine tephra is composed entirely of sideromelane clasts. However, these clasts differ from those of the Lava Cascade deposit in they are smaller, smoother, and less angular. The

mean clast size (M_d) and sorting coefficients (σ) for each layer in the deposit are similar to those of Strombolian eruptions (Figure 2.5). Smaller grain sizes and well-sorted layers indicate that fragmentation was more efficient at South Sugarpine and that the eruption was more explosive. Construction of a small cinder cone, rather than spatter ramparts, indicates strombolian activity rather than hawaiian-style fire-fountaining (e.g. McGetchin et al., 1974; Francis and Oppenheimer, 2004; Parfitt, 2004; Valentine and Gregg, 2008). Limited stratification of the tephra blanket suggests there were slight variations in eruption intensity throughout tephra-producing phases of activity. Together, the vent morphology, grain size distribution, sorting, and juvenile componentry of the South Sugarpine deposit indicate that this vent was the result of low-energy strombolian activity.

Eruptions of the Lava Butte and Mokst Butte vents produced the largest cinder cones and tephra deposits. Detailed analyses of the Lava Butte tephra indicate that the eruption included both strombolian and brief phases of violent strombolian activity. These interpretations are made based on tephra characteristics and eruption styles described by Heiken (1978), Arrighi et al. (2001), Pioli et al. (2008), and Valentine and Gregg (2008). Alternating layers of lapilli and ash indicate that efficient fragmentation took place during rhythmic pulses of explosive activity (e.g. Pioli et al., 2008; Valentine and Gregg, 2008). The well-sorted layers of the deposit are indicative of fall deposits from well-developed eruption columns. Variations in stratigraphy and juvenile components of the Lava Butte tephra suggest there were three main phases of activity: Phase I was characterized by low magma flux and intermittent strombolian activity, which produced lapilli layers dominated by moderately vesicular tachylite clasts. Phase II

was characterized by high magma flux and pulsatory strombolian to violent strombolian explosions, which produced finely stratified layers of lapilli and ash dominated by increasing proportions of vesicular sideromelane clasts. Phase III was characterized by low magma flux and intermittent strombolian activity similar to Phase I, which produced lapilli layers dominated by tachylite clasts (Figures 2.4 and 2.7).

2.5.5. Controls on Explosive Mafic Eruptions

The mechanisms that control eruption styles during explosive mafic activity are poorly understood. To address this problem, I examine the variables that might have controlled eruption style during activity at the NWRZ (Table 2.5). These include SiO₂ content, estimated H₂O content, estimated temperature, and total eruptive volume.

NWRZ vents exhibit a range in chemical composition, minimum pre-eruptive H₂O contents (from plagioclase), and erupted volumes, making this an excellent location to examine the effects of each of these variables on the eruption style of individual vents.

Estimated temperatures do not show enough variation to affect eruption style.

Table 2.5. Physical controls on eruption style.

Vent	Eruption style	Total eruptive volume (10 ⁶ m ³)*	SiO ₂ (wt. %) [†]	H ₂ O (wt. %) [§]	Temp. (°C) [#]
Gas Line	Hawaiian	1.1	55.34	1.0	1137±30
Lava Cascade	Hawaiian	38.7	54.67	1.3	1144±26
South Sugarpine	Low-energy strombolian	101.6	52.68	0.7	1181±62
Lava Butte	High-energy strombolian	309.2	55.95	2.5	1114±98
Mokst Butte	High-energy strombolian	381.9	56.89	0.8	1133±88

*Eruptive volumes are from McKay et al. 2009. [†]SiO₂ contents are from bulk rock lava (McKay et al., 2009) and tephra (Table 2.2) XRF analyses. [§]H₂O contents are the maximum measured from the plagioclase-liquid hygrometer (Lange et al., 2009), shown in Figure 2.11.

[#]Magma temperatures are estimated from thermodynamic modeling in MELTS (Ghiorso and Sack, 1995; Asimow and Ghiorso, 1998), shown in Figure 2.10.

To address the problem of what controls eruption style, the ratio of fragmented material (cinder cone material and tephra blanket) to total erupted material is used as a measure of eruption intensity. Figure 2.16 shows that there is no correlation between either H₂O or SiO₂ content and the eruption intensity of NWRZ vents. However, there does appear to be a correlation between eruption intensity and total eruptive volume (Table 2.5). Lava Butte and Mokst Butte erupted total volumes several orders of magnitude larger than other NWRZ vents; these vents also produced the largest cinder cones and the greatest volumes of tephra (Table 2.1 and 2.5). The South Sugarpine vent erupted an intermediate total volume of material and produced a small cinder cone (Table 2.1 and 2.5). The Gas Line and Lava Cascade vents erupted small total volumes and produced spatter ramparts rather than cinder cones and relatively small tephra blankets (Table 2.1 and 2.5). Thus, although there is likely a minimum H₂O content required to generate highly explosive activity, it appears that eruptive volume (and, by inference, volumetric eruption rate; e.g., Pioli et al., 2009), rather than H₂O content, exerted the primary control on eruption styles of NWRZ vents. Small to intermediate volumes of lava that emerged along fissure systems were primarily effusive, with associated hawaiian-style activity along the fissure vents. The elongate geometry of the fissure systems suggests that they were not active for long enough to focus into a single vent (i.e. eruption durations of hours to days). Somewhat larger volumes of lava erupting from focused vents (e.g. South Sugarpine) generated low-energy strombolian activity that produced small cinder cones and associated small tephra blankets. The largest erupted volumes occurred at Lava Butte and Mokst Butte vents. Here the extent and volume of tephra produced, together with the patterns of grain size and componentry preserved in

the stratigraphy, are consistent with high-energy strombolian activity punctuated by short phases of violent strombolian activity. Violent strombolian activity, in turn, indicates mass eruption rates that are higher than those feeding strombolian activity (Pioli et al., 2009).

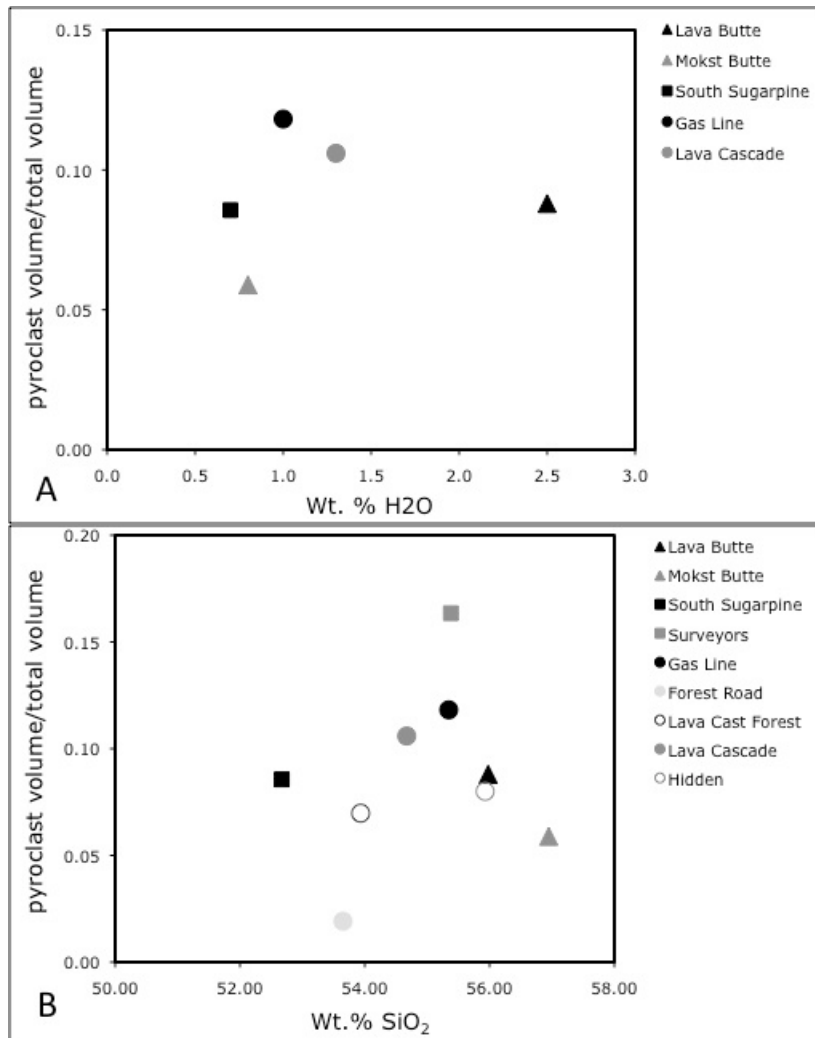


Figure 2.16. Relationships between eruption intensity, as measured by the ratio of fragmented material to total erupted material, and H₂O (A) and SiO₂ (B) contents. There is no correlation between eruption intensity and either H₂O or SiO₂.

The effects of inferred changes in mass eruption rate on eruption style are particularly well demonstrated by the eruption sequence at the Gas Line and Lava Butte vents. Here the magma composition (including H₂O content) remained constant

throughout the eruption. However, the eruption went through various stages of activity, from initiation along a fissure that produced spatter ramparts and the small Gas Line lava flows to focused activity at the Lava Butte vent that produced a large cinder cone and a relatively large tephra deposit. It appears that the transition in geometry from an elongate fissure to a focused scoria cone increased the magma effusion rate, which in turn increased the fragmentation efficiency of the eruption. The volume of magma erupted at the Lava Butte vent may have also played a role in eruption style. It has been suggested that violent strombolian eruptions require the development of a complete scoria cone, which promotes gas segregation in the conduit and, in turn, highly efficient fragmentation and sustained eruption columns (Pioli et al., 2009). Since the erupted volume at Lava Butte (and also at Mokst Butte) was sufficiently large, the eruption duration was long enough to allow for the formation of a complete scoria cone, which may have initiated gas segregation and contributed to brief phases of violent strombolian activity.

2.5.6. Implications for Hazards

The close proximity of Newberry Volcano to developed areas, particularly the city of Bend, Oregon (Figure 2.1), means that future mafic activity poses significant hazards to regional transportation, infrastructure, agriculture, and public health. Despite the abundance of past mafic activity at Newberry, hazards posed by this type of eruption to nearby central Oregon communities have not been fully addressed. From this perspective, it is important to note that the NWRZ eruptive episode appears to have lasted for at least decades and that eruption styles varied considerably from vent to vent, producing extensive lava flows and multiple tephra blankets. Lava flows covered areas

that are now transected by major railroad, power, and gas lines, one major highway, and multiple housing developments. Flows from the Lava Butte vent dammed the Deschutes River in several locations (Jensen et al., 2009), causing long-term flooding upstream (Jensen, 2006) and possible catastrophic flooding downstream. If such an eruptive episode were to occur today, lava flows could cause extensive damage to central Oregon communities and tephra production could pose even broader hazards if winds were blowing toward developed areas.

Geochemical evidence for a shallow magma storage system below Newberry Volcano has additional implications for hazards. Rather than one eruption focused spatially and temporally at a main vent, magmas of the NWRZ were distributed among multiple vents scattered across a large area. Recent mapping and paleomagnetic work on older mafic lava flows at Newberry Volcano indicate that past eruptive episodes have also involved multiple vents (Jensen et al., 2009; McKay et al., 2009; Donnelly-Nolan et al., 2010). In fact, it appears that multi-vent eruptive episodes have also occurred along the main axis of the central Oregon Cascades, where there are hundreds of recent mafic vents that are similar to Newberry vents in that they follow regional fault systems and have erupted a range of chemical compositions (e.g. Wells, 1990; Priest, 1990; Taylor, 1990; Scott and Gardner, 1992; Conrey et al., 2000). Current deformation in the Three Sisters region has been interpreted as evidence of a shallow magmatic intrusion along this section of the Cascades (Wicks et al., 2002; Dzurisin et al., 2006; Dzurisin et al., 2009). The intrusion appears to have stalled in the shallow crust (Riddick, 2011), but additional inputs of magma into this region could trigger an eruptive episode similar to the NWRZ and other eruptive events that have taken place in the Cascades. Regional hazard

assessments need to address the possibility that shallow mafic storage systems can develop over time and eventually produce long-lived (decades to a century) multi-vent eruptions that occur over large spatial areas.

2.6. Conclusions

By focusing in detail on the tephra produced during the NWRZ eruption, I have: 1) estimated minimum H₂O contents for magmas erupted during the first phases of activity; 2) constrained the genetic relationship between magma batches erupted at different vents; and 3) shown that the eruption style at individual vents was strongly correlated to eruptive volume. Estimated minimum values of $\geq 1-2.5$ wt.% H₂O from plagioclase phenocrysts are consistent with the interpretation that Newberry magmas are subduction-related and that this is a rear-arc Cascade volcano (e.g. Carlson et al., 2008; Donnelly-Nolan, 2008; Donnelly-Nolan et al., 2008; Donnelly-Nolan, 2009; Graham et al., 2009; Grove et al., 2009; Rowe et al., 2009; Donnelly-Nolan, 2010). The crustal assimilation model presented here indicates that a complex network of shallow magma storage areas developed below the volcano and supplied chemically distinct magmas to vents scattered over a broad spatial area. Finally, the correlation between eruptive volume and eruption style indicates that at some mafic vents, the volume of eruptible magma might be a more important control on eruption style than chemical composition or magmatic H₂O content.

The formation of a complex storage system and subsequent eruption of chemically distinct magmas from multiple NWRZ vents demonstrates the complexity of mafic magma systems. Although activity along the NWRZ was essentially one eruptive

episode, it was not a simple eruption of a single batch of magma. Rather, an extensive network of small storage areas developed below the volcano and distributed magma to multiple vents scattered over a broad area. Past eruptions from multiple vents on the flanks of Newberry (Sherrod et al., 1997; Jensen et al., 2009; McKay et al., 2009; Donnelly-Nolan et al., 2010) and along the main axis of the central Oregon Cascades (e.g. Wells, 1990; Priest, 1990; Taylor, 1990; Scott and Gardner, 1992; Conrey et al., 2000) suggest that the development of shallow mafic storage systems and subsequent multi-vent eruptions is common in this section of the Cascades. This type of activity has significant implications in terms of hazards, especially in central Oregon where the population is expanding rapidly and there are hundreds of recent mafic vents in the region, suggesting that future activity is likely. If future mafic eruptions at Newberry Volcano occur from multiple vents scattered over a broad spatial area, impacts on regional transportation, infrastructure, agriculture, and public health would be severe. For this reason, it is important to specifically address multi-vent mafic activity in regional hazard assessments.

The correlation between eruptive volume and eruption style at individual vents also has implications in terms of hazards. During the NWRZ eruption, many of the vents produced small total eruptive volumes and were characterized by effusive activity, but a few vents (i.e. Lava Butte and Mokst Butte) were characterized by relatively large total eruptive volumes and by explosive activity. This suggests that even if the dominant activity during multi-vent eruptions is effusive, explosive activity can occur at some vents if eruptive volumes are large enough. Thus, from a hazards perspective, it is important to consider abrupt transitions from effusive to explosive behavior. Hazard

assessments for Newberry Volcano need to specifically address multi-vent activity spanning a range of eruptive styles, from effusive hawaiian-style activity to explosive strombolian and violent strombolian activity.

2.7. Bridge Between Chapter II and Chapter III

In Chapter II, I presented detailed textural characteristics, chemical compositions, and pre-eruptive magmatic H₂O contents of tephra from mafic vents of the northwest rift zone of Newberry Volcano. I used these data to infer eruption styles at individual vents and to show that activity at the northwest rift zone was not a simple monogenetic eruption. Rather, it appears that a complex network of shallow magma storage areas developed below the volcano and supplied chemically distinct magmas to vents scattered over a broad spatial area. These vents were characterized by a range in eruptive styles, which was likely controlled by the total eruptive volume at each vent. This work expands our understanding of explosive mafic activity in central Oregon and draws attention to the hazards that mafic eruptions pose to nearby communities.

In the next chapter, I expand my investigation of explosive mafic eruptions to three recent mafic vents in the central Oregon High Cascades. I present detailed maps of the tephra deposits from each of these vents, along with chemical compositions and detailed textural characteristics of the tephra. As in Chapter II, I use these data to infer eruption styles at each vent and to expand our understanding of recent mafic activity in central Oregon. In particular, I focus on estimating the extent of trace tephra deposits from mafic vents because even very small amounts of tephra deposition would pose significant hazards to the region.

CHAPTER III

PHYSICAL VOLCANOLOGY OF TEPHRA DEPOSITS FROM THREE RECENT CINDER CONE ERUPTIONS IN THE CENTRAL OREGON HIGH CASCADES

This chapter includes coauthored material with Dr. K.V. Cashman, Dr. P.J. Wallace, Dr. D.M. Ruscitto, and Dr. D.G. Gavin. The analytical work was performed entirely by me and the writing is entirely mine. Drs. Cashman, Wallace, and Gavin provided guidance during field and analytical work, as well as editorial assistance.

3.1. Introduction

Cinder cone eruptions are the most common type of volcanic activity on land and in many places they occur in clusters, resulting in cinder cone fields. These fields are usually dominated by extensive lava flows, thus it is often assumed that the eruptions were predominantly effusive and that tephra production was limited. This assumption persists in part because tephra preservation at cinder cones is often poor. Tephra deposits can be easily eroded or reworked by biotic activity, or covered by subsequent lava flows from the same vent or other vents within the field. Consequently, reconstructions of original tephra deposits can be extremely difficult, especially in areas that were once covered by very thin deposits. For these reasons, it is likely that at many cinder cone vents tephra production is often either underestimated or not accounted for at all. This is the case in the central Oregon Cascades, where there are hundreds of cinder cones but

few of the tephra deposits have been mapped, despite the fact that determining the volume and extent of these deposits is necessary for assessing eruptive histories and volcanic hazards.

Here I examine tephra deposits from three cinder cones in the central Oregon Cascades: Four-in-One Cone, Collier Cone, and Sand Mountain. Each of these vents produced at least one cinder cone, multiple lava flows, and tephra blankets that, prior to this study, had not been mapped. These vents were chosen because they are each young (≤ 3000 yr B.P.) and represent a range in cinder cone morphologies, which may be a reflection on eruption style. For each vent, I present isopach maps of the tephra deposit as preserved on dry land; for Collier Cone I estimate the extent of the trace deposit based on tephra preserved in lake sediments. Although trace deposits on land can be quickly removed by erosion or obscured by biotic activity, wet sediments preserve very thin (millimeters to centimeters) layers of tephra. I use the isopach maps to calculate volume estimates for each deposit and to compare differences between minimum estimates, based only on deposits ≥ 25 cm thick, and maximum estimates, which include deposits ≤ 25 cm. Additionally, I examine the physical characteristics of each tephra deposit, including stratigraphic changes in grain size, juvenile components, and microtextural characteristics. These, along with volume calculations, are used to interpret the eruption style at each vent.

This work shows that: 1) at least one recent cinder cone in the central Oregon Cascades (Sand Mountain) produced a surprisingly large volume of tephra; and 2) trace tephra deposits contribute significantly to the total volume of tephra, thus volume estimates that do not include trace deposits have the potential to be significantly

underestimated. As in Chapter II, this study focuses on tephra production because it represents the most explosive phases of activity and thus is an indicator of eruption style. Tephra production can also represent the most widespread hazard posed by cinder cones; even very small amounts of tephra (<1 cm) can impact transportation, agriculture, and public health. Thus, from a hazards perspective, it is important to determine the extent of tephra deposits produced by Cascade cinder cones. This work also has broader impacts for hazard assessments in cinder cone fields worldwide, where uncertainties in future vent positions, clustering of vents, and challenges in reconstructing tephra deposits due to poor preservation make hazard assessments difficult (e.g. Bebbington and Cronin, 2011).

3.2. Geologic Setting

The cinder cones in this study are located in the central Oregon High Cascades, which makes up the central section of the Cascade volcanic arc. Volcanism here is associated with the subduction of the Juan de Fuca plate beneath the North American plate. Although volcanism along much of the arc is focused at major central volcanoes, the dominant form of Holocene activity in the central section of the arc has been the production of large and small cinder cones (e.g. Sherrod and Smith, 1990; Sherrod et al., 2004; Hildreth, 2007). Regional extension in this region (e.g. Wells, 1990; Priest, 1990; Taylor, 1990; Conrey et al., 2000) has promoted the eruption of voluminous mafic lavas from vents aligned parallel to the axis of extension. Multi-vent eruptive episodes have occurred along these regional fault systems, forming extensive chains of shield volcanoes, cinder cones, and spatter vents that have erupted a range of chemical compositions (e.g. Wells, 1990; Priest, 1990; Taylor, 1990; Scott and Gardner, 1992;

Conrey et al., 2000; Deligne, 2012). The cinder cone vents in this study are all part of larger chains or clusters of vents representing some of the most recent mafic activity in the central section of the arc (≤ 3000 yr B.P.). Four-in-One Cone and Collier Cone are part of a cluster of vents that were active ≤ 2300 yr B.P. on the north flank of North Sister (Figure 3.1). The oldest vent in this cluster is Yapoah Crater, which sits stratigraphically above silicic tephra thought to be from the 2000-2300 yr B.P. Rock Mesa - Devil's Hill vents located ~ 15 km to the south (Sherrod et al., 2004). Although portions of the tephra deposit from Yapoah Crater were mapped as part of this study, the entire extent of the deposit was not determined. Radiocarbon ages indicate that the Yapoah Crater, Four-in-One Cone, and Collier Cone cluster of vents were active within several hundred years of each other (Sherrod et al., 2004). The Sand Mountain chain of vents are also part of a larger cluster, in this case a ~ 9 km chain of large and small cinder cones, spatter vents, and extensive lava flows. Like the Yapoah Crater, Four-in-One Cone, and Collier Cone cluster of vents, the Sand Mountain vents were likely active within several hundred years of each other (Deligne et al., 2012).

Future activity in this section of the Cascades is likely; current deformation in the Three Sisters region has been interpreted as evidence of a shallow magmatic intrusion (Wicks et al., 2002; Dzurisin et al., 2006; Dzurisin et al., 2009). The intrusion appears to have stalled in the shallow crust (Riddick, 2011), but additional inputs of magma into the region could trigger an eruptive episode. If magma inputs are mafic in composition, which seems likely based on the regional tectonic regime dominated by extensional fault systems, as well as the dominance of mafic activity throughout the Holocene, future eruptive episodes could produce new cinder cones similar to those described here.

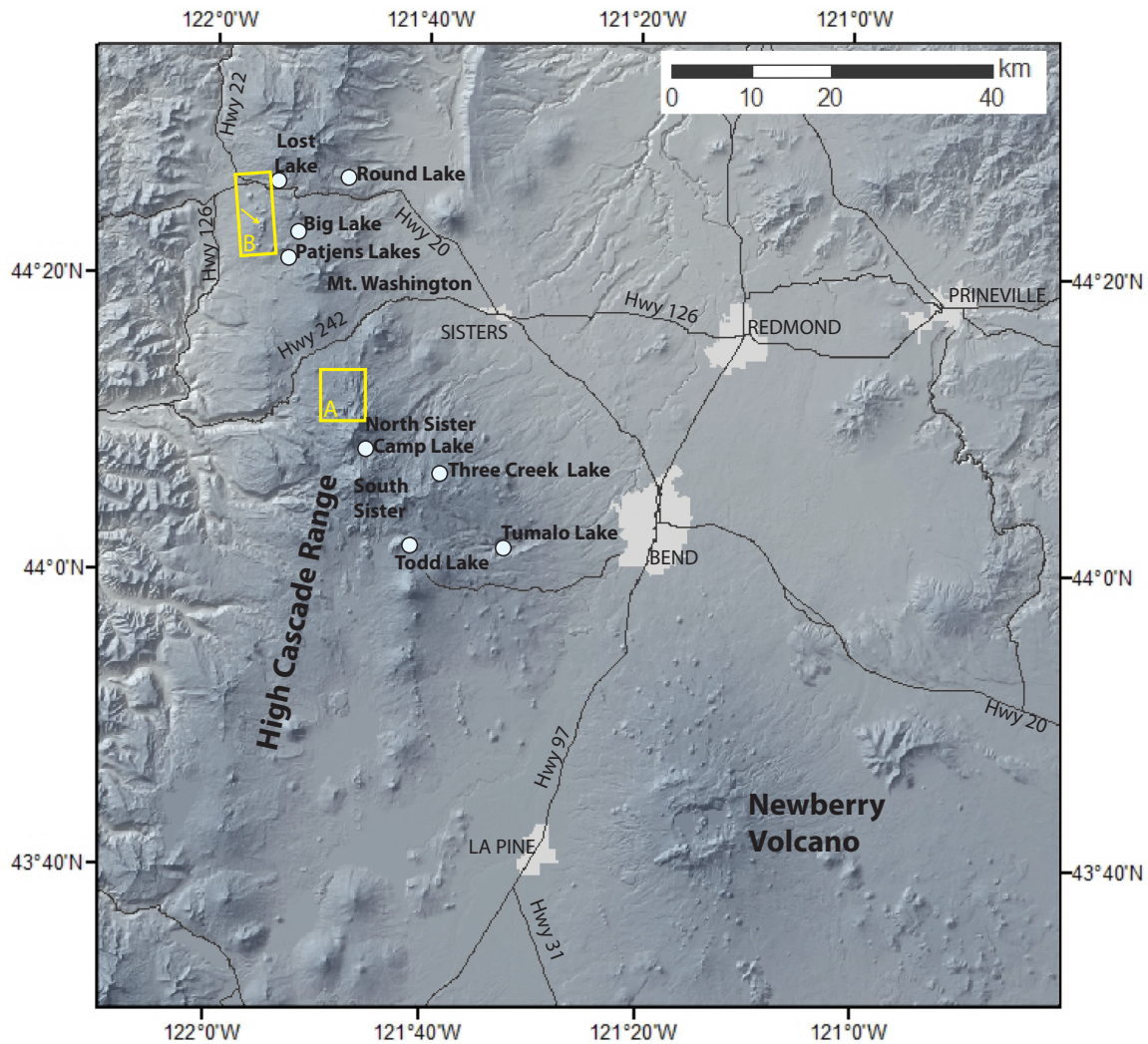


Figure 3.1. Map showing the location of the central Oregon High Cascades and densely populated areas. The Four-in-One Cone, Collier Cone, and Yapoah Crater cluster of vents are located in the yellow box marked A. The Sand Mountain volcanic chain is located in the yellow box marked B. The Sand Mountain vents discussed here are in the central section of the chain, indicated with a yellow arrow. Circles represent regional lakes that were cored as part of this and other studies. In addition to the cinder cones examined in this study, numerous cinder cone vents are scattered throughout this section of the High Cascades and on the flanks of Newberry Volcano (visible as small dots scattered throughout the region).

3.2.1. Four-in-One Cone

Four-in-One Cone is located ~6 km northwest of North Sister (Figure 3.1). The “cone” is actually a chain of overlapping cinder cones erupted from a fissure system trending N. 10° E. Four of the vents are located at Four-in-One Cone and two additional

vents are located ~1 km to the south (Sherrod et al., 2004). The length of the entire chain of vents is ~2 km and the section of overlapping cones that make up Four-in-One Cone is ~1 km long. The highest cone in the Four-in-One Cone complex, located at the south end of the overlapping vents, is ~68 m tall. Each of the cones are breached to the northwest by basaltic andesite (~56 wt% SiO₂) to andesite (58-59 wt% SiO₂) lava flows (Sherrod et al., 2004) that extend ~4 km from the vents. Large sections of cone material have been rafted to the northwest by these flows. The tephra blanket is well exposed to the east of the vents, where it lies stratigraphically above tephra and lava from Yapoah Crater. A radiocarbon age of 1980±160 ¹⁴C yr B.P. was obtained from charred needles and twigs in the lower 20 cm of the Four-in-One tephra deposit, ~300 m east of the vents (Scott, 1990; Sherrod et al., 2004).

3.2.2. Collier Cone

Collier Cone is located on the flank of North Sister (Figure 3.1) ~3 km northwest of the summit and ~3 km southeast of Four-in-One Cone. The cone is ~150 m high and is breached to the west by multiple flows of basaltic andesite, andesite, and dacite lava flows (Schick, 1994; Sherrod et al., 2004) that extend ~14 km to the west of the vent. The SiO₂ content of these flows ranges from 56 to 64 wt% (Schick, 1994; Sherrod et al., 2004; Deardorff, 2011). The lavas contain troctolite xenoliths that are interpreted to be mafic cumulates, as well as silicic xenoliths similar in composition to the Obsidian Cliffs, located ~4 km to the southwest of the vent (Schick, 1994). The southwest side of the cone is mantled by glacial till deposited during the late Neoglacial phase of ice advance (Sherrod et al., 2004). Tephra from Collier Cone is well exposed to the east of the vent,

where it lies stratigraphically above tephra from Yapoah Crater. Collier Cone lava flows surround and overlap the southern vents associated with Four-in-One Cone, as well as the southern portion of the Four-in-One Cone tephra deposit. A radiocarbon age of 1600 ± 100 ^{14}C yr B.P. was obtained from charcoal beneath Collier Cone tephra (Sherrod et al., 2004).

3.2.3. Sand Mountain

Sand Mountain is located ~9 km northwest of Mt. Washington and ~23 km northwest of Four-in-One and Collier Cones (Figure 3.1). The Sand Mountain alignment is a N 10° E trending chain of cinder cone and spatter vents ~9 km long. The chain consists of 41 distinct vents, 22 of which created cinder cones of various sizes (Taylor, 1965). The Sand Mountain cone is the largest cinder cone in the chain at ~230 m high. Basalt to basaltic andesite (51.6 to 53.2 wt% SiO_2) lava flows make up an extensive flow field to the west of Sand Mountain. These flows repeatedly interacted with the McKenzie River system and dammed the river in several locations (Deligne et al., 2012). New mapping of the Sand Mountain lava flow field constrains the age of the vents to ca. 3000 yr B.P. and paleomagnetic data indicate that activity spanned a century or less (Deligne et al., 2012). As at Four-in-One Cone and Collier Cone, the Sand Mountain tephra blanket is well exposed to the east of the vents.

3.3. Methods

3.3.1. Field Methods

Tephra thickness measurements were made in both proximal (<1 km from the vent) and distal (>1 km from the vent) sections of each deposit from hand-dug trenches, auger holes, and lake sediment cores. Measurements were made at 14 locations in the Four-in-One Cone deposit, 61 locations in the Collier Cone deposit, and 92 locations in the Sand Mountain deposit. Fewer measurements were made in the relatively small Four-in-One Cone deposit, while the larger Collier Cone and Sand Mountain deposits required more measurements to constrain the geographical extent of each deposit. Trenches were dug in flat, sparsely vegetated locations. At each location, the total depth of the deposit was noted and complete stratigraphic descriptions were made. Criteria used to identify individual stratigraphic units exposed in trenches include grain size, grading, sorting, color, apparent lithic content, loose crystals, and vesicularity. Complete stratigraphic samples were collected from locations where the stratigraphy was judged to be representative of the entire deposit, based on what was observed elsewhere. Auger holes were made in flat, sparsely vegetated locations where sediments were dry and also in meadows and fens where sediments were wet. At each auger location the total depth of the deposit was noted, stratigraphic descriptions were made, and in some cases samples were collected from different stratigraphic units. Criteria used to identify stratigraphic units in auger holes include distinct changes in grain size, color, apparent lithic content, and vesicularity. Lake sediments were recovered in 1-m drives using a 5-cm diameter Livingstone piston sampler (Wright et al., 1983) from a platform anchored in the deepest section of each lake. Sediments from lakes and fens not accessible by road were

recovered from shallow areas near the shore, rather than from a platform on the lake. In addition to collecting my own sediment cores, I also obtained samples of mafic tephra preserved in cores collected by other workers.

3.3.2. Sample Preparation and Analytical Methods

Each sample suite was dry sieved at one-phi intervals for grain size distribution measurements. Sample suites from Four-in-One Cone and Collier Cone were separated into three juvenile components that differ in vesicularity: 1) tan, highly vesicular scoria (sideromelane), 2) black, less vesicular scoria (tachylite), and 3) dense fragmented lava (e.g. Heiken, 1978; Valentine et al., 2005; Pioli et al., 2008). Componentry was determined for all grain size fractions from 0 to -5 ϕ (1 to 32 mm). Due to the small grain size of the Sand Mountain tephra ($>0 \phi$ for all but two layers), these samples were not separated into juvenile components. Petrographic thin sections were made from representative sideromelane and tachylite clasts from the bottom and top of each stratigraphic sequence. Thin sections were examined in backscattered imaging mode on a FEI Quanta 200 FEG Environmental SEM at the University of Oregon. The textural and chemical examinations presented here focus on the sideromelane component of each deposit because it is least affected by late-stage degassing and crystallization (e.g. Erlund et al., 2009). Bulk tephra analyses were performed on sideromelane clasts by X-ray fluorescence (XRF) for major elements and inductively coupled plasma mass spectrometry (ICP-MS) for trace elements at the GeoAnalytical Laboratory at Washington State University.

Tephra samples from lake sediments were collected from split cores and organic content was estimated by loss on ignition (Heiri et al., 2001). Samples for XRF and ICP-MS analyses were cleaned in an ultrasonic bath, dried, and sideromelane clasts were handpicked and sent to the GeoAnalytical Laboratory at Washington State University. The tephra layers preserved in lake sediments were correlated to source vents based on the thickness of each layer, stratigraphic position within the core, sedimentation rates in each lake, and chemical and physical characteristics of the tephra clasts.

Thickness measurements were used to create isopach maps, which in turn were used to calculate volume estimates using the fallout calculation of Pyle (1989) and assuming exponential decay of the thickness with distance. A plot of tephra thickness versus dispersal area ($A^{1/2}$) was used to integrate two straight-line segments to calculate volumes (Fierstein and Nathenson, 1992). In addition to estimating the volumes of each tephra deposit, volumes of cone material and lava flows produced by each vent were also estimated. Cone volumes were calculated based on the average height and radius of each cinder cone and on the average depth and radius of the summit crater, if present. Lava flow areas were measured using an image processing program (ImageJ; Abramoff et al., 2004); volumes were estimated based on an average flow thicknesses of 10 m. Dense rock equivalents (DRE) were calculated using values in McKnight and Williams (1997).

3.4. Results

The tephra deposits produced by Four-in-One Cone, Collier Cone, and Sand Mountain are strikingly different, both in the relative size of each deposit and in the physical characteristics of the tephra itself. Here I present isopach maps, detailed

stratigraphic descriptions, grain size distributions, relative abundance of juvenile components, microtextural characteristics, and bulk chemistry for each of the three deposits. Tephra layers preserved in regional lake sediments are also described and correlated to source vents based on physical and chemical characteristics. Isopach maps created from tephra thickness measurements are shown Figure 3.2. Volume estimates for each tephra deposit, cinder cone, and associated lava flows are listed in Table 3.1. Tephra volumes are estimated based on the areas covered by ≥ 25 cm of tephra (Figure 3.2) and do not account for portions of the deposits that were covered by subsequent lava flows or have since been eroded or reworked. Thus, the tephra volumes in Table 3.1 represent minimum estimates.

3.4.1. Isopach Maps

3.4.1.1. *Four-in-One Cone*

The Four-in-One Cone tephra deposit is the least extensive of the three, with an area of ~ 1.4 km² and a volume of ~ 0.002 km³ (Figure 3.2 and Table 3.1). In addition to producing the smallest tephra deposit, Four-in-One Cone also produced the smallest cinder cone, lava flows, and total eruptive volume (Table 3.1). The tephra deposit thins rapidly to < 10 cm ~ 1.5 km east of the vent area; to the west the deposit thins even more rapidly, suggesting that the eruption was short-lived and prevailing winds deposited most of the tephra to the east and southeast. Pockets of tephra cover proximal sections of the Four-in-One Cone lava flows to the northwest of the vents, indicating that some tephra production occurred after effusive activity. However, the individual cones that make up Four-in-One Cone are breached in the direction of the lava flows and large sections of

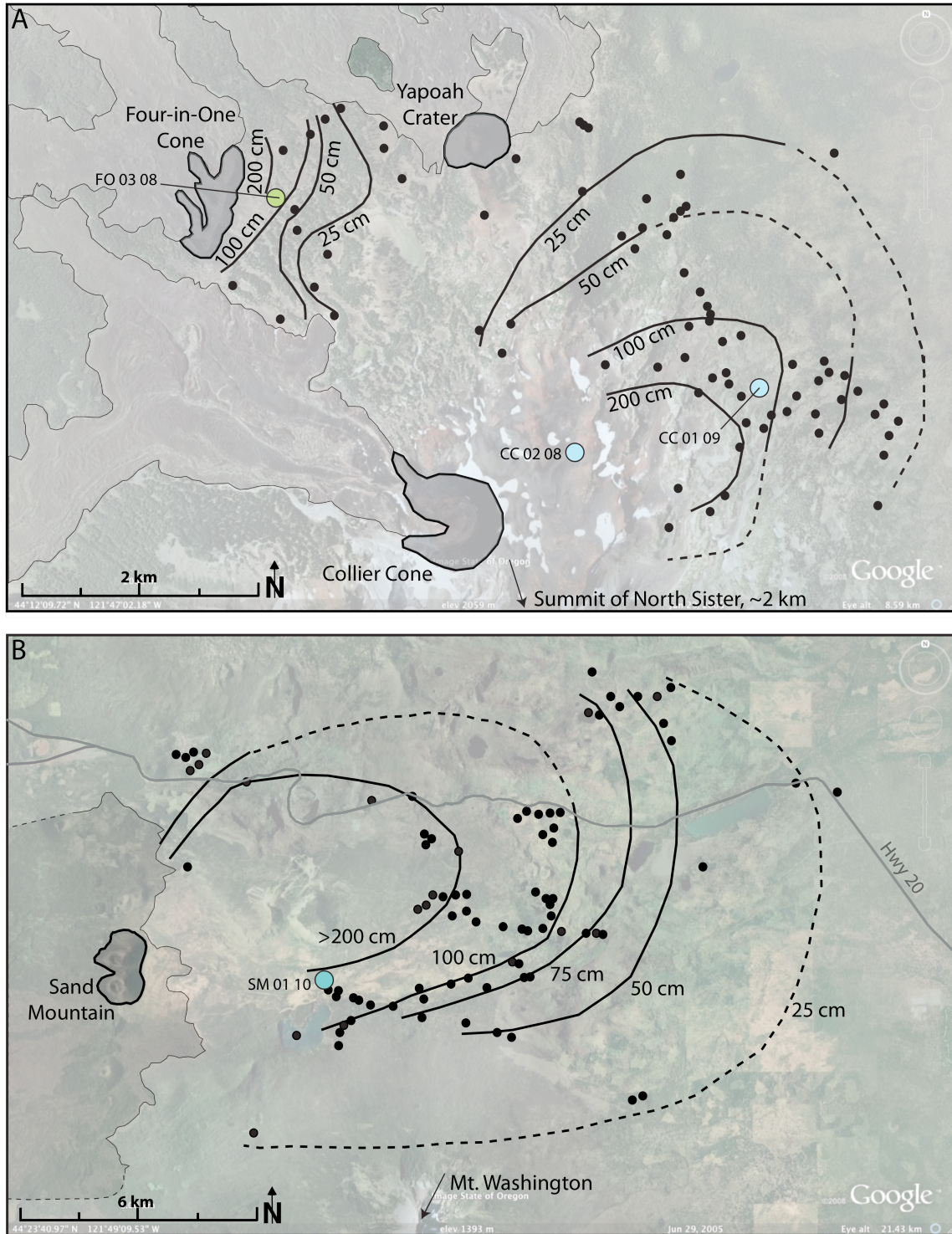


Figure 3.2. Isopach maps for the Four-in-One Cone (A), Collier Cone (A) and Sand Mountain (B) tephra deposits. Black circles represent locations where tephra thickness measurements were made, colored circles represents locations where the complete stratigraphy was described and sampled. Lava flows from each vent are outlined in thin black lines. Sand Mountain lava flows are after Deligne et al. (2012). Images are from Google Earth.

Table 3.1. Volumes of eruptive products.

Vent name	Tephra area (km ²)	Tephra (km ³)	Cinder cone (km ³)	Lava flows (km ³)	Total ¹ (km ³)
Four-in-One Cone	1.36	0.002	0.004	0.036	0.032
Collier Cone	14.73	0.037	0.024	0.154	0.154
Sand Mountain	153.87	0.387	0.043	0.259 ²	0.362

¹Total eruptive volumes are DRE equivalents calculated using values in McKnight and Williams (1997). ²Sand Mountain lava flow volume is from N.I. Deligne, personal communication.

rafted cone material are present in the flows. This indicates that the cones were rafted apart by lava during or after construction and that subsequent phases of explosive activity did not rebuild them. This along, with the limited amount of tephra on the lava flows, indicate that the most explosive phases of activity occurred prior to effusive activity.

3.4.1.2. Collier Cone

The Collier Cone tephra deposit covers an area of ~14.7 km² and has a volume of ~0.04 km³; both values are an order of magnitude larger than the Four-in-One Cone deposit (Figure 3.2 and Table 3.1). Collier Cone also produced a larger cinder cone, lava flows, and a greater total eruptive volume than Four-in-One Cone (Table 3.1). Like the Four-in-One Cone deposit, the Collier Cone deposit thins rapidly to the west of the vent, indicating that the eruption was short-lived and prevailing winds deposited most of the tephra to the northeast (Figure 3.2). However, glacial erosion during the Neoglacial phase of ice advance and lava flows to the south and west of the vent make it difficult to determine the extent of the deposit in those directions. Tephra deposits are present to the southeast of the cone, but the steep slopes of North Sister and glacial erosion have obscured the original extent of the tephra blanket in that direction. Unlike the Four-in-One Cone deposit, the Collier Cone deposit maintains a greater thickness over a much

larger area in the direction of dispersal, with >1 m of tephra occurring up to ~3 km northeast of the vent (Figure 3.2). Collier Cone is breached in the direction of the lava flows, indicating that it was rafted apart by lava during or after construction and that subsequent phases of explosive activity did not rebuild the cone. As at Four-in-One Cone, this indicates that the most explosive phases of activity occurred prior to the effusion of lava.

3.4.1.3. *Sand Mountain*

The Sand Mountain tephra deposit covers an area of ~154 km² and has a volume of ~0.39 km³; both values are an order of magnitude larger than the Collier Cone deposit and two orders of magnitude larger than the Four-in-One Cone deposit (Figure 3.2 and Table 3.1). Sand Mountain also produced substantially larger cinder cones, lava flows, and total eruptive volume than both Four-in-One Cone and Collier Cone (Table 3.1). The Sand Mountain deposit maintains a greater thickness over a much larger area than either of the other deposits, with ≥2 m of tephra occurring up to ~ 9 km from the vent and ≥1 m of tephra occurring ~12 km from the vent (Figure 3.2). Although the deposit is well-exposed to the east of the vents, to the west it is obscured by the extensive Sand Mountain lava flow field and the steep slopes and dense vegetation of the Western Cascades, making it very difficult to trace the extent of the tephra deposit in that direction. For this reason, the deposit was not mapped to the west of the vents and the tephra area and volume in Table 3.1 are likely significantly underestimated. The Sand Mountain cinder cones are not breached by lava flows, indicating that if rafting of the cones occurred at any time during the eruption, explosive phases of activity continued

either during or after the effusion of lava. Either scenario would result in rebuilding sections of the cones that had been rafted apart by lava flows.

3.4.2. Stratigraphy of the Tephra Deposits

In the following sections I describe the stratigraphy of the three deposits in detail. Representative stratigraphic columns, grain size distributions from each major layer of the deposits, and Inman Graphical Standard Deviation (IGSD) sorting coefficients (σ_s) and median grain sizes (Md_s) are given for each vent. In addition to stratigraphic descriptions of sample trenches dug in each tephra deposit, the stratigraphy of regional lake sediments (Figure 3.1) are also described in this section. Mafic tephra layers preserved in lake sediments are correlated to source vents based on stratigraphic position, lake sedimentation rates, and physical characteristics of the tephra clasts.

3.4.2.1. *Four-in-One Cone*

Tephra from Four-in-One Cone lies stratigraphically above the lava flow and a distinctive, crystal-rich tephra layer from Yapoah Crater (Figure 3.2). In various locations, Four-in-One Cone tephra also overlies an orange paleosol that contains discontinuous lenses of white ash interpreted to be from the Rock Mesa - Devil's Hill chain of vents (Sherrod et al., 2004). Complete stratigraphic samples were collected from a representative ~236 cm section of the proximal deposit (~0.5 km east of the vents) exposed in a stream channel (Figure 3.2). Here the deposit is dominated by massive, medium to coarse lapilli (≤ 32 mm) layers (Figure 3.3). The lower layer of the deposit is ~167 cm thick and is clast supported with little to no fine material present. Average clast

sizes range from 4-16 mm (Figure 3.3), with occasional larger clasts (16-64 mm) that are highly vesicular and glassy in appearance. This layer is well-sorted ($\sigma=1.55$) from the base of the deposit to ~79 cm depth, where it grades to poorly-sorted ($\sigma=2.37$) and average clast size increases to 8-32 mm (Figures 3.3 and 3.4). At ~69 cm depth there is an erosional contact that indicates fluvial incision into the basal layer (Figure 3.3). Above this contact, there is a ~25 cm thick, poorly-sorted ($\sigma=2.13$) lapilli layer with average clast sizes ranging from 4-16 mm and occasional larger clasts ≤ 32 mm (Figures 3.3 and 3.4). At ~44 cm depth this layer grades into a thin (~8 cm) well-sorted ($\sigma=1.63$) coarse ash layer with average clast sizes ranging from 0.25-1 mm and occasional lapilli clasts ≤ 16 mm (Figure 3.3 and 3.4). At ~36 cm depth this layer grades into the upper section of the deposit, which is a well-sorted ($\sigma=1.55$) lapilli layer with average clast sizes ranging from 4-16 mm and occasional larger clasts ≤ 32 mm (Figures 3.3 and 3.4). This upper layer contains weathered brown tephra and is penetrated by roots.

3.4.2.2. *Collier Cone*

The Collier Cone tephra lies stratigraphically above crystal-rich tephra from Yapoah Crater (Figure 3.2) and, in various locations, either glacial till or an orange paleosol that contains discontinuous lenses of white ash, again interpreted to be from the Rock Mesa - Devil's Hill chain of vents (Sherrod et al., 2004). Two representative stratigraphic sections of the Collier Cone deposit were exposed in trenches located ~1.1 km (CC-02-08) and ~2.75 km (CC-01-09) northeast of the vent (Figures 3.2 and 3.5). The first trench (CC-02-08) exposed ~200 cm of Collier Cone tephra but did not reach the base of the deposit. The second trench (CC-01-09) exposed ~120 cm of tephra and did

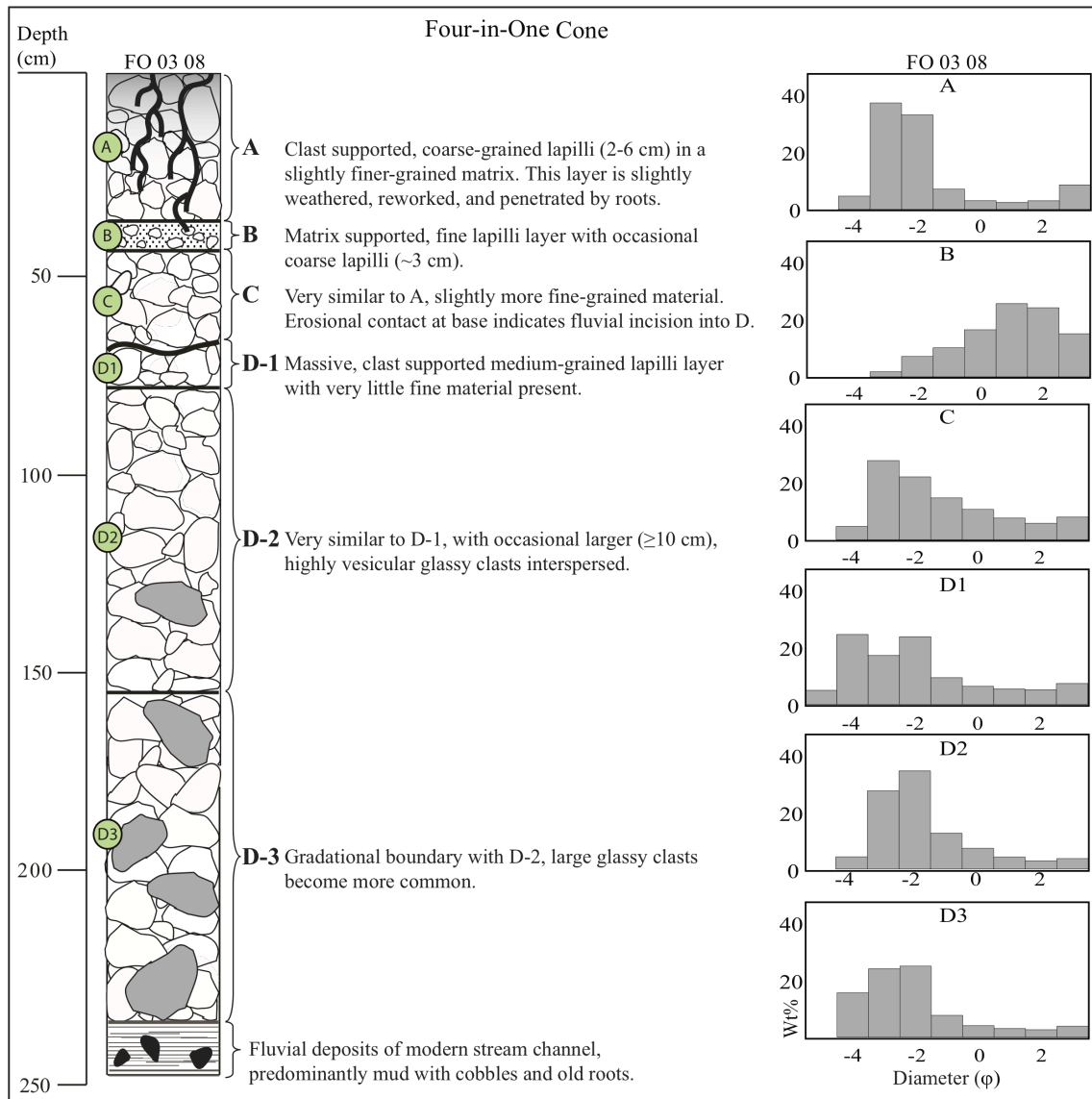


Figure 3.3. Representative stratigraphic column and grain size distributions of the Four-in-One Cone tephra deposit. Sample trench locations are shown in Figure 3.2 (labeled *FO 03 08*). Colored circles represent locations where samples were collected for grain size, componentry, and chemical analyses.

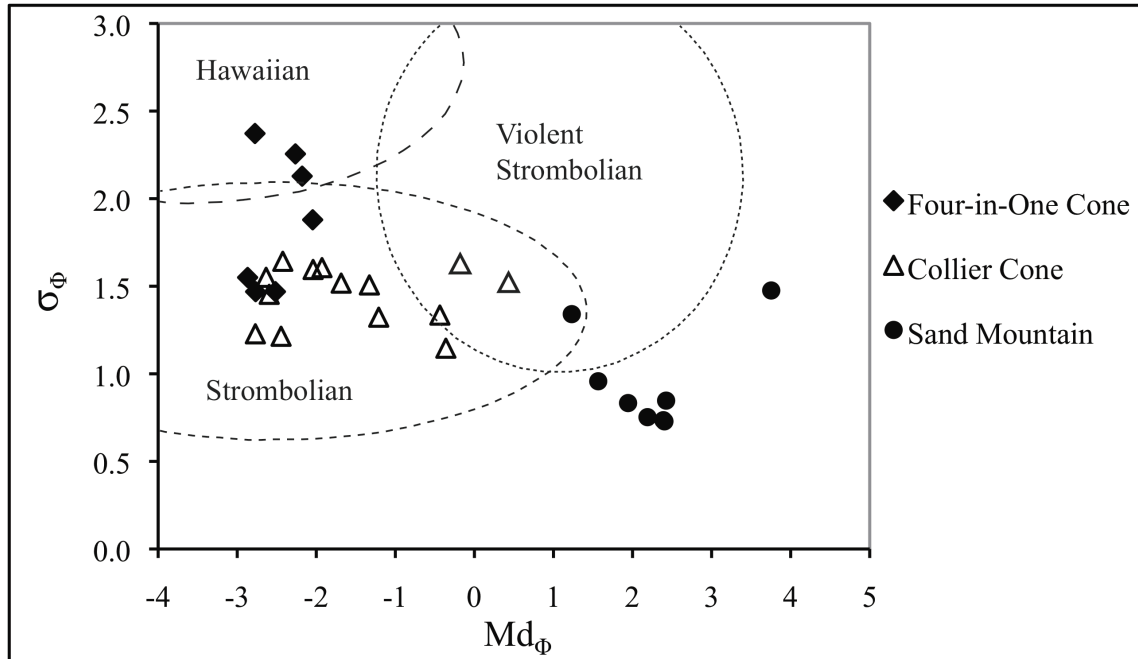


Figure 3.4. Inman sorting coefficients (σ_{ϕ}) and median grain sizes (Md_{ϕ}) for the Four-in-One Cone, Collier Cone, and Sand Mountain tephra deposits. Fields defining eruption styles are after Walker and Croasdale (1972), Parfitt (1998), Houghton and Gonnermann, (2008), and Pioli et al. (2008).

reach the base of the deposit. The more proximal deposit (CC-02-08) consists of one massive well-sorted ($\sigma=1.57$) lapilli layer with average clast sizes ranging from 4-16 mm (Figures 3.4 and 3.5). The deposit is crudely stratified and grades to smaller average clast sizes, ranging from 1-4 mm, in the upper ~20 cm (Figure 3.5). The entire deposit is characterized by highly vesicular tan and black clasts and occasional clasts of white, sugary glass that contains pyroxene and troctolite clumps. Flat clasts that appear to be broken ribbon-like fragments are common throughout the entire deposit.

The second trench (CC-01-09) exposed a more representative stratigraphy of the distal Collier Cone deposit, which is characterized by alternating layers of medium to fine lapilli and coarse ash (Figure 3.5). This observation is made based on the stratigraphy observed at multiple locations where trenches were dug or auger holes were made. The

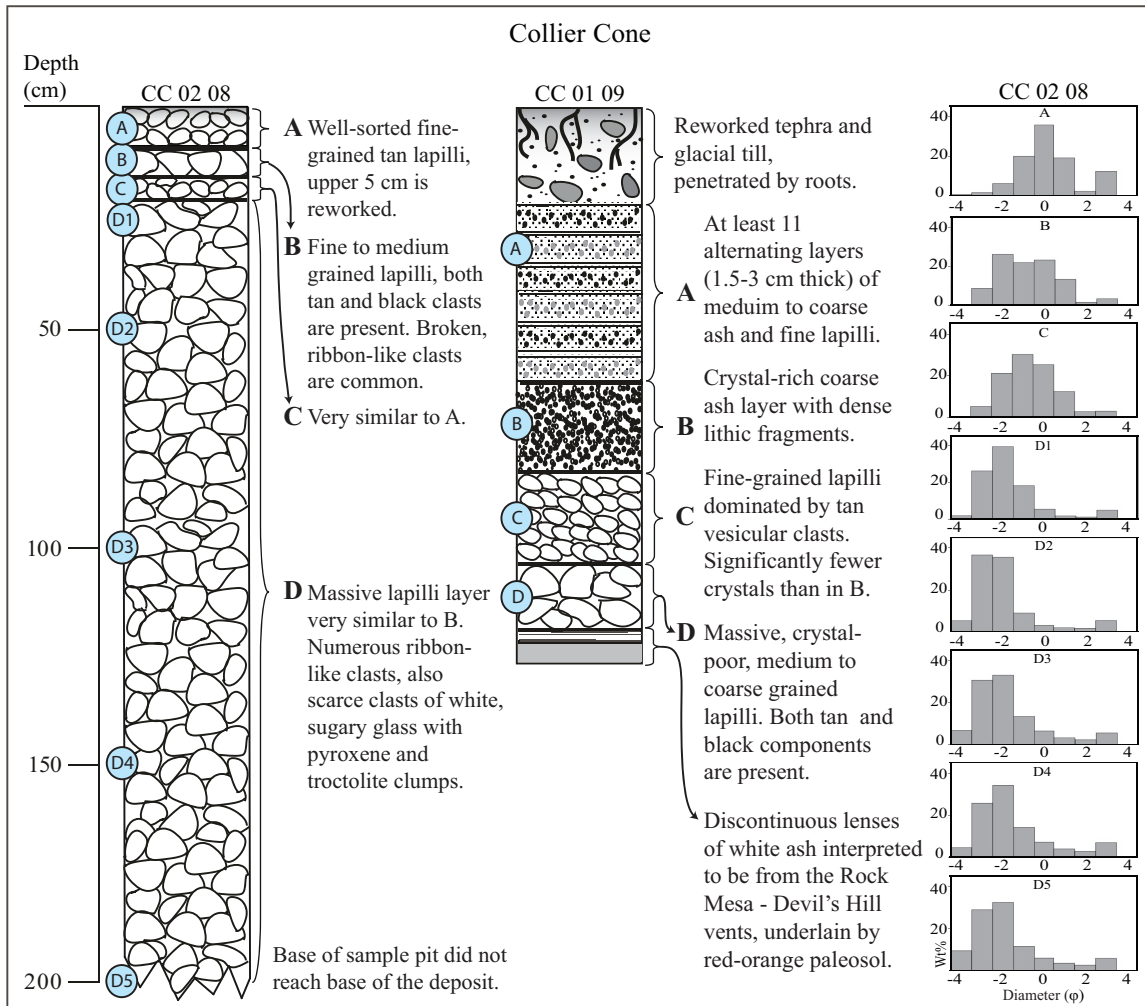


Figure 3.5. Representative stratigraphic columns and grain size distributions of the Collier Cone tephra deposit. Sample trench locations are shown in Figure 3.2 (labeled *CC 02 08* and *CC 01 09*). Stratigraphic units are labeled and described to the right of each column. Colored circles represent locations where samples were collected for grain size, componentry, and chemical analyses.

lower layer of CC-01-09 is ~17 cm thick and consists of one massive, well-sorted lapilli layer characterized by highly vesicular clasts with average sizes ranging from 4-16 mm (Unit D; Figure 3.5). Above this layer there is another very similar lapilli layer that is ~20 cm thick and consists of highly vesicular clasts with smaller average grain sizes ranging from 1-4 mm (Unit C; Figure 3.5). These two layers appear to correlate with the massive lapilli layers exposed in the proximal deposit (CC-02-08; Figures 3.2 and 3.5). Above

these two layers there is a crystal-rich layer ~20 cm thick that contains dense lithic fragments and abundant olivine and plagioclase crystals several millimeters in size. The next ~40 cm of the deposit is characterized by ~11 alternating layers of coarse ash and fine lapilli that vary in thickness from ~1.5-3 cm. This layer is overlain by ~23 cm of reworked Collier tephra.

3.4.2.3. *Sand Mountain*

The Sand Mountain deposit is striking in that it is consistently fine-grained at every location where it was recorded, making it easily recognizable in the field. The deposit lies stratigraphically above a gray clay-rich paleosol that contains rounded pebbles and cobbles and, in many locations, abundant lenses of charcoal. The tephra sequence is significantly compacted and although auguring is possible, digging trenches by hand proved to be extremely difficult. For this reason, the sample trench described here was excavated by backhoe. The trench was located ~5 km east of the vent (Figure 3.2) and exposed a ~156 cm section of the deposit (Figure 3.6).

In addition to being uniformly fine-grained, the Sand Mountain deposit is strikingly different from both the Four-in-One Cone and Collier Cone deposits in that it is characterized by hundreds of interbedded layers of fine, medium, and coarse ash (Figure 3.6). Lapilli sized clasts are absent throughout the entire deposit. The lower section of the deposit is ~40 cm thick and contains very well-sorted ($\sigma=0.74$), finely laminated ash layers that vary in thickness from <1 mm to ~4 cm (Figures 3.4 and 3.6). Average clast sizes range from 63-125 μm in the finest ash layers and from 0.25-0.5 mm in the coarser ash layers (Figure 3.6). At ~116 cm depth there is a distinctive coarse ash layer that is ~2

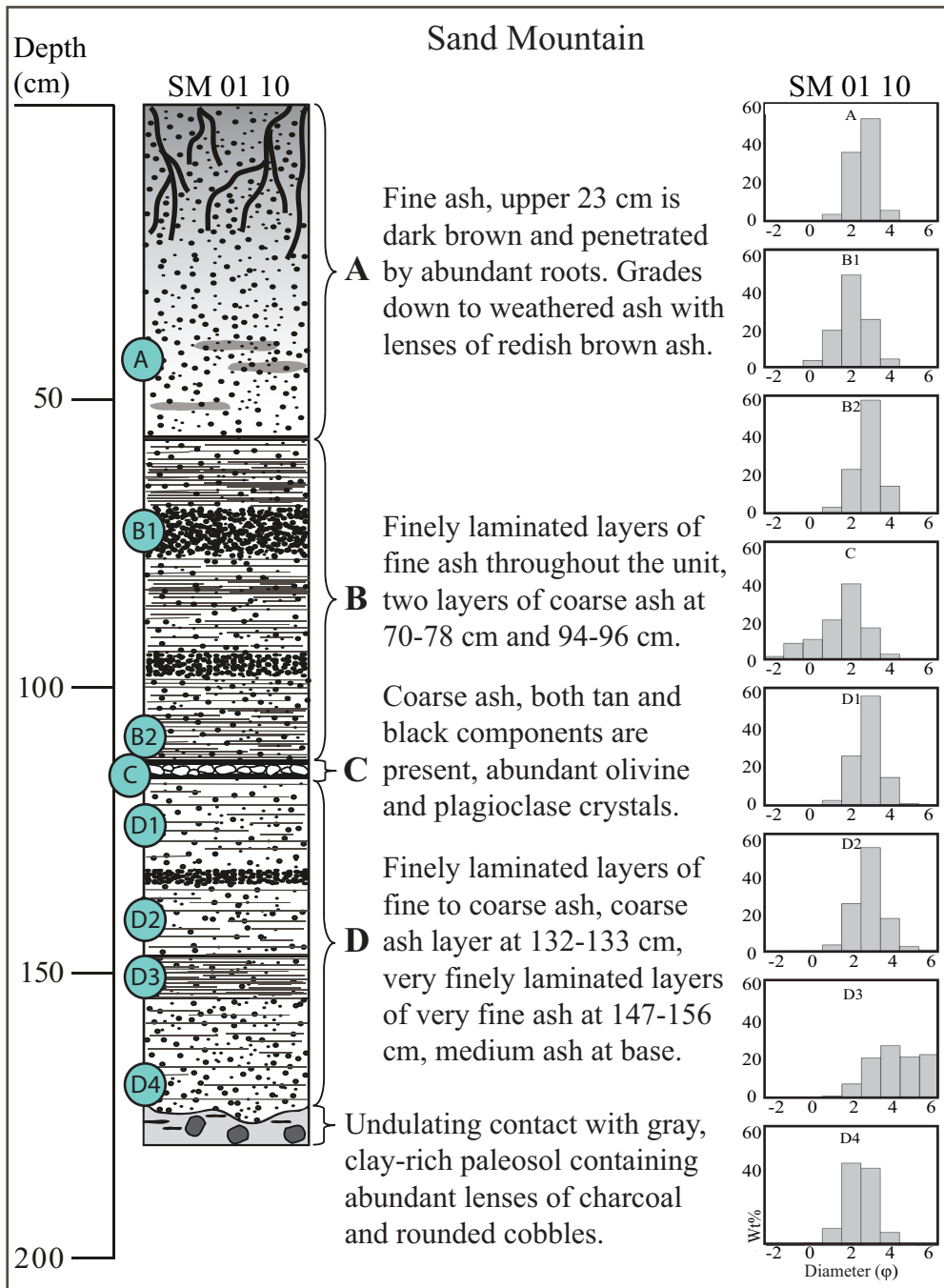


Figure 3.6. Representative stratigraphic column and grain size distributions of the Sand Mountain tephra deposit. Sample trench locations are shown in Figure 3.2 (labeled *SM 01 10*). Colored circles represent locations where samples were collected for grain size, componentry, and chemical analyses.

cm thick and contains average clast sizes ranging from 0.25-0.5 mm (Figure 3.6). This layer was observed in multiple auger holes and lake sediment cores and appears to be continuous throughout the deposit. Above this layer, there is a ~57 cm thick section that is very similar to the lower section of the deposit (Figure 3.6). Finely laminated layers of very fine ash <1 mm to several millimeters in thickness are punctuated by two layers of coarse ash, one ~2 cm thick located at ~96 cm depth and the other ~8 cm thick located at ~78 cm depth (Figure 3.6). Above the 78 cm layer there is another ~57 cm thick section that differs from the section below only in that it contains weathered, oxidized clasts (Figure 3.6). The upper ~23 cm of this section is reworked and penetrated by roots.

3.4.3. Stratigraphy of Lake Sediments

Regional lakes cored as part of this or other studies are shown in Figure 3.1 and listed in Table 3.2. Sediment cores collected as part of this study are from Big Lake, Lost Lake, Patjens Lakes, and Round Lake. Tephra samples from sediment cores collected at other lakes listed in Table 3.2 are courtesy of S.A. Marcott at Oregon State University and C.J. Long at the University of Wisconsin Oshkosh. In the following sections I correlate tephra preserved in lake sediments to source vents based on stratigraphic position, lake sedimentation rates, and physical characteristics of the tephra clasts. For chemical correlations between tephra preserved in lake sediments and possible source vents, see Section 3.4.6.

Table 3.2. Mafic tephra layers preserved in lake sediments.

Lake name	Latitude (N)	Longitude (W)	Tephra depth (cm)
Big Lake	44° 22.37	121° 52.62	12-?
Camp Lake ¹	44° 07.92	121° 45.65	45-50
Lost Lake	44° 26.01	121° 54.35	30-?
Patjens Lakes	44° 21.12	121° 53.40	17.5-51.5
Round Lake	44° 26.57	121° 47.17	94.5-95.5 and 115.5-194.5
Three Creek Lake ²	44° 05.93	121° 37.71	87-88
Todd Lake ²	44° 01.69	121° 41.09	95-96
Tumalo Lake ²	44° 01.31	121° 32.63	74-75

¹Courtesy of S.A. Marcott at Oregon State University. ²Courtesy of C.J. Long at the University of Wisconsin Oshkosh.

3.4.3.1. *Big Lake*

Big Lake is located ~4 km east-southeast of the Sand Mountain vents (Figure 3.1). Based on the Sand Mountain isopach map (Figure 3.2), the tephra deposit is likely 100-200 cm thick at this location. However, the compacted nature of the deposit made it extremely difficult to drive the sampler by hand and collect a complete stratigraphic core. A short (45 cm) core was recovered that consists of ~12 cm of dark brown gyttja in the upper section and ~33 cm of fine-grained, dark brown to black tephra in the lower section. Tephra exposed in the core consist of well-sorted, finely laminated ash layers very similar to those observed in the Sand Mountain sample trench described above (Figure 3.6). For this reason, the tephra layer is interpreted to be from Sand Mountain. However, the depth of the deposit as preserved in Big Lake could not be determined.

3.4.3.2. *Lost Lake*

Lost Lake is located ~5 km north-northeast of the Sand Mountain vents (Figure 3.1). The lake is shallow (2.7 m in the deepest location) and surrounded by fens, particularly along the southeast shore. Two partial cores were recovered from Lost Lake, both consisting of medium (~4 mm in diameter), very loosely consolidated lapilli that

either fell out of the sampler before the core could be recovered or fell apart as soon as it was removed from the sampler. No stratigraphic changes in grain size, grading, sorting, color, or apparent lithic content were noted in either core. Tephra in both cores are intermixed with organic material, including small woody fragments and abundant grass and roots. Both cores appear to consist of reworked tephra interpreted to be from the 1950 ± 150 ^{14}C yr B.P. eruption of the Lost Lake chain of vents (Sherrod et al., 2004), which are located <1 km west of the lake. This interpretation is made based on the relatively large grain size of the tephra, which indicates deposition proximal to the source vent. Additionally, the tephra recovered from lake sediments resemble tephra exposed west of the lake, at the base of the Lost Lake chain of vents.

3.4.3.3. *Patjens Lakes*

The Patjens Lakes are four small lakes located ~ 5 km southeast of the Sand Mountain vents (Figure 3.1) and ~ 2.5 km from the nearest road access. Since they are not accessible by road, sediment cores were collected from a fen located on the south shore of the largest lake, rather than from a platform anchored in the deepest portion of the lake. An 88-cm core was recovered from the fen (Figure 3.7). The upper section of the core consists of uniform, consolidated red-brown sediments with abundant roots. At ~ 17.5 cm there is a gradational contact with a fine-grained mafic tephra layer interpreted to be from Sand Mountain. This interpretation is based on other thickness measurements for the Sand Mountain tephra deposit (Figure 3.2) and on the size of the tephra clasts, which are uniformly fine grained. At ~ 51.5 cm there is a sharp contact between the mafic tephra layer and a brown, silty clay layer that contains occasional rounded pebbles and

abundant sand-sized white flecks that appear to be weathered pumice clasts (Figure 3.7). This layer becomes increasingly sandy toward the bottom. At ~81.5 cm there is a gradational contact between the sandy clay layer and a silicic tephra layer ~4 cm thick. This layer is interpreted to be from the 7478-7620 cal yr B.P. eruption of Mt. Mazama (Hallett et al., 1997), based on thickness and grain size. The stratigraphic position of the presumed Mt. Mazama tephra supports the interpretation that the mafic tephra layer above is from Sand Mountain. At ~85.5 cm there is a sharp contact between the silicic tephra and a brown, silty clay layer similar to the layer above (Figure 3.7).

3.4.3.4. Round Lake

Round Lake is located ~13 km northeast of the Sand Mountain vents (Figure 3.1). A 398-cm core was recovered that consists primarily of uniform brown gyttja punctuated by multiple tephra layers (Figure 3.8). Two very thin (<0.3 cm) layers of mafic fine ash occur at 94.5-95.5 cm depth (Figure 3.8). At 115.5-194.5 cm depth there is a 79 cm-thick layer of mafic tephra (Figure 3.8) that consists of multiple, finely laminated layers of very fine to coarse ash, similar to those observed in the Sand Mountain sample trench (Figure 3.6). At 250.5-251.5 cm depth there are two thin (<0.5 cm) unidentified mafic tephra layers, followed by 14 cm of silicic tephra at 267-281 cm depth (Figure 3.8). The silicic tephra layer is interpreted to be from the 7478-7620 cal yr B.P. eruption of Mt. Mazama (Hallett et al., 1997), based on thickness, stratigraphic position, and grain size. At 381-382 cm depth there is a 1 cm-thick layer of unidentified mafic tephra (Figure 3.8).

Radiocarbon dates of 1790 and 11,910 cal yr B.P. were obtained from plant material recovered at 90 cm and 352 cm depth (C.J. Long, personal communication).

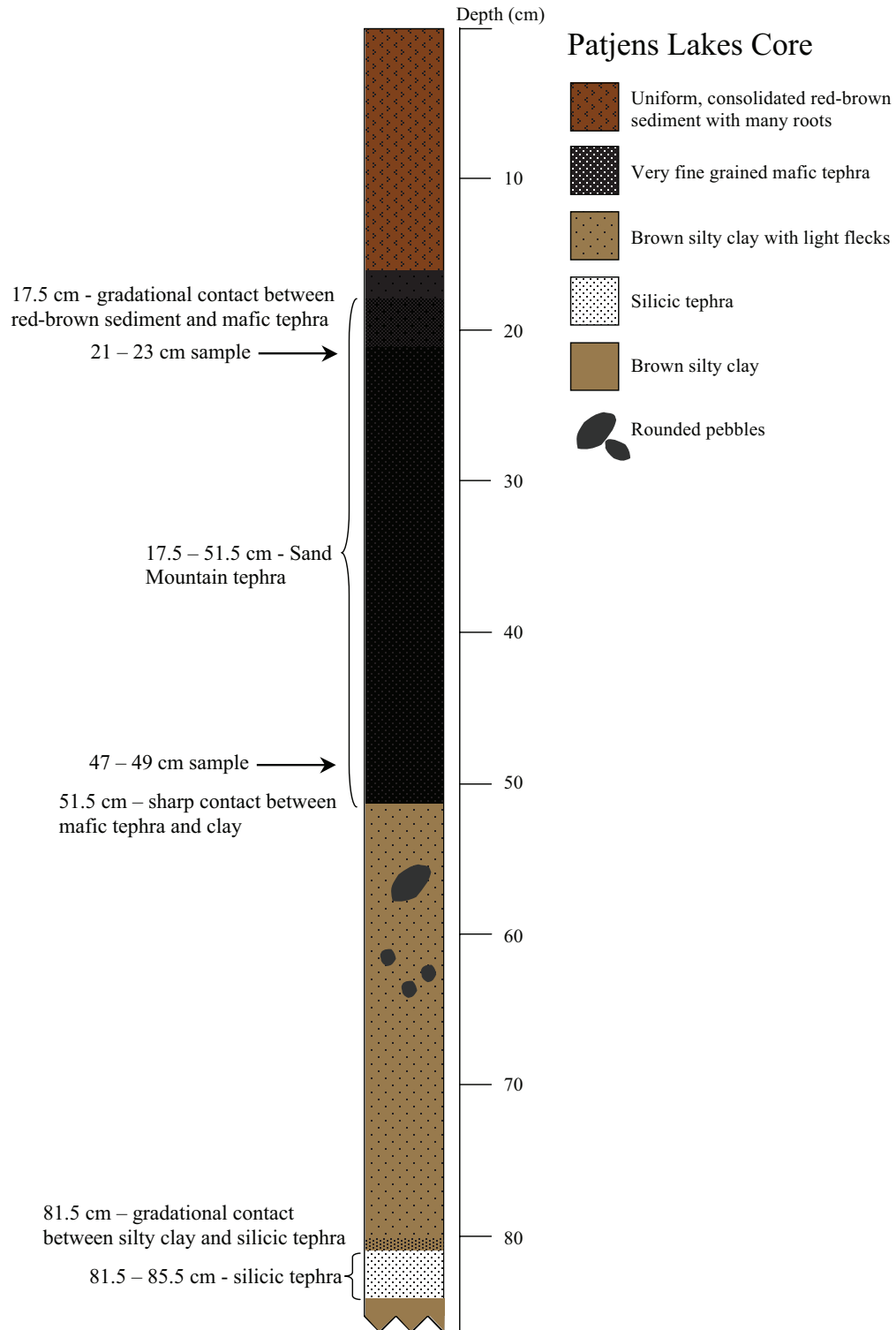


Figure 3.7. Representative stratigraphic column of Patjens Lakes sediments. The lake location is shown in Figure 3.1 and Table 3.2. Descriptions of the sediment layers are located to the right of the stratigraphic column and tephra layers are identified to the left. Arrows indicate locations where samples were collected for chemical analyses.

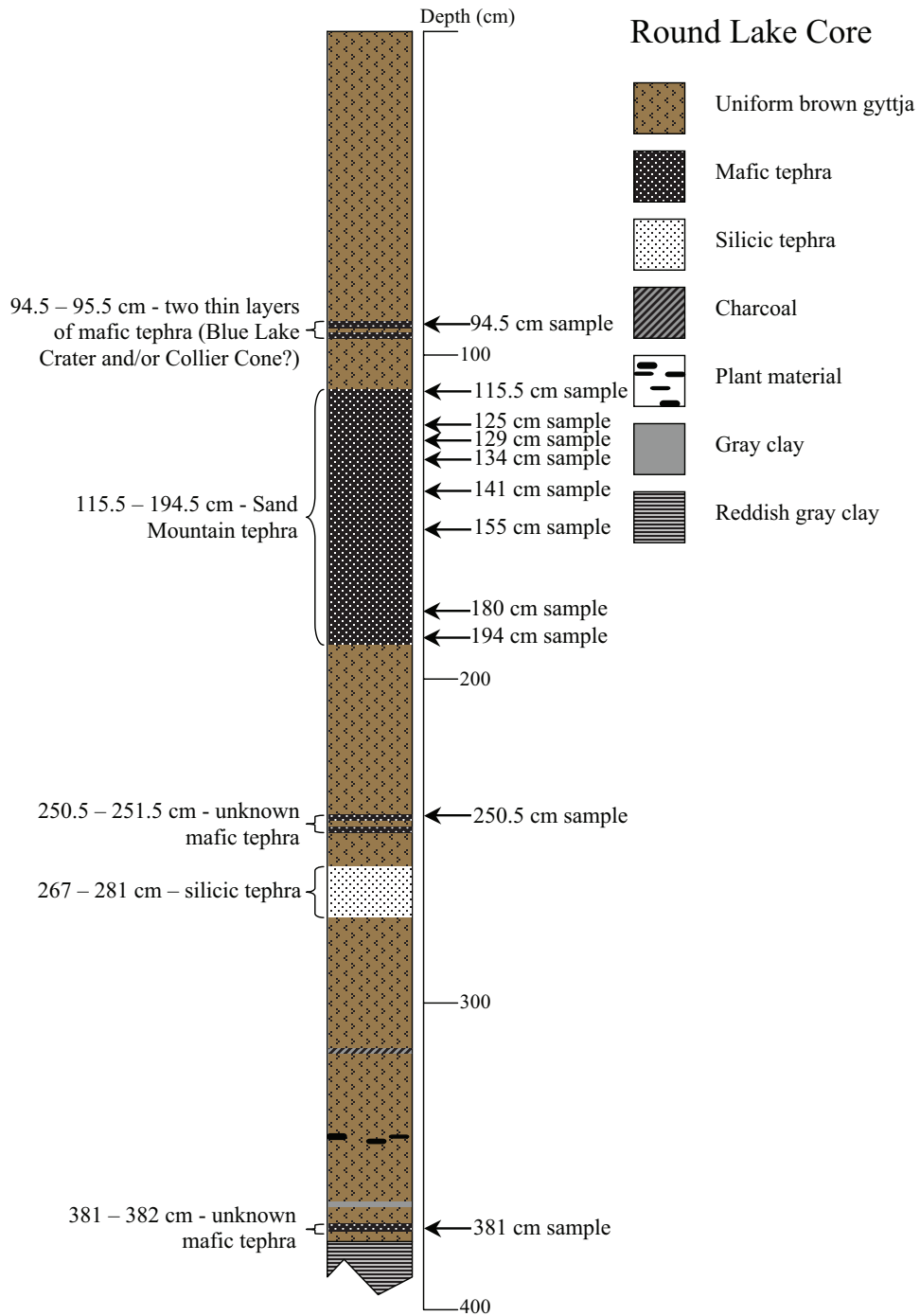


Figure 3.8. Representative stratigraphic column of Round Lake sediments. The lake location is shown in Figure 3.1 and Table 3.2. Descriptions of the sediment layers are located to the right of the stratigraphic column and tephra layers are identified to the left. Arrows indicate locations where samples were collected for loss on ignition and chemical analyses.

These dates, along with estimated ages for Mt. Mazama tephra, were used to estimate sedimentation rates that indicate eruption ages of ~2060 cal yr B.P. for the two thin layers of mafic tephra at 94.5-95.5 cm depth and ~3250 cal yr B.P. for the tephra layer at 115.5-194.5 cm depth (C.J. Long, personal communication). Loss on ignition results for samples collected from 115.5-194.5 cm depth indicate very little organic content (Table 3.3), suggesting that the entire 79 cm-thick tephra layer was deposited quickly, from a single eruptive episode.

The small grain size (<0.25 mm) of tephra clasts at 94.5-95.5 cm depth indicates that these layers were deposited distally from the source. Based on stratigraphic position, radiocarbon dates obtained from plant material in the lake core, and estimated sedimentation rates, there are several possible source vents for these layers, including the 1330±140 ¹⁴C yr B.P. eruption of Blue Lake crater, located ~4 km southeast of Round Lake, the 1600±100 ¹⁴C yr B.P. eruption of Collier Cone, the 1980±160 ¹⁴C yr B.P. eruption of Four-in-One Cone, and ≤2300 yr B.P. eruption of Yapoah Crater (Sherrod et al., 2004). The limited extent of the Four-in-One Cone tephra deposit indicates this is an unlikely source (Figure 3.2). Chemical correlations between tephra sampled from the lake core and tephra from both Blue Lake crater and Collier Cone indicate that one or both layers could be trace deposits from either of these two vents (see Section 3.4.6.).

Table 3.3. Loss on ignition results for tephra from the Round Lake core.

Depth in core (cm)	Dry bulk density (g/cm ³)	LOI (% dry weight)
125	1.4323	0.53
134	1.2847	0.57
141	1.3406	0.94
155	1.4552	0.54

The stratigraphic position of the tephra layer at 115.5-194.5 cm depth suggests this layer is from Sand Mountain. The estimated age of ~3250 cal yr B.P., based on radiocarbon dates obtained from plant material and estimated lake sedimentation rates, correlates with the ca. 3000 yr B.P. estimate of the Sand Mountain eruption from Deligne et al. (2012). Additionally, tephra thickness measurements made near Round Lake (Figure 3.2) correlate with the thickness of this layer. Similarities between the laminated layers of very fine to coarse ash in the lake core and the layers exposed in the Sand Mountain sample trench (Figure 3.6) also support this conclusion, as do chemical correlations (see Section 3.4.6).

3.4.3.5. *Mafic Tephra in Other Lake Sediments*

In addition to the lake cores described above, Table 3.2 lists regional lakes cored by other workers. Samples from mafic tephra layers preserved in sediments from Camp Lake, Three Creek Lake, Todd Lake, and Tumalo Lake were obtained and correlated to Collier Cone. Sediments from Camp Lake, located ~6.5 km southeast of Collier Cone (Figure 3.1), are described in Marcott et al. (2009). The Camp Lake core records ~4 cm of mafic tephra located at 46 cm depth. This layer is attributed to Collier Cone based on stratigraphic position ~5 cm above tephra attributed to the Rock Mesa - Devil's Hill chain of vents, and on grain size (Marcott et al., 2009). The chemical composition of tephra sampled from the Camp Lake core supports the interpretation of Collier Cone as the source vent (see Section 3.4.6).

Sediment cores recovered by C.J. Long from Three Creek Lake, Todd Lake, and Tumalo Lake (Figure 3.1 and Table 3.2) each contain a thin (≤ 0.5 cm) mafic tephra layer

located above a thin white tephra layer interpreted to be from the Rock Mesa - Devil's Hill vents. Estimated sedimentation rates indicate that in each lake, the mafic layer was deposited ~400 to 700 years after the silicic, presumably Rock Mesa - Devil's Hill, layer (C.J. Long, personal communication). Additionally, the tephra clasts preserved in all three lakes are small (<0.25 mm), indicating they were deposited distally from the source.

Collier Cone is a likely source vent for the tephra layers preserved in each of these lakes. The age of the Collier Cone eruption (1600 ± 100 ^{14}C yr B.P.; Sherrod et al., 2004) fits with the stratigraphic position and estimated sedimentation rates for each lake. Although there are several other possible vents of similar age (e.g. the 1330 ± 140 ^{14}C yr B.P. eruption of Blue Lake crater and the associated spatter cone chain of vents, the 1950 ± 150 ^{14}C yr B.P. eruption of the Lost Lake chain of cones, the 1980 ± 160 ^{14}C yr B.P. eruption of Four-in-One Cone, and several different eruptions of Belknap Crater; Sherrod et al., 2004), Collier Cone is the most likely source based on location. All of the other vents except Blue Lake crater and the associated spatter cone chain are located northwest of Collier Cone. If tephra from any of these vents were deposited in Three Creek Lake, Todd Lake, or Tumalo Lake, the same tephra would also have been deposited in Camp Lake (Figure 3.1). Since Camp Lake records just one mafic tephra layer that is clearly correlated to Collier Cone, the mafic tephra layers in Three Creek Lake, Todd Lake, and Tumalo Lake are more likely to be from Collier Cone than from any of these other vents. Blue Lake crater and the associated spatter cone chain, located north of Collier Cone and northwest of the three lakes, are also possible source vents. However, since Collier Cone is located closer to these lakes (<30 km) than Blue Lake crater and the spatter cone chain

(>30 km), it is more likely that the tephra layers are from Collier Cone. Sufficient material for chemical analyses was not be recovered from any of these lake cores.

3.4.4. Juvenile Components of the Tephra Deposits

Juvenile components of the tephra deposits from Four-in-One Cone and Collier Cone are similar those identified from mafic vents at Newberry Volcano (Chapter II, Section 2.4.2). As at Newberry, three juvenile components were identified in the Four-in-One Cone and Collier Cone deposits: 1) tan, highly vesicular scoria (sideromelane), 2) black, less vesicular scoria (tachylite), and 3) dense fragmented lava. Each component is very similar to the representative examples shown in Figure 2.6 of Chapter II. Clasts with flattened shapes and relatively smooth surfaces identified in the Lava Butte deposit (Figure 2.6, Chapter II) were not identified in the Four-in-One Cone and Collier Cone deposits. However, the proximal section of the Collier Cone deposit (CC 02 08; Figures 3.2 and 3.5) does contain numerous broken, ribbon-like fragments shown in Figure 3.9. Relative proportions of tan vesicular scoria, black less vesicular scoria, and dense lava fragments from Four-in-One Cone and Collier Cone are shown in Figure 3.10.

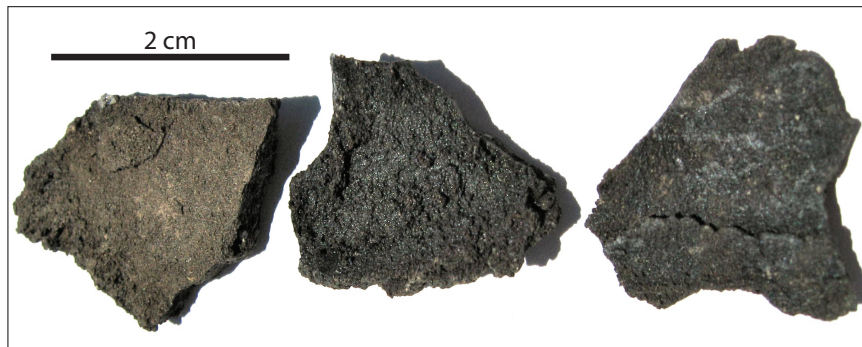


Figure 3.9. Photo of juvenile tephra clasts from the Collier Cone deposit that resemble broken, ribbon-like fragments (as described in Figure 3.5).

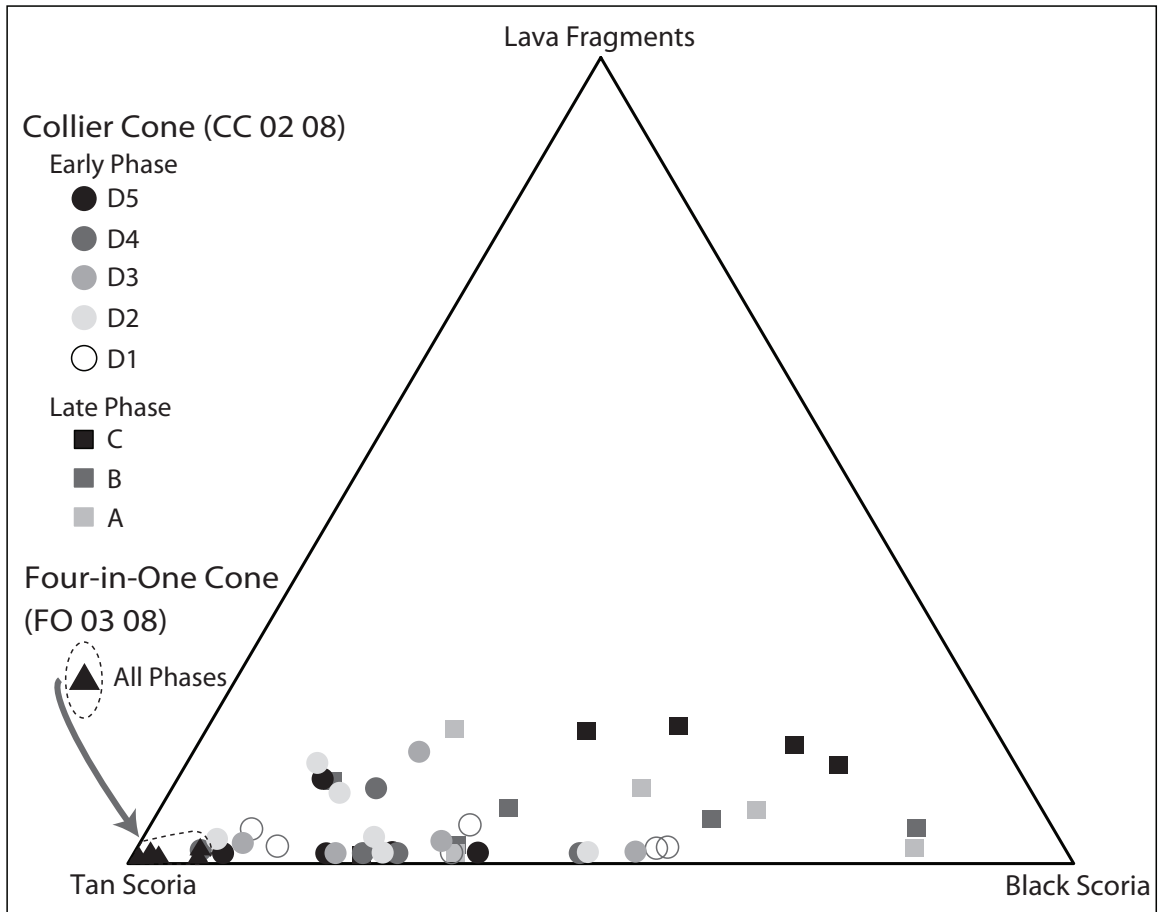


Figure 3.10. Componentry of juvenile tephra from the Four-in-One Cone and Collier Cone deposits. All stratigraphic horizons of the Four-in-One Cone deposit (Figure 3.3) are dominated by tan scoria, indicated by triangle symbols surrounded by a dashed line. Stratigraphic horizons A-D of the Collier Cone tephra deposit (Figure 3.5) are shown by square and circle symbols. In general, tan scoria dominates during the early phases of activity; black scoria and lava fragments become increasingly more common during later phases of activity.

Juvenile components in the Four-in-One Cone deposit are similar to those produced by the Lava Cascade and South Sugarpine vents at Newberry Volcano (Chapter II, Section 2.4.2). Like the Lava Cascade and South Sugarpine clasts, tephra clasts from Four-in-One Cone have angular shapes and are glassy in appearance. Unlike the Newberry deposits, which consist only of tan, highly vesicular clasts, the Four-in-One Cone deposit also contains small amounts of black scoria and dense lava fragments

(Figure 3.10). Loose olivine and plagioclase crystals ~1 mm in diameter are also present, but rare.

The Collier Cone deposit contains all three juvenile components (Figure 3.10) as well as abundant loose olivine and plagioclase crystals ~1 mm in diameter. Tan sideromelane clasts differ from those in the Four-in-One Cone deposit in having smooth outer edges and smaller vesicles that are more uniform in size. They resemble clasts from the Lava Butte vent at Newberry Volcano (Chapter II, Section 2.4.2), as well as clasts described by Heiken (1978) and Pioli et al. (2008). Tan vesicular scoria dominates during the early phases of activity and black scoria and lava fragments become increasingly more common during later phases of activity.

Due to the very small grain sizes of the Sand Mountain tephra deposit, juvenile clasts were not separated into different components. Instead, representative clasts were sampled from the entire stratigraphy of the deposit and examined under a stereo microscope. Although the proportions of each clast type were not determined quantitatively, two juvenile components were identified: vesicular sideromelane clasts and denser tachylite clasts. Abundant loose olivine and plagioclase crystals are also present. Sideromelane and tachylite clasts are characterized by blocky, equant shapes and are denser than the sideromelane and tachylite clasts in the Four-in-One Cone and Collier Cone deposits. Both these characteristics, along with the uniformly small grain size of the Sand Mountain tephra, indicate that interaction with water likely occurred during tephra-producing phases of the eruption (e.g. Büttner et al., 1999; Dellino and Kyriakopoulos, 2003; see Chapter IV for further discussion of interaction with water during the Sand Mountain eruption).

3.4.5. Microtextural Characteristics of Tephra

Tan scoria clasts from Four-in-One Cone, Collier Cone, and Sand Mountain are all moderately crystalline and characterized by abundant plagioclase microphenocrysts and microlites (Figure 3.11). Plagioclase crystals are elongate in cross-section and tabular in three dimensions. In clasts from Four-in-One Cone and Collier Cone, plagioclase crystals are often aligned. Less abundant olivine and pyroxene are also present, both as euhedral microphenocrysts and as microlites. Scoria clasts from Four-in-One Cone and Collier Cone are characterized by round microvesicles that vary in size from ~1mm - 25 μm in cross sectional diameter. In some cases, vesicles appear to have deformed around individual or multiple crystals (e.g. Figure 3.11B). Clasts from Sand Mountain are characterized by smaller microvesicles, generally $\leq 100 \mu\text{m}$ in cross sectional diameter. Sand Mountain clasts are also characterized by numerous micro-fractures (Figure 3.11C), suggesting that syn-eruptive interaction with water may have occurred (e.g. Büttner et al., 1999; Dellino and Kyriakopoulos, 2003; see Chapter IV for further discussion of interaction with water).

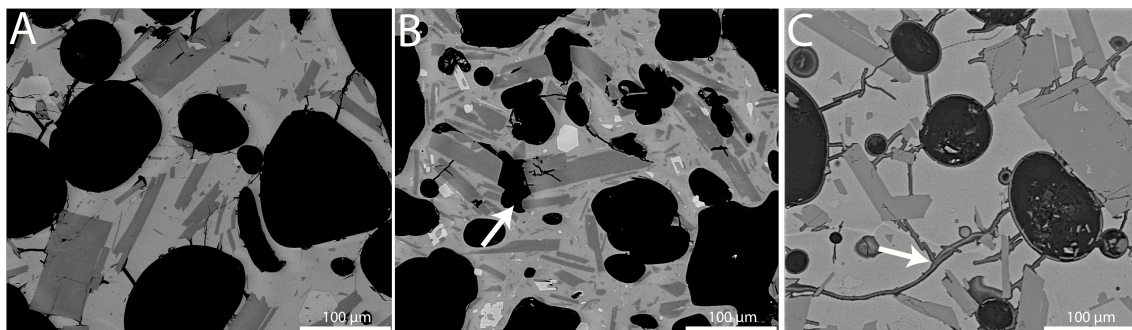


Figure 3.11. SEM images of tan tephra clasts from Four-in-One Cone (A), Collier Cone (B), and Sand Mountain (C). Arrows indicate examples of vesicles deformed around crystals (B) and microfractures that could be indicative of syn-eruptive interaction with water (C).

3.4.6. Tephra Compositions

Bulk compositions of juvenile tephra from the Four-in-One Cone, Collier Cone- and Sand Mountain sample trenches are listed in Table 3.4. Bulk compositions of tephra sampled from lake cores are listed in Table 3.5. Variations in major elements are not sufficient to correlate tephra preserved in lake cores to individual source vents. Trace element variations, however, support the stratigraphic correlations made in Sections 3.4.3.3 through 3.4.3.5. Figure 3.12 shows trace element data for tephra sampled from lake cores and tephra from known vents. In the Round Lake core, the stratigraphic position of the double tephra layer at 94.5 cm (Figure 3.8) suggests that Blue Lake crater, Collier Cone, Four-in-One Cone, or Yapoah Crater could be a possible source vent for one or both layers. Trace element data do not show a strong chemical correlation between these layers and tephra from Four-in-One Cone or Yapoah Crater (Figure 3.12A). However, there is a strong correlation between these layers and tephra from both Blue Lake crater and Collier Cone (Figure 3.12B and C), indicating that either vent could be the source for one or both layers. The tephra layers preserved from 115.5-194 cm in Round Lake (Figure 3.8) and from 17.5-51.5 cm in Patjens Lakes (Figure 3.7) both show strong chemical correlation to tephra from Sand Mountain (Figure 3.12D). The mafic tephra layer preserved in Camp Lake is strongly correlated to tephra from Collier Cone (Figure 3.12C).

Table 3.4. Bulk chemical analyses of tephra samples from Four-in-One Cone, Collier Cone, and Sand Mountain.

Vent	Four-in-One Cone		Collier Cone		
Lat (N)	44° 12.656		44° 11.540		
Long (W)	121° 48.318		121° 46.486		
Sample	FO 03 08 A	FO 03 08 D3	CC 02 08 A	CC 02 08 D1	CC 02 08 D5
wt%					
SiO ₂	54.40	52.68	57.26	57.03	57.14
Al ₂ O ₃	18.47	19.25	18.07	18.19	18.05
FeO*	7.82	7.84	7.35	7.29	7.19
MgO	4.86	5.52	3.62	3.72	3.77
CaO	8.14	8.96	7.01	7.20	7.25
Na ₂ O	3.86	3.62	4.38	4.33	4.35
K ₂ O	0.86	0.64	0.92	0.89	0.88
TiO ₂	1.17	1.11	1.12	1.09	1.09
P ₂ O ₅	0.28	0.23	0.15	0.14	0.14
MnO	0.13	0.14	0.13	0.13	0.13
ppm					
Rb	13	8	15	14	14
Sr	558	584	516	524	527
Y	20	19	17	18	17
Zr	125	104	99	97	94
Nb	8	7	4	4	4
Ba	301	231	299	295	303
Ni	35	43	14	16	15
Cu	76	90	55	55	54
Zn	75	68	77	73	74
Cr	75	102	27	36	36
Ce	25	25	21	20	18
Ga	18	18	19	19	18
La	12	11	9	9	9
Nd	16	15	12	12	12
V	205	201	213	207	204
Th	2	1	1	1	1
U	1	0	1	1	1
Ta	1	0	0	0	0
Sm	4	4	3	3	3
Pb	4	3	4	4	4

Table 3.4. Continued.

Vent	Collier Cone				Sand Mountain		
Lat (N)	44° 11.779				44° 23.057		
Long (W)	121° 45.302				121° 52.021		
Sample	CC0109A	CC0109B	CC0109C	CC0109D	SM0110B	SM0110C	SM0110D3
wt%							
SiO ₂	55.27	56.40	55.18	56.54	50.64	50.82	50.66
Al ₂ O ₃	19.44	18.93	19.51	18.50	18.84	18.61	17.25
FeO*	6.39	6.53	6.21	7.44	9.23	9.18	9.08
MgO	5.30	4.87	5.63	3.78	6.50	6.63	8.10
CaO	8.03	7.33	8.06	7.27	8.61	8.54	9.04
Na ₂ O	3.75	3.94	3.67	4.27	3.42	3.45	3.16
K ₂ O	0.78	0.89	0.78	0.84	0.71	0.71	0.73
TiO ₂	0.81	0.85	0.75	1.09	1.52	1.51	1.47
P ₂ O ₅	0.12	0.13	0.10	0.15	0.40	0.39	0.37
MnO	0.11	0.12	0.11	0.13	0.14	0.14	0.15
ppm							
Rb					9	9	9
Sr					643	578	801
Y					27	29	27
Zr					165	166	155
Nb					14	14	14
Ba					277	276	297
Ni					110	122	159
Cu					66	71	76
Zn					73	76	81
Cr					186	198	292
Ce					40	38	40
Ga					21	18	19
La					19	18	14
Nd					22	22	22
V					194	192	199
Th					1	0	2
U					2	0	0
Ta							
Sm							
Pb					5	5	5

Sample locations are shown in Figure 3.2. Chemical analyses of major elements were performed by X-ray fluorescence (XRF) and trace elements by inductively coupled plasma mass spectrometry (ICP-MS) at the GeoAnalytical Laboratory at Washington State University. Major element analyses are normalized to 100% volatile-free with iron calculated as FeO and indicated as FeO*.

Table 3.5. Bulk chemical analyses of tephra samples from lake cores.

Lake name	Camp Lake	Patjens Lakes		Round Lake			
Lat (N)	44° 07.92	44° 21.12		44° 26.57			
Long (W)	121° 45.65	121° 53.40		121° 47.17			
Tephra depth (cm)	45-47	21-23	47-49	94.5	115.5	129	180
wt%							
SiO ₂	57.71	51.67	51.43	53.63	53.45	53.56	51.15
Al ₂ O ₃	17.97	18.54	17.91	20.02	17.92	17.97	16.51
FeO*	6.60	7.32	7.98	6.19	7.64	7.45	8.39
MgO	3.88	6.50	7.41	5.62	5.52	5.95	8.71
CaO	7.11	9.29	9.26	9.30	8.96	8.70	9.28
Na ₂ O	4.44	3.71	3.31	3.51	3.71	3.86	3.28
K ₂ O	0.94	0.83	0.73	0.59	0.84	0.80	0.74
TiO ₂	1.068	1.519	1.480	0.860	1.403	1.237	1.456
P ₂ O ₅	0.161	0.500	0.356	0.163	0.408	0.355	0.332
MnO	0.124	0.133	0.136	0.114	0.142	0.129	0.150
ppm							
Rb	14	9	10	9	11	8	8
Sr	487	761	747	618	625	981	716
Y	16	25	25	13	23	19	21
Zr	88	150	148	73	151	148	140
Nb	5	13	11	4	12	10	11
Ba	284	310	284	225	331	333	272
Ni	22	121	136	73	61	97	162
Cu	56	55	62	60	72	53	56
Zn	73	82	86	64	81	85	78
Cr	34	253	284	107	122	104	340
Ce	14	40	39	19	33	44	38
Ga	19	18	20	16	16	18	16
La	12	20	16	8	20	23	16
Nd	12	19	23	11	22	26	23
V	195	194	197	157	192	167	196
Th	1	2	2	0	0	0	0
U	0	2	3				
Pb	16	8	3	6	4	5	3

Lake locations are shown in Figure 3.1. Chemical analyses were performed by X-ray fluorescence (XRF) and inductively coupled plasma mass spectrometry (ICP-MS) at the GeoAnalytical Laboratory at Washington State University. Major element analyses are normalized to 100% volatile-free with iron calculated as FeO and indicated as FeO*.

Table 3.5. Extended.

Lake name	Round Lake		
Lat (N)	44° 26.57		
Long (W)	121° 47.17		
Tephra depth (cm)	194	250.5	381
wt%			
SiO ₂	51.35	57.54	58.93
Al ₂ O ₃	17.05	16.98	17.01
FeO*	8.62	7.06	6.62
MgO	6.96	5.06	4.36
CaO	9.34	7.26	6.61
Na ₂ O	3.55	3.57	3.73
K ₂ O	1.02	0.84	1.21
TiO ₂	1.504	1.181	1.117
P ₂ O ₅	0.452	0.389	0.302
MnO	0.151	0.125	0.120
ppm			
Rb	11	12	22
Sr	887	484	419
Y	24	19	22
Zr	158	127	122
Nb	10	10	7
Ba	503	306	375
Ni	109	81	59
Cu	66	53	50
Zn	85	80	75
Cr	235	126	77
Ce	43	33	28
Ga	17	16	17
La	20	14	16
Nd	28	19	16
V	202	161	157
Th	0	0	0
U			
Pb	5	8	13

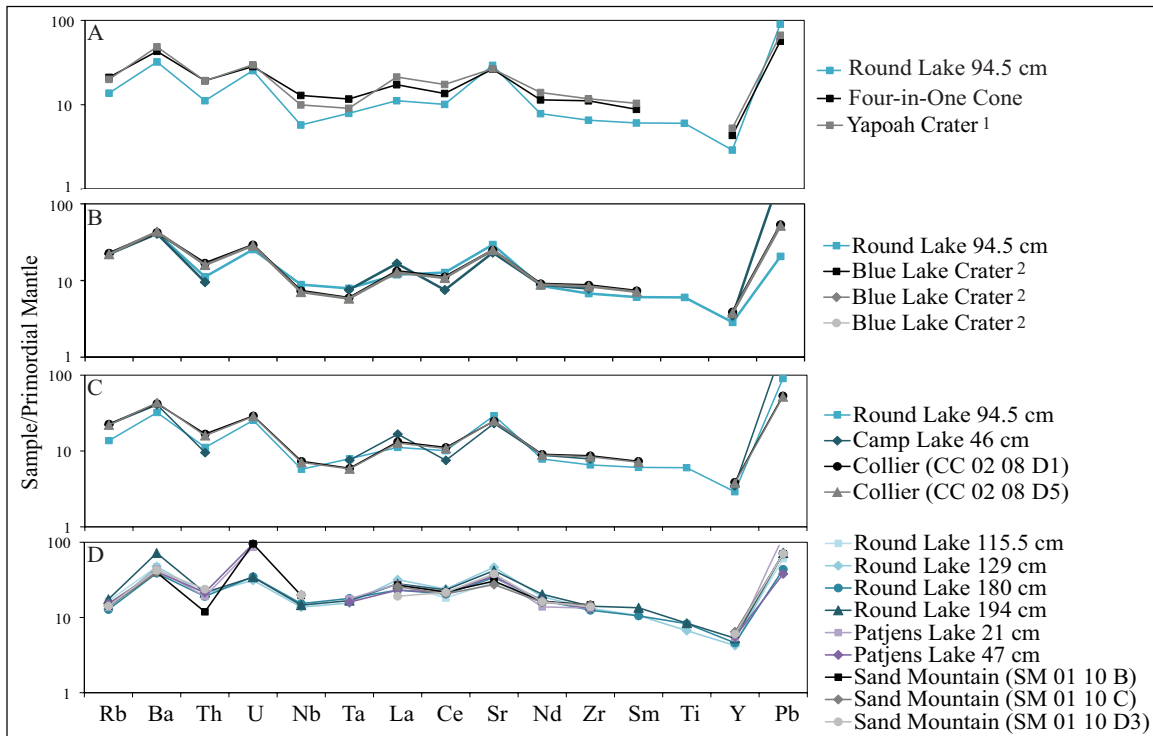


Figure 3.12. Trace element data for tephra from lake sediments and known vents. Trace elements are normalized to average primordial mantle. The double tephra layer preserved at 94.5 cm in Round Lake (Figure 3.8) is chemically correlated to tephra from Blue Lake crater (B) and Collier Cone (C), but not to tephra from Four-in-One Cone and Yapoah Crater (A). Tephra layers preserved from 115.5-194 cm in Round Lake (Figure 3.8) and from 17.5-51.5 cm in Patjens Lakes (Figure 3.7) are chemically correlated to Sand Mountain (D). The tephra layer preserved in Camp Lake is chemically correlated to Collier Cone (C). ¹Blue Lake Crater and ²Yapoah Crater data are courtesy of E.R. Johnson and D.M. Ruscitto, respectively.

3.5. Discussion

Mafic eruptions are classified along a spectrum ranging from low-energy hawaiian activity, to strombolian activity, to violent strombolian and plinian activity (e.g. Walker, 1973; Parfitt, 2004; Valentine and Gregg, 2008). At many mafic vents, transitions between eruption styles occur throughout the duration of the eruption. These transitions are controlled by changes in eruption dynamics, in particular by changes in the mass flux of magma and gas and in the degree of magma fragmentation (e.g. Walker, 1973; Parfitt, 2004; Pioli et al., 2008; Valentine and Gregg, 2008). Thus, classification

systems for mafic eruptions use the degree of fragmentation and the area covered by the tephra blanket to determine eruption style (e.g. Walker, 1973). Other parameters that are often used to interpret eruption style include grain size distributions and sorting of individual tephra layers, characteristics of juvenile components, and the total volume of the tephra deposit. In the following sections, I compare these parameters for the Four-in-One Cone, Collier Cone, and Sand Mountain tephra deposits to other well-documented mafic eruptions and use these comparisons to make interpretations about eruption style.

3.5.1. Volume Estimates of the Tephra Deposits

Reconstructing accurate isopachs for tephra deposits produced by cinder cones can be difficult because the deposits are easily eroded, reworked by biotic activity, or covered by subsequent lava flows from the same vent or other vents within the same cinder cone field. It can be especially difficult to reconstruct areas covered by trace deposits (in this case, <25 cm) because thin deposits are often eroded or reworked quickly. For these reasons, tephra production at many cinder cone vents is often either underestimated or not accounted for at all. At the vents described in this study, areas covered by <25 cm of tephra were not mapped because the deposits were not preserved. This is especially true of the Collier Cone and Sand Mountain deposits, where steep slopes, vegetation, glacial erosion, and lava flows have obscured nearly all tephra <25 cm thick. Since the trace deposits were not mapped, tephra area and volume calculations listed in Table 3.1 represent minimum estimates. In this section, I use tephra deposits preserved in regional lake sediments, along with comparisons to other well-documented

cinder cone eruptions, to estimate the original extent of trace tephra deposits and to estimate maximum tephra volumes.

Tephra layers preserved in lake sediments and correlated to Collier Cone can be used to estimate the original extent of the Collier Cone deposit. Figure 3.13 shows isopachs based on tephra layers preserved in Camp Lake, Round Lake, Three Creek Lake, Todd Lake, and Tumalo Lake. Since these isopachs are poorly constrained by just one or two points rather than multiple thickness measurements, their shapes have been very roughly approximated as ellipses. Figure 3.14 shows thinning trends for the Four-in-One Cone, Collier Cone, and Sand Mountain deposits, based on the isopach maps in Figure 3.2. These trends were used to make minimum tephra volume estimates listed in Table 3.1. The dashed line in Figure 3.14 for Collier Cone represents the thinning trend based on trace deposit isopachs (Figure 3.13). Using the two thinning trends for Collier Cone, the estimated maximum volume for the deposit is 0.069 km^3 , nearly twice as large as the minimum estimate of 0.037 km^3 (Table 3.6).

To test the accuracy of extrapolating volume estimates based on just a few locations where trace deposits are preserved in lake sediments, I compare thinning trends and minimum and maximum volume estimates for historic 1995 eruption of Cerro Negro, Nicaragua (Hill et al., 1998) and the 1943-52 eruption of Paricutin, Mexico (Fries, 1953; Luhr and Simkin, 1993; Figure 3.14 and Table 3.6). Paricutin in particular is a good analog for Sand Mountain because the isopachs for both deposits cover similar areas (Figure 3.15). I also compare thinning trends and volumes for older, but well documented, eruptions of Cinder Cone, California, USA (Clynne and Muffler, 2010) and Sunset Crater, Arizona, USA (Ort et al., 2008; Figure 3.14 and Table 3.6). The extent of

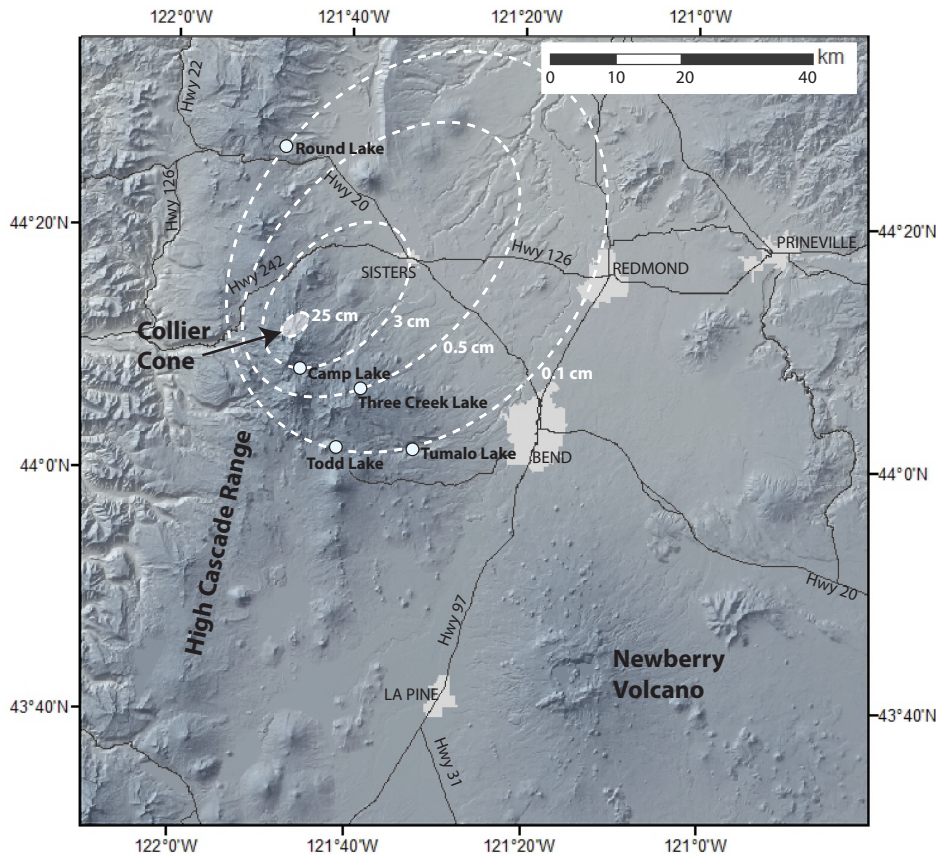


Figure 3.13. Estimated isopachs for trace deposits from Collier Cone, based on tephra preserved in Camp Lake, Round Lake, Three Creek Lake, Todd Lake, and Tumalo Lake.

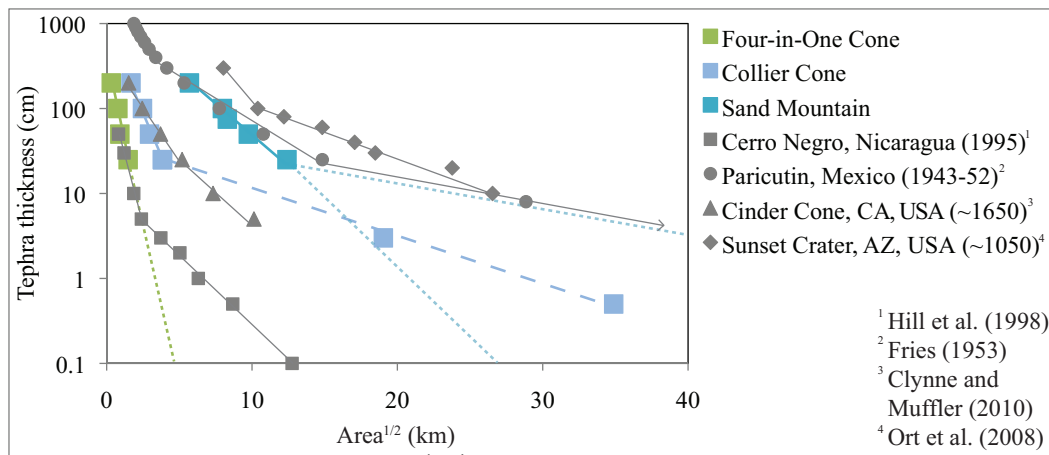


Figure 3.14. Plot showing thickness (cm) versus dispersal area ($Area^{1/2}$) for Cascade tephra deposits. Thinning trends for deposits produced by other cinder cone eruptions are shown in gray. For Cascade vents, points connected by solid lines are derived from isopachs ≥ 25 cm (Figure 3.2); Collier Cone points connected by the dashed line are derived from trace deposits preserved in lake sediments (Figure 3.13). The thinning trend for Paricutin, Mexico, extends to 0.1 cm, with a corresponding value of $242.24 \text{ km}^{1/2}$.

Table 3.6. Minimum and maximum volume estimates for tephra deposits.

Vent name	Minimum volume (km ³)	Maximum volume (km ³)
Four-in-One Cone	0.002	0.003
Collier Cone	0.037	0.069
Sand Mountain	0.387	1.13
Cerro Negro, Nicaragua (Hill et al., 1998)	0.002	0.003
Paricutin, Mexico (Fries, 1953; Luhr and Simkin, 1993)	0.325	1.3
Cinder Cone, USA (Clynne and Muffler, 2010)	0.024	0.035
Sunset Crater, USA (Ort et al., 2008)	0.486	0.972

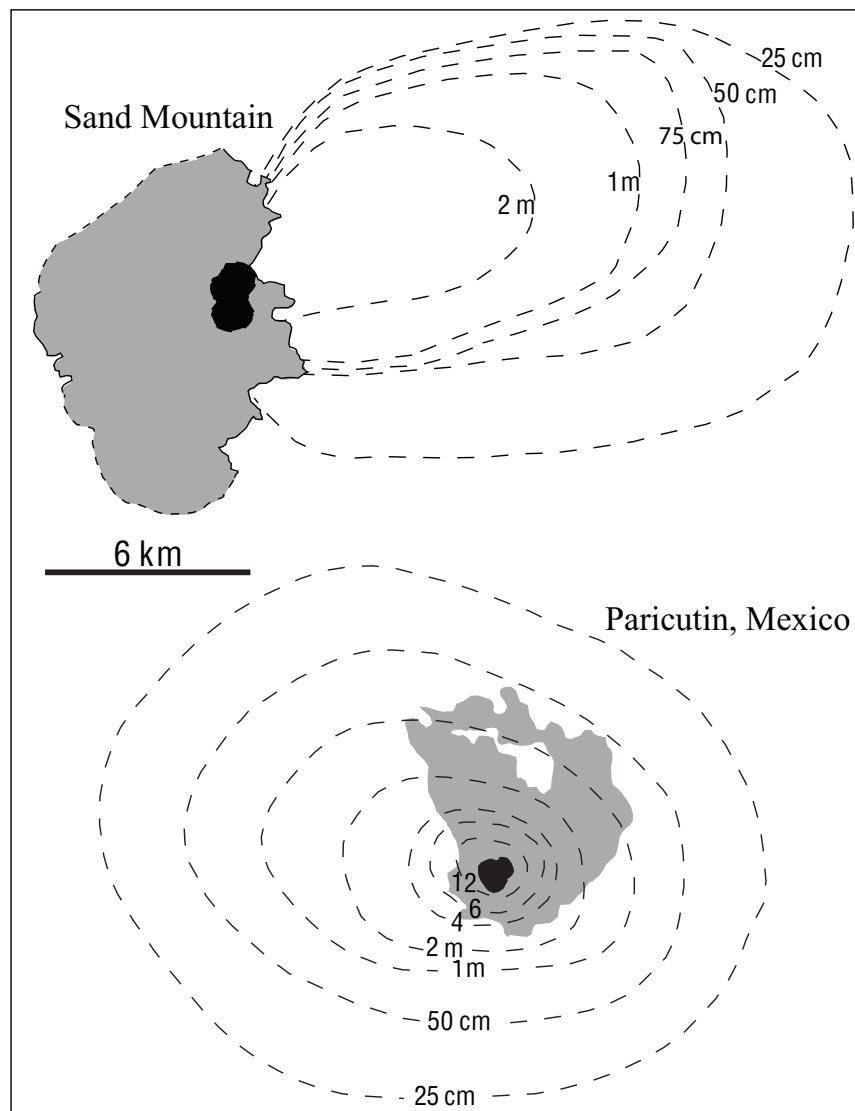


Figure 3.15. Isopach maps for Sand Mountain and Paricutin, Mexico. Black represents cinder cone vents, gray represents lava flows (Sand Mountain lava flows are after Deligne et al., 2012), dashed lines represent tephra thicknesses.

the tephra deposits produced by Cerro Negro and Parícutin are very well constrained because they were documented during or shortly after each eruption, before erosion or biotic activity could remove or rework portions of the deposits. Thus, volume estimates of the original tephra blankets, including trace deposits as thin as 0.1 cm, are much more accurate than at older vents. Cinder Cone and Sunset Crater are not historic eruptions, but the tephra deposits from these vents have been mapped to 5 cm at Cinder Cone and 10 cm at Sunset Crater (Clynn and Muffler, 2010; Ort et al., 2008).

Minimum volumes listed in Table 3.6 for Cerro Negro, Parícutin, Cinder Cone, and Sunset Crater represent estimates based only on areas covered by ≥ 25 cm of tephra and thus are comparable to minimum estimates for Four-in-One Cone, Collier Cone, and Sand Mountain. Maximum estimates are based on areas covered by the entire mapped deposits (≥ 0.1 cm for Cerro Negro and Parícutin, ≥ 5 cm for Cinder Cone, and ≥ 10 cm for Sunset Crater). These estimates range from 1.5 to 4 times larger than minimum estimates (Table 3.6), which implies that the maximum estimate for Collier Cone, based on limited locations where tephra is preserved in lake sediments, is reasonable.

Trace deposits of tephra from Four-in-One Cone and Sand Mountain were not identified in regional lakes cored as part of this study, so maximum volumes cannot be estimated from tephra preserved in lake sediments. Instead, the thinning trends for trace deposits from Cerro Negro and Parícutin (Figure 3.14) are used to make maximum volume estimates for Four-in-One Cone and Sand Mountain. These vents are good proxies because the thinning trends for deposits ≥ 25 cm are very similar (Figure 3.14). Based on the Cerro Negro and Parícutin thinning trends, maximum volume estimates for Four-in-One Cone and Sand Mountain are 0.003 km^3 and 1.13 km^3 , respectively (Table

3.6). Although this approach is an improvement on the minimum estimates in Table 3.6, these maximum volumes are still likely to be underestimated because they do not account for tephra deposited to the west of the vents, where steep topography, vegetation, or lava flows obscured the original deposits.

The differences between minimum and maximum volume estimates in Table 3.6 are significant, especially for vents where very thin (0.1 cm) trace deposits can be measured. These deposits cover large areas and contribute substantially to the total volume. Using historic eruptions as proxies for older eruptions demonstrates that if trace deposits are not accounted for, tephra volumes can be significantly underestimated. This is true even for relatively young vents (≤ 3000 years) like Collier Cone and Sand Mountain, where tephra blankets preserved on dry land do not accurately record the original volume of the deposit. Since tephra production represents the most explosive phases of activity, interpretation of eruption styles are likely to be skewed toward less explosive eruptions if no attempt is made to estimate the original extent of trace deposits.

3.5.2. Interpretation of Eruption Styles

As discussed earlier in this section, the classification system described by Walker (1973) uses the degree of fragmentation to infer eruption style. From this perspective, large tephra clasts indicate low fragmentation efficiency and small clasts indicate high fragmentation efficiency and thus more explosive eruptions. Additionally, alternating layers of ash and lapilli indicate changes in eruption style throughout the duration of activity. Physical characteristics of the juvenile components of tephra deposits can be used to further quantify differences between eruption styles. Highly vesicular clasts are

produced during energetic phases of activity with high lava flux, while less vesicular clasts are produced during phases of low energy and low lava flux (e.g. Heiken, 1978; Pioli et al. 2008).

Detailed examinations of the tephra deposits presented here indicate that the Four-in-One Cone eruption was characterized by low-energy strombolian activity, the Collier Cone eruption by high-energy strombolian to violent strombolian activity, and the Sand Mountain eruption by violent strombolian activity that may have been particularly explosive due to syn-eruptive interaction with water. These interpretations are made based on the physical characteristics of tephra clasts, the volumes of erupted products, and interpretations of various mafic eruption styles from the literature. Interpretations of eruption styles for vents of the northwest zone of Newberry Volcano, discussed in Chapter II, are also used to draw comparisons between cinder cone vents at Newberry and in the High Cascades.

Four-in-One Cone shares characteristics with both the Lava Cascade vent and the South Sugarpine vent at Newberry Volcano (Chapter II, Sections 2.4.1 and 2.5.4). Like the South Sugarpine vent, Four-in-One Cone produced small cinder cones and a limited tephra blanket, although the volumes of both cone material and tephra for Four-in-One Cone are greater than South Sugarpine vent. The Four-in-One Cone deposit is dominated by tan, highly vesicular sideromelane clasts that are similar in appearance to those of the South Sugarpine deposit. However, the Four-in-One Cone deposit also contains glassy, highly vesicular, angular clasts that have ragged edges, similar to those of the Lava Cascade deposit and indicative of fire-fountaining activity (e.g. Parfitt, 1998; Parfitt, 2004; Francis and Oppenheimer, 2004; Valentine and Gregg, 2008; Stovall et al., 2010).

Mean clast size (Md_n) and sorting coefficients (σ_n) for the Four-in-One Cone deposit range between those of the Lava Cascade and South Sugarpine deposits and plot within the fields defining both hawaiian and strombolian eruption styles (Figure 3.4). Together, the grain size distributions, sorting, and componentry of the Four-in-One Cone deposit indicate the eruption was characterized by phases of both hawaiian and strombolian activity. The elongate shape of Four-in-One Cone is consistent with this interpretation. The eruption occurred from multiple vents along a fissure system and constructed a series of overlapping cones ~1 km long (Figure 3.2). During phases of vent migration along this fissure system, the eruption was likely characterized by bursts of fire-fountaining activity that produced tephra deposits consistent with hawaiian-style eruptions. However, the overlapping cinder cones that make up Four-in-One Cone indicate that activity became focused at individual vents several times throughout the eruptive episode. The construction of small cinder cones, as opposed to spatter ramparts or spatter cones, during these phases of activity indicate that eruption intensity increased from hawaiian-style fire-fountaining to low-energy strombolian activity (e.g. McGetchin et al., 1974; Francis and Oppenheimer, 2004; Parfitt, 2004; Valentine and Gregg, 2008). The limited Four-in-One Cone tephra deposit was likely produced during these low-energy strombolian phases of activity.

Collier Cone shares characteristics with Lava Butte at Newberry Volcano (Chapter II, Sections 2.4.1 and 2.5.4) in that both vents produced relatively large cinder cones and tephra deposits characterized by alternating layers of lapilli and ash. Mean clast size (Md_n) and sorting coefficients (σ_n) for the Collier Cone deposit are similar to those of Lava Butte and plot within the fields defining both strombolian and violent

strombolian eruption styles (Figure 3.4). The alternating lapilli and ash layers exposed in sample trench CC-01-09 (Figure 3.2), along with the generally well-sorted nature of the deposit, indicate that phases of activity were characterized by rhythmic pulses of explosive activity, efficient fragmentation, and deposition from well-developed eruption columns (e.g. Pioli et al.; Valentine and Gregg, 2008). Together these indicate that, like Lava Butte, the Collier Cone eruption was characterized by intermittent phases of both strombolian and violent strombolian activity. However, the minimum volume estimate of the Collier Cone tephra deposit is an order of magnitude larger than that of Lava Butte, and the tephra blanket covers a larger area. This could be the result of better preservation at Collier Cone because it is younger (~1600 yr B.P., as opposed to ~7000 yr B.P. for Lava Butte), but the difference in size suggests that even if the Lava Butte deposit has been significantly eroded or reworked, the original deposit was likely much smaller than that of Collier Cone. Greater tephra production at Collier Cone implies either longer or more frequent phases of explosive violent strombolian activity.

The Sand Mountain tephra deposit is unlike any other cinder cone deposit described in Chapters II and III. It is comparable in volume and extent to the deposit produced by Paricutin, Mexico (Figure 3.14 and Table 3.6), which is often described as a “type” example of violent strombolian activity (e.g. Macdonald, 1972; Walker, 1973; Pioli et al., 2008). This, along with the uniformly small grain size and very well sorted nature of the Sand Mountain deposit indicates that the eruption was characterized by highly explosive activity similar to that described as violent strombolian (e.g. Pioli et al.; Valentine and Gregg, 2008). However, violent strombolian activity is strongly pulsatory, which produces tephra deposits characterized by multiple layers of fine to coarse ash and

lapilli (e.g. Pioli et al.; Valentine and Gregg, 2008). The Sand Mountain deposit differs from violent strombolian deposits in that it is composed entirely of ash; lapilli sized clasts are completely absent. This indicates that highly explosive activity was sustained rather than pulsatory. Additionally, Sand Mountain tephra clasts are characterized by blocky, equant shapes and are denser than clasts observed in typical strombolian and violent strombolian deposits. Both these characteristics suggest that interaction with water may have occurred during tephra-producing phases of the eruption (e.g. Büttner et al., 1999; Dellino and Kyriakopoulos, 2003). Although the Sand Mountain eruption appears to have been similar to that of Paricutin in terms of the volume of tephra that was produced, interaction with external water may have contributed to phases of activity more explosive than violent strombolian (i.e. subplinian).

3.5.3. Implications for Hazards

Although the cinder cones in this study are not located near populated areas, the central section of the Cascade arc is characterized by hundreds of other cinder cone vents, many of which are located in or near large population centers (Figure 3.1). The presence of multiple volcanic fields means that future activity is likely and could anywhere in the region, in close proximity to urban areas. Such activity would pose significant hazards to regional transportation, infrastructure, agriculture, and public health. The Sand Mountain eruption, for example, occurred <5 km from a popular ski area and one of the major east-west transportation corridors across the state of Oregon. Lava flows from the Sand Mountain vents covered areas that are now transected by multiple sections of the state highway system and several flows dammed the McKenzie River system. If such an

eruption were to occur today, lava flows would severely impact transportation and drinking water supplies; tephra production would bury large sections of major transportation routes and tourist destinations in >25 cm of tephra, and, depending on wind directions, would likely deposit trace thicknesses in urban areas.

Despite the abundance of past mafic activity in the region, the hazards posed to central Oregon communities by cinder cone eruptions have not been fully addressed. In particular, only a few of the tephra deposits produced by regional cinder cones have been mapped, despite the fact that determining the volume and extent of these deposits is necessary for assessing eruptive histories and volcanic hazards. In addition to mapping tephra deposits from regional cinder cones, it is also important to consider the original extent that these deposits might have covered. As shown in Figures 3.13 and Table 3.6, trace deposits can cover large areas and contribute significantly to the total volume of the deposit. Since common classification systems for eruption style (e.g. Walker, 1973) depend entirely on quantifying tephra production, accurate tephra volume estimates are necessary. Additionally, identifying trace deposits is important because even very small amounts of tephra (<1 cm) can impact transportation, agriculture, and public health. Thus, from a hazards perspective, it is important to determine the extent of trace deposits produced by Cascade cinder cones. This work also has broader impacts for hazard assessments in cinder cone fields worldwide, where challenges in reconstructing tephra deposits due to poor preservation make hazards assessments difficult.

3.6. Conclusions

By focusing in detail on tephra produced by Cascade cinder cones, I have shown that: 1) a range of eruption styles has occurred at recent Cascade vents, ranging from low-energy strombolian activity at Four-in-One Cone to highly explosive violent strombolian and perhaps subplinian activity at Sand Mountain; 2) tephra layers preserved in sediments from regional lakes can be used to estimate the original extent of Cascade deposits that have been eroded or reworked; and 3) trace tephra deposits contribute significantly to the total volume of tephra produced by cinder cones, thus volume estimates that do not include trace deposits have the potential to be significantly underestimated.

Establishing the range of eruption styles that have occurred at recent mafic vents in the Cascades is important in terms of hazard assessment. The results reported here show that at least two recent mafic vents in the central Oregon Cascades (Collier Cone and Sand Mountain) produced a significant tephra blanket and could have easily deposited trace amounts of tephra on modern urban areas. Future mafic activity in this section of the Cascades is likely and could occur anywhere within a broad region; for this reason, it is important that communities in central Oregon are prepared for renewed mafic activity, including tephra production.

Preservation of trace deposits in lake sediments has important implications for reconstructing tephra deposits that have been eroded or reworked by biotic activity. The work reported here shows that tephra deposits <25 cm thick can contribute up to 75% of the total volume of the deposit. Since thin deposits can be easily eroded or reworked in relatively short periods of time, this suggests that tephra production at many cinder cone vents worldwide has been significantly underestimated. Traditional classification systems

of eruption style are based solely on tephra production, thus inaccurate estimates of tephra deposits could result in a general interpretation that cinder cones are rarely explosive. Examining nearby lakes, seasonal meadows, and fens for tephra layers preserved in wet sediments offers a potential solution to the problem of reconstructing the extent of original deposits that have since been eroded or reworked.

3.7. Bridge Between Chapter III and Chapter IV

In Chapter III, I presented isopach maps and physical descriptions of tephra for three recent cinder cone eruptions in the central Oregon High Cascades. I use these data to infer eruption styles and to show that each cinder cone was characterized by a different style of activity. One of the most intriguing results of this work is the mapping of the widespread and fine-grained tephra deposit produced by Sand Mountain. To understand the dynamics that produced this unusual tephra deposit, further investigation into the Sand Mountain eruption is needed. In Chapter IV, I build upon Chapter III by examining the Sand Mountain eruption in detail and investigating the role that syn-eruptive interaction with water played in the production of such an unusually large, fine-grained tephra deposit. As in Chapters II and III, this investigation is used to draw attention to the range of activity that can occur at mafic vents and the importance of addressing the hazards of mafic eruptions in the Cascades.

CHAPTER IV

EVIDENCE FOR WATER-MAGMA INTERACTION DURING THE SAND MOUNTAIN CINDER CONE ERUPTION, CENTRAL OREGON CASCADES

This chapter is in preparation for publication in *Geology*. Coauthor K.V. Cashman provided editorial assistance and guidance during analytical work. I performed the field and laboratory work and was the primary author.

4.1. Introduction

The large volume and unusually small grain size of the Sand Mountain tephra deposit indicate this eruption was characterized by energetic, explosive behavior similar to what has been described as violent Strombolian or subplinian (e.g. Arrighi et al., 2001; Pioli et al. 2008; Valentine and Gregg, 2008). These types of explosive mafic eruptions are often driven by high pre-eruptive volatile contents (e.g. Johnson et al., 2008; Pioli et al., 2009), but pre-eruptive H₂O and CO₂ contents measured from olivine-hosted melt inclusions from Sand Mountain are comparable to those of other Cascade cinder cones that did not produce such large-volume, fine-grained tephra deposits (Ruscitto, 2010).

The unusual nature of the Sand Mountain deposit prompted an investigation on the effect that syn-eruptive interaction with water might have had on tephra production. The 2010 eruption of Eyjafjallajökull, Iceland, demonstrated that interaction with external water (in this case glacial melt water) generates large amounts of very fine-grained tephra. Similar eruptions could occur in the Cascades and would have severe

regional consequences, especially on air transportation. For this reason, I examine the role that external water might have played in the Sand Mountain eruption. I also assess the possible sources of water that might have fueled phreatomagmatic activity.

4.2. Background

Phreatomagmatic activity occurs when rising magma interacts with external water at or near the surface of the earth, producing steam explosions that violently fragment the magma (e.g. Sheridan and Wohletz, 1983; Wohletz and McQueen, 1984). This activity differs from magmatic eruptions, which are driven solely by the exsolution of volatiles (primarily H₂O and CO₂) from the melt. If surface or groundwater is available in the vent area during eruptive activity, both processes can occur simultaneously and persist throughout the eruptive episode. The presence of external water greatly increases the fragmentation efficiency of phreatomagmatic eruptions as compared to volatile driven eruptions. Two different mechanisms are variously thought to exert the most control on increased magma fragmentation in the presence of external water: 1) fuel-coolant interaction (FCI) processes, which are driven by the water/melt mass ratio and contact geometry of the rising melt with water (e.g. Wohletz and Sheridan, 1983; Wohletz and McQueen, 1984); and 2) interactions between magma and impure coolants, or sediment-laden water, where sediment particles enhance fragmentation and the ability of magma to mix with large volumes of coolant (e.g. White, 1996; Schipper et al., 2011).

The nature of phreatomagmatic deposits is controlled by the overall energy of the system, with tuff rings, tuff cones, pyroclastic surge deposits, and maars resulting from the most explosive interactions (e.g. Waters and Fisher, 1971; Wohletz and McQueen,

1984). Since fragmentation during this type of activity is closely linked to the degree of magma interaction with water, sorting and grain size distributions of pyroclastic deposits can be used to identify the extent of water-magma interactions (e.g. Waters and Fischer, 1971; Sheridan and Wohletz, 1983; Fisher and Schmincke, 1984), as can microtextural textural characteristics of the ash particles (e.g. Wohletz 1983; Büttner et al., 1999; Dellino and Kyriakopoulos, 2003; Heiken, 1972).

As discussed in Chapter III, the tephra deposit produced by Sand Mountain is strikingly different from tephra deposits produced by other mafic vents in the central Oregon Cascades in that it is much larger in volume, more widespread, and uniformly smaller in grain size (Chapter III, Figures 3.2, 3.4, 3.6, and Table 3.1). These characteristics all indicate that rising magma may have interacted with water during the Sand Mountain eruption. To evaluate this possibility, I compare volumes, grain sizes, and sorting of the Sand Mountain deposit to deposits from other mafic vents in the Cascades that do not show indications of interacting with water. I also compare microtextural features of Sand Mountain tephra to tephra from Collier Cone, where there is no indication that interaction with water occurred, and to tephra from the 2010 eruption of Eyjafjallajökull, Iceland, where interaction with water did occur. These comparisons are used to identify microtextural features of Sand Mountain tephra that are indicative of water-magma interaction. Finally, I consider possible external water sources that might have interacted with the Sand Mountain eruption and evaluate the likelihood of each water source based on physical characteristics of the tephra deposit.

4.3. Methods and Results

Sampling and analytical methods for quantifying characteristics of the Sand Mountain tephra deposit, as well as tephra deposits from other cinder cone vents in the Cascades, are described in detail in Chapter III, Section 3.3. In this chapter, I compare the results of these analyses to other phreatomagmatic deposits documented in the literature. In particular, I use the 2010 eruption of Eyjafjallajökull as a comparison because activity was characterized by two distinct phases: 1) an early phase during which explosive activity was entirely volatile driven; and 2) a later phase during which highly explosive activity was primarily phreatomagmatic (Figure 4.1). Thus, tephra clasts from Eyjafjallajökull show characteristics of both magmatic and phreatomagmatic fragmentation. Additionally, the effects of widespread ash dispersal from the Eyjafjallajökull eruption are well documented and provide a good comparison for hazards posed by potential phreatomagmatic activity in the Cascades. Samples from Eyjafjallajökull are courtesy of M. Pistolesi at the Università di Pisa, Italy. Figure 4.1 shows the location of the 2010 vents and locations where tephra samples were collected. Representative clasts from these samples, along with clasts from the complete stratigraphy of the Sand Mountain deposit (Chapter III, Figure 3.6) and clasts from Collier Cone (Chapter III, Figure 3.5), were examined in backscattered imaging mode on a FEI Quanta 200 FEG Environmental SEM at the University of Oregon.

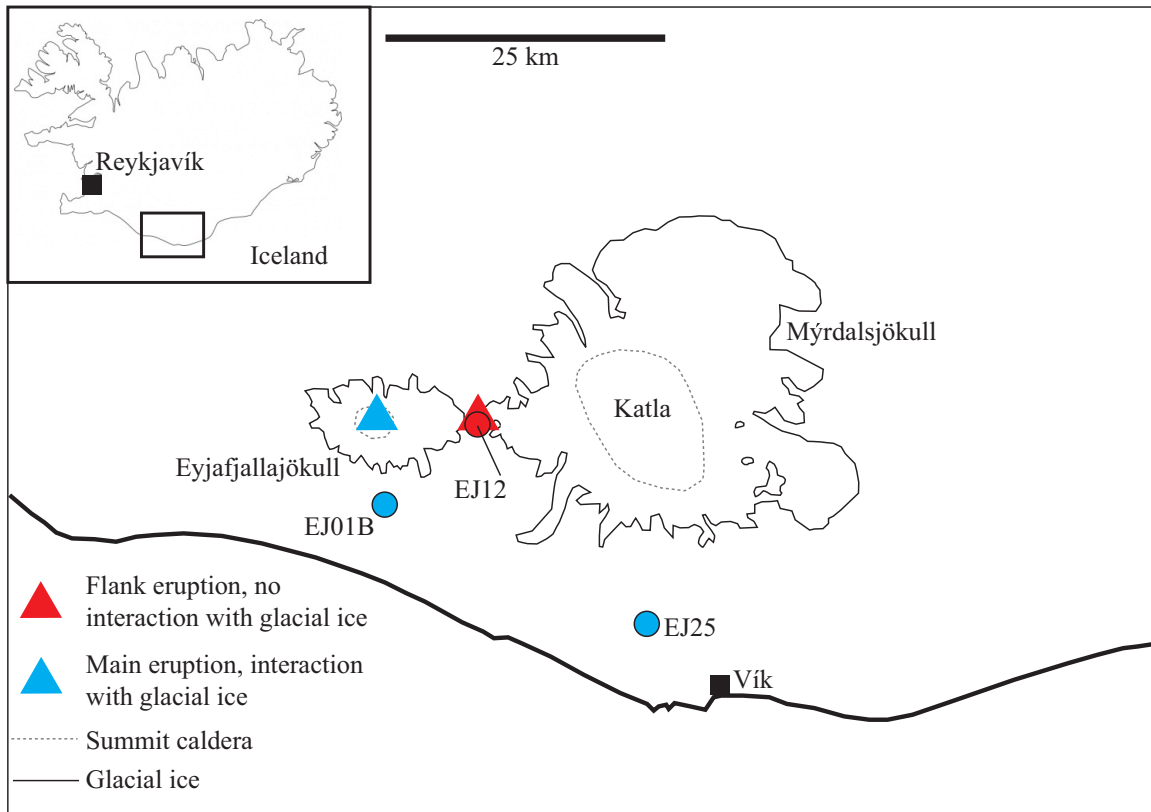


Figure 4.1. Map showing the locations of the 2010 eruption of Eyjafjallajökull, Iceland. Circles indicate locations where tephra was sampled during magmatic activity (red) and phreatomagmatic activity (blue). Tephra samples are courtesy of M. Pistolesi.

4.3.1. Typical Cascade Cinder Cone Deposits

The cinder cones described in Chapters II and III produced small tephra deposits ($<0.1 \text{ km}^3$) dominated by well sorted to poorly sorted layers of predominantly lapilli-sized clasts (Figure 4.2). The Collier Cone deposit, which is the largest measured from central Oregon cinder cones (aside from Sand Mountain), has a volume of $\sim 0.07 \text{ km}^3$. Traceable tephra deposits from central Oregon cinder cones rarely extend beyond a few km from the vent, except where thin tephra layers can be identified in lake sediments (e.g. Collier Cone; Chapter III). Moreover, significant thicknesses ($\geq 25 \text{ cm}$) of tephra are limited to areas $<5 \text{ km}$ from the vent.

4.3.2. Sand Mountain – An Unusual Tephra Deposit

The Sand Mountain eruption produced at least $\sim 0.4 \text{ km}^3$ of tephra based on the isopach map in Chapter III (Figure 3.2). However, this value is likely significantly underestimated because it does not account for tephra deposited to the west of the vents, or for deposits $< 25 \text{ cm}$ thick. Comparisons with other tephra deposits of similar size suggest that $\sim 1 \text{ km}^3$ is a reasonable estimate for the Sand Mountain deposit (Chapter III; Table 3.6). In addition to having a much larger volume than other Cascade cinder cones, the Sand Mountain tephra deposit is also much more widespread. The area covered by $\geq 200 \text{ cm}$ of tephra at Sand Mountain is covered by $< 20 \text{ cm}$ at Collier Cone (Chapter III, Figure 3.2). The 25 cm isopach for the Sand Mountain deposit extends up to $\sim 18 \text{ km}$ from the vent, as opposed to $\sim 5 \text{ km}$ from the vent at Collier Cone (Chapter III, Figure 3.2). Trace deposits from Sand Mountain have not been identified, but they presumably extended much farther (see comparisons to Parícutin, Mexico; Chapter III, Section 3.5.1). The large volume and widespread area covered by the Sand Mountain deposit indicate that the eruption was much more explosive than other cinder cone eruptions described in this study.

In addition to producing an unusually large volume of tephra, the Sand Mountain eruption also produced uniformly fine-grained clasts. Figure 4.2 shows grain sizes and sorting coefficients for Cascade cinder cones, including Sand Mountain and Collier Cone. The Sand Mountain deposit is very well sorted and is dominated by ash-sized (4 to 1ϕ) rather than lapilli-sized clasts (Figure 4.2). Activity at other Cascade cinder cones can be described as hawaiian, strombolian, or violent strombolian based on the grain size and sorting of the deposits, but the majority of the Sand Mountain deposit does not fall into

any of these fields. Grain size and sorting data from Taal, Philippines, is also shown in Figure 4.2 (Water and Fisher, 1971). This eruption was characterized by phreatomagmatic activity that produced wet pyroclastic surge deposits. Although the Sand Mountain deposit resembles Taal in terms of grain size distributions, Sand Mountain tephra layers are much better sorted. As discussed in Chapter III (Section 3.4.2.3), individual layers within the deposit are very thin (millimeters to centimeters), laminar, and show no cross stratification. These bedding features, along with the extremely well-sorted nature of the deposit, indicate that the Sand Mountain sequence is dominated by fall deposits rather than pyroclastic surge deposits, which are characterized by cross-bedding and poorly-sorted layers (Figure 4.2).

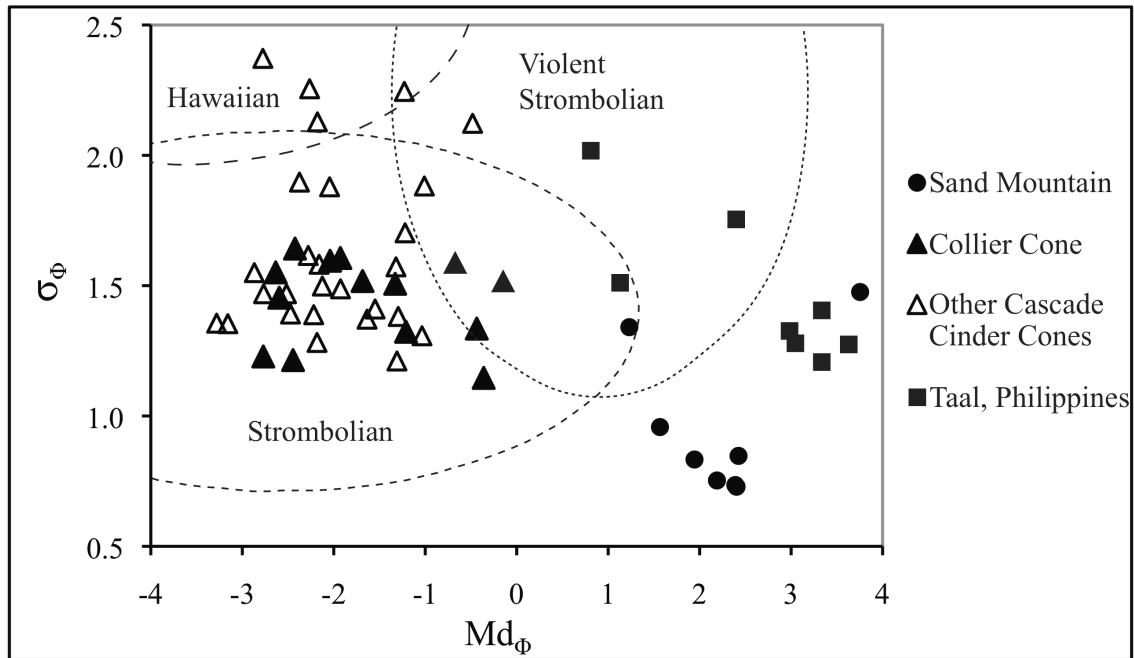


Figure 4.2. Inman sorting coefficients (σ_e) and median grain sizes (Md_e) for tephra deposits from Sand Mountain, Collier Cone, and other cinder cones in the central Oregon Cascades (Chapters II and III). Fields defining eruption styles are after Walker and Croasdale (1972), Parfitt (1998), Houghton and Gonnermann, (2008), and Pioli et al. (2008). Data from Taal, Philippines, represents phreatomagmatic activity that produced wet surge deposits (Water and Fisher, 1971).

4.3.3. Microtextural Characteristics of Tephra

SEM images of tephra clasts from Eyjafjallajökull, Collier Cone, and Sand Mountain are shown in Figure 4.3. Tephra clasts from the early phase of activity at Eyjafjallajökull, before interaction with glacial ice occurred, have rounded or fluidal shapes and abundant microvesicles (Figure 4.3A). Tephra produced by Cascade cinder cones (Chapters II and III), represented here by clasts from Collier Cone, are highly vesicular and frothy in appearance (Figure 4.3B). Like magmatic Eyjafjallajökull clasts, they have fluidal shapes and abundant microvesicles. In contrast, phreatomagmatic phases of the Eyjafjallajökull eruption produced denser clasts with blocky, equant shapes and stepped fractures (Figure 4.3C), all characteristics of brittle fragmentation caused by interaction with water (e.g. Wohletz 1983; Büttner et al., 1999; Dellino and Kyriakopoulos, 2003; Heiken, 1972). Sand Mountain clasts show similar blocky, equant shapes and fractured surfaces, as well as a paucity of vesicles (Figure 4.3D). Additionally, clast surfaces show evidence of very fine micro-scale cracking that indicates rapid quenching by water (Figure 4.3E; e.g. Büttner et al., 1999; Dellino and Kyriakopoulos, 2003). Importantly, these microtextural features are present throughout the entire stratigraphy of the Sand Mountain deposit.

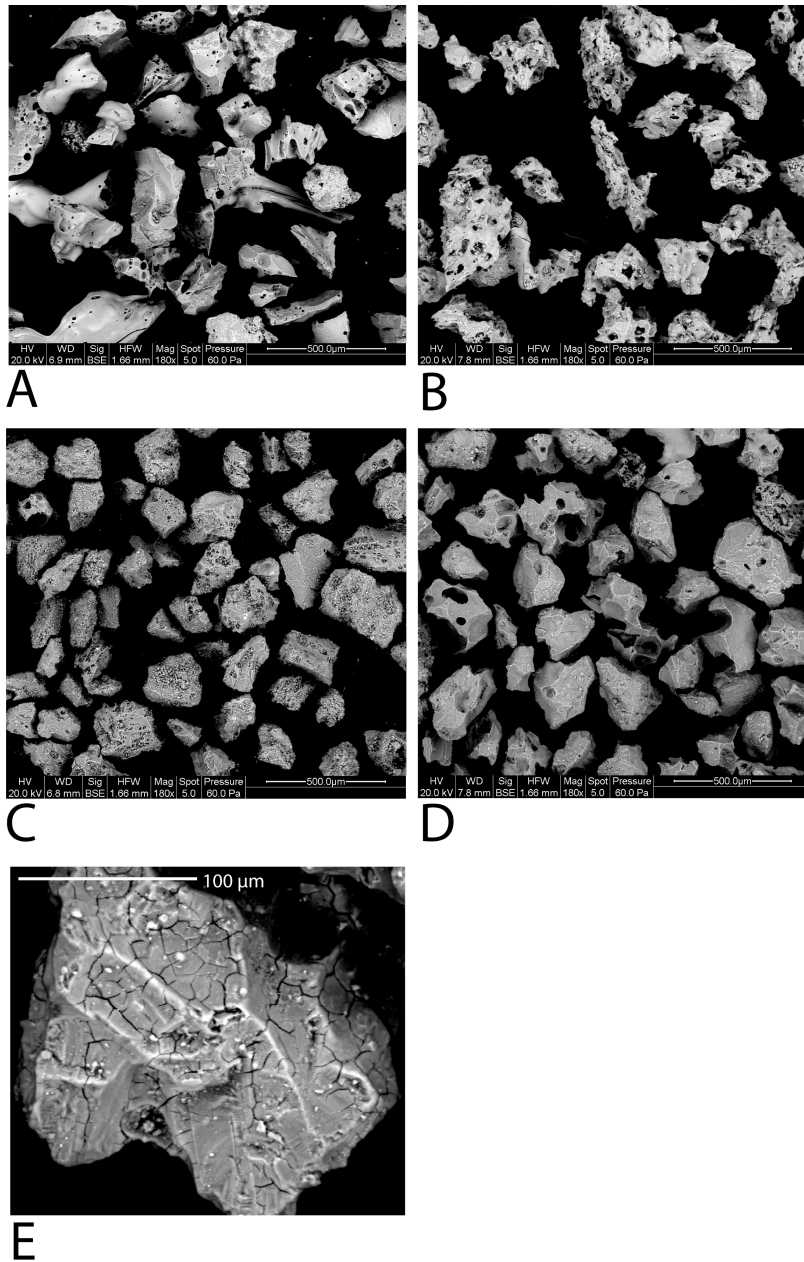


Figure 4.3. SEM images of tephra clasts from Eyjafjallajökull, Iceland, Collier Cone, and Sand Mountain. (A) Magmatic clasts from Eyjafjallajökull are highly vesicular and have fluidal shapes. (B) Clasts from Collier Cone resemble magmatic clasts from Eyjafjallajökull in being highly vesicular with fluidal shapes. (C) Phreatomagmatic clasts from Eyjafjallajökull are denser than magmatic clasts and have blocky, equant shapes and stepped fractures indicative of brittle fragmentation (e.g. Wohletz 1983; Büttner et al., 1999; Dellino and Kyriakopoulos, 2003; Heiken, 1972). (D) Clasts from Sand Mountain also have blocky, equant shapes and stepped fractures. (E) Sand Mountain clast showing micro-scale cracking that indicates rapid quenching by water (e.g. Büttner et al., 1999; Dellino and Kyriakopoulos, 2003).

4.4. Discussion

Microtextural characteristics of the Sand Mountain tephra clearly show that magma interacted with water, resulting in a protracted and highly explosive tephra-producing eruption. There is no evidence of tuff cones, tuff rings, or maars associated with the Sand Mountain vents. Additionally, although the deposit is characterized by hundreds of finely laminated ash layers, there is no evidence of wet pyroclastic surge deposits. Together these observations indicate the eruption was characterized by phreatomagmatic activity, but that ash particles were transported by an eruption column rather than by wet base surges typically associated with phreatomagmatic eruptions. The eruption may have been similar to phreatomagmatic phases of the 2010 Eyjafjallajökull eruption. Fall deposits from Eyjafjallajökull sampled 9-10 km from the vent in the direction of dispersal (i.e. a comparable location to the Sand Mountain sample trench described in Chapter III, Section 3.4.2.3) are well sorted, fine-grained, completely dominated by ash-sized clasts (3 to 1 ϕ), and contain very rare lapilli (Dellino et al., 2012). Grain size distributions reported in Dellino et al. (2012) are very similar to those of Sand Mountain (Chapter III, Figure 3.6). However, the volume of tephra produced by Sand Mountain is considerably larger than Eyjafjallajökull (at least $\sim 0.4 \text{ km}^3$ and likely $\sim 1 \text{ km}^3$, compared to $\sim 0.14 \text{ km}^3$ for Eyjafjallajökull; Gudmundsson et al., 2011). This indicates that either the Sand Mountain eruption was much more explosive, or that activity was prolonged over a longer period of time.

The Eyjafjallajökull eruption demonstrated the hazards associated with fall deposits produced by phreatomagmatic activity. Since it is apparent that this type of activity occurred at Sand Mountain, but likely on a larger scale, it is important to

determine the source of water that interacted with the vents. Possible water sources in the region include glaciers, heavy winter snowpack, surface water, and groundwater. In the following section I examine each of these possibilities to evaluate their likelihood as a water source during the Sand Mountain eruption.

4.4.1. Glacial Ice and Snow in the Central Oregon High Cascades

Glacial ice in the central Oregon Cascades is presently limited to elevations above ~2300 m, well above the elevation of the Sand Mountain vents (1450 m). The eruption occurred during the Neoglacial phase of ice advance, ~2 to 8 ka in central Oregon, but this advance did not reach the elevation of the vents (Marcott et al., 2009). Thus, interactions with glacial ice can be ruled out. However, the region receives heavy annual snowfall. More than 75% of the annual precipitation falls during winter months, most of which falls as snow at Sand Mountain. To estimate average snowpack in the vent region during the time of the eruption, modern mean monthly precipitation and temperature data were obtained from the Hogg Pass station of the Natural Resources Conservation Service SNOTEL network, located ~6 km northeast of Sand Mountain and at the same elevation as the base of the cinder cones. Data from 1980 to 2010 record maximum snow water equivalent depths of ~1.5 m (Figure 4.4), which convert to a maximum snow depth of ~4 m (spring snowpack with 40% density). Based on reconstructions of equilibrium-line altitudes during the Neoglacial, winter snowfall was ~23% greater than present and summer temperatures were ~1.4 °C cooler (Marcott et al., 2009). This suggests that at the time of the Sand Mountain eruption, winter and spring snow depths could have been ≥ 5 m. Cooler temperatures would have resulted in earlier accumulation of snow during

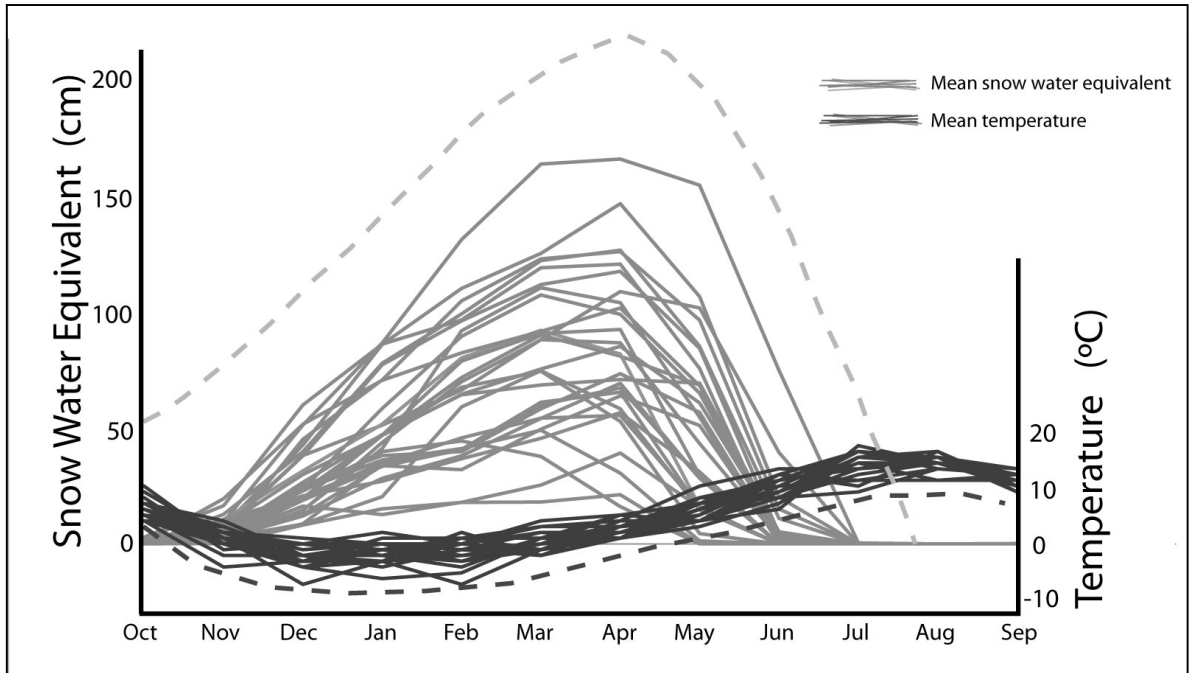


Figure 4.4. Historic records and Neoglacial estimates for snowpack and temperatures in the central Oregon Cascades. Solid gray lines represent mean snow water equivalents from 1980 to 2010 (data from the Natural Resources Conservation Service SNOTEL network). The dashed gray line represents Neoglacial snow water equivalents, which are estimated at ~23% greater than present (Marcott et al., 2009). Solid black lines represent mean temperatures from 1980 to 2010 (data from the Natural Resources Conservation Service SNOTEL network). The dashed black line represents Neoglacial temperatures, which are estimated at ~1.4 °C colder than present (Marcott et al., 2009).

autumn months and later melting during summer months (Figure 4.4). If the Sand Mountain eruption occurred during winter or spring, heavy accumulations of snow could have contributed to phreatomagmatic activity.

Syn-eruptive interaction with deep snow could cause phreatomagmatic activity for a limited time, but as the eruption progressed the availability of melt water would quickly decrease. Construction of a cinder cone would further restrict interaction between melt water and magma at the vent. In this scenario, as the eruption continued there would likely be a transition from phreatomagmatic to magmatic activity, as evidenced by a

change in grain size and clast characteristics (e.g. Dellino et al., 2012). The Sand Mountain deposit is consistently well sorted and fine-grained, with tephra clasts that exhibit microtextural features indicative of syn-eruptive interactions with water throughout the entire stratigraphy of the deposit (Figures 4.2 and 4.3). This consistency in sorting, grain size distribution, and microtextural features indicates that phreatomagmatic occurred throughout all the phases of tephra production. Thus, although deep snow may have contributed to phreatomagmatic activity early in the eruption, water continued to be available after the supply of snow would have been exhausted. It is possible that magma interacted with heavy winter or spring snowpack during early phases of activity, but snowmelt was not the dominant source of water throughout the eruption.

4.4.2. Surface and Groundwater Patterns in the Central Oregon High Cascades

The central Oregon High Cascades are characterized by a complex relationship between young mafic lava flows and groundwater flow. Discharge from spring systems on both the east and west slopes of the High Cascades indicate that much of the regional precipitation flows as groundwater through young permeable lava flows (e.g. Manga, 1997; James et al., 2000; Gannett and Lite, 2004; Jefferson et al., 2006). Surface runoff is largely absent, although there are perched lakes throughout the High Cascades. Most of these lakes are dammed by lava flows and have no outlets, indicating that water percolates through the lava dams and enters the groundwater system.

Perched lakes and fens presently exist in the Sand Mountain region and likely existed during the time of the eruption. Although lakes or fens could have supplied external water during eruptive activity, characteristics of the Sand Mountain deposit

suggest this was not the case. Phreatomagmatic eruptions that interact with large volumes of surface or groundwater (i.e. supplied by a lake or by water-saturated sediments) typically produce wet pyroclastic surge deposits that are poorly sorted and display surge bedforms (e.g. the Taal deposit; Figure 4.2). The well-sorted layers, uniformly ash-sized clasts, and lack of surge bedforms in the Sand Mountain deposit are all characteristic of fall deposits rather than a surge deposits. Thus, large lakes or water-saturated sediments can be eliminated an external water source during the eruption. A small lake or fen could have supplied limited water during early phases of activity, but would have been exhausted as the eruption continued. Since the Sand Mountain deposit shows evidence of phreatomagmatic activity throughout the duration of tephra production, but no evidence of wet surge deposits, the water supply was likely small in volume but was continuously being supplied to the vent area. This suggests that groundwater, rather than surface water, played an important role during eruptive activity.

Hydrologic studies show that water sourced in the Sand Mountain area is discharged from springs and seeps into Clear Lake, directly west of the Sand Mountain vents, and into the upper McKenzie River channel (Jefferson et al., 2006). The combined mean discharge from these springs is $\sim 14.5 \text{ m}^3/\text{s}$. The estimated thickness of the aquifers ranges from ~ 30 to 120 m and they are thought to follow shallow flow paths controlled by extensive young lava flows. Seepage velocities for these aquifers are estimated to range between 1×10^{-6} and $7 \times 10^{-6} \text{ m/s}$. Moreover, the total discharge measured from springs is greater than the amount of precipitation received by individual catchments, indicating that additional groundwater is supplied from outside the catchment boundaries and suggesting that the complex stratigraphy of lava flows in the Sand Mountain region

plays a more important role in controlling regional water flow than surface topography.

The aquifers in the Sand Mountain area described by Jefferson et al. (2006) are contained within the Sand Mountain lava field. This field is mapped as originating from the Sand Mountain vents (Sherrod et al., 2004; Jefferson et al., 2006), although recent detailed mapping of individual flows shows that some of the lava flows pre-date tephra-producing phase of the Sand Mountain eruption (N. Deligne, personal communication). Pleistocene basalt flows, which probably contain aquifers similar to those described by Jefferson et al. (2006), underlie the Sand Mountain vents and likely underlie the Sand Mountain lava flow field (Sherrod et al., 2004). The presence of multiple, young, mafic lava flows in the vent area prior to the eruption suggests that an extensive, complex groundwater system, similar to the system that exists today, was available to the vent region during the time of the eruption. Since winter precipitation is estimated to be ~23% greater in the Neoglacial (Marcott et al., 2009), the total water flux of this groundwater system was likely to be greater, making more water available to the vent region.

Groundwater flows through both the porous matrix of breccia layers separating individual flows and through fractures in denser sections of basaltic lava (Saar and Manga, 2004). Flow through fracture-dominated aquifers is probably higher than in aquifers dominated by matrix porosity, where low to moderate hydraulic conductivity prevents the flow of water to the vents and phreatomagmatic activity cannot be maintained (e.g. Aranda-Gomes and Luhr, 1996; Nemeth et al., 2001). The high discharge rate of springs below Sand Mountain suggests that fracture-dominated lava flows underlie the Sand Mountain vents. Additionally, the location of the vents along a regional fault system (e.g. Wells, 1990; Priest, 1990; Taylor, 1990; Scott and Gardner,

1992; Conrey et al., 2000) indicates that the lava flows directly underling the vents are likely highly fractured, providing further evidence that fracture dominated water flow rates could have been fast enough to sustain phreatomagmatic activity. Grain size evidence indicates that the flow of water through young, porous, highly fractured lava was sufficient to produce unusually large volumes of fine-grained tephra, but too low to create wet pyroclastic surge deposits. Regardless of the velocity of water flow in the vent region, the system would need time to recharge in order to sustain phreatomagmatic activity. This suggests that eruptive activity was long lived, perhaps decades, and may have occurred from multiple vents.

4.5. Conclusions

The Sand Mountain tephra deposit is unusual as compared to deposits produced by other Cascade cinder cones in this study. The deposit more closely resembles that of the 2010 eruption of Eyjafjallajökull, Iceland, in that it is very well sorted, uniformly small grained, and composed of tephra clasts that exhibit features indicative of interaction with water. All tephra clasts in the Sand Mountain deposit are <2 mm in diameter and a substantial portion of the deposit is $\leq 125 \mu\text{m}$. The total volume of tephra is considerably larger than that of Eyjafjallajökull and several orders of magnitude larger than deposits produced by other Cascade cinder cones. These observations all indicate that the Sand Mountain eruption interacted with external water during tephra-producing phases of activity. Groundwater flow through highly fractured, young lava flows below the vent region likely sustained highly explosive phreatomagmatic eruptions, but did not supply enough water to produce wet pyroclastic surge deposits.

CHAPTER V

CONCLUSIONS

In this dissertation I investigated the eruption dynamics of recent mafic vents in the central Oregon Cascades. Detailed studies of the tephra deposits produced by these vents were used to constrain the chemical evolution of magmas, pre-eruptive magmatic H₂O contents, syn-eruptive interaction with external water, and eruption style. These investigations show that recent mafic activity in central Oregon has been characterized by a wide range in eruption styles, varying from low-energy hawaiian activity to explosive phreatomagmatic activity. Rather than restate the conclusions made in Chapters II, III, and IV, in this chapter I summarize the hazards posed by mafic activity in central Oregon and make suggestions as to how communities can prepare for future mafic eruptions.

The central section of the Cascade arc, including Newberry Volcano, is characterized by hundreds of cinder cone vents, many of which are located in or near populated areas. The presence of multiple volcanic fields means that future mafic activity is likely and could occur anywhere in the region. Despite the abundance of past mafic activity in central Oregon, the hazards posed by cinder cone eruptions have not been fully addressed. Only a few of the tephra deposits from cinder cones have been mapped, even though determining the volume and extent of these deposits is necessary for assessing eruptive histories and volcanic hazards.

The mafic eruptions described in Chapters II, III, and IV occurred from multiple vents scattered across a large area. At each cluster of vents (i.e. the northwest rift zone of

Newberry Volcano, the Four-in-One Cone, Collier Cone, and Yapoah Crater cluster on the flank of North Sister, and the Sand Mountain chain of vents), activity appears to have lasted for decades to several centuries. Multiple lava flows were produced that covered areas presently transected by major highways, railroads, power and gas lines, and housing developments. In several cases, lava flows dammed major rivers, causing long-term flooding upstream and possible catastrophic flooding downstream. If lava flows were to interact with these river systems today, flooding would affect regional transportation and infrastructure, public and private property, and drinking water supplies.

In addition to lava flows, these clusters of vents also produced large and small tephra deposits. In many cases, tephra production represents the most widespread hazard posed by mafic activity because it is dispersed by wind. It has the potential to disrupt air and ground transportation and can negatively impact agriculture, tourism and public health throughout a widespread area. The 2010 eruption of Eyjafjallajökull, Iceland, demonstrated that a relatively small eruption can greatly impact regional air travel. Since future mafic activity in central Oregon could persist for decades to centuries, regional communities need to be prepared for intermittent, but long-term, tephra production from multiple sources.

In Chapter III, I showed the importance of estimating the extent of trace tephra deposits, both in terms of interpreting eruption style and assessing potential hazards. By correlating tephra deposits preserved in lake sediments to individual source vents, I showed that small amounts of tephra from Collier Cone were likely deposited in modern urban areas (Chapter III, Figure 3.13). Even very small amounts of tephra (<1 cm) can impact regional transportation, agriculture, outdoor recreation, and public health. The

proximity of central Oregon communities to hundreds of cinder cone vents associated with Newberry Volcano and the High Cascades indicates that if future eruptions occur, tephra deposition in urban areas is very likely. The regional economy in central Oregon is driven largely by agriculture and outdoor recreation, both of which would be negatively impacted by long-term tephra deposition.

I also showed in Chapter III that phreatomagmatic activity during the Sand Mountain eruption produced an unusually large volume of tephra. This eruption was likely similar to the 2010 eruption of Eyjafjallajökull in that interaction with water produced very fine-grained tephra that was deposited over a wide area. The identification of recent phreatomagmatic cinder cone eruptions in the Cascades has significant implications for regional hazard assessments. Groundwater patterns indicate that there is a constant flux of water throughout broad areas of the region, making phreatomagmatic activity likely. Thus, from a hazards perspective, not only do the spatial and temporal likelihoods of renewed mafic activity need to be considered, but hazard assessments also need to address groundwater flow patterns.

Heavy winter and late spring snowpack should also be considered in regional hazard assessments. Although there is no direct evidence that the Sand Mountain eruption interacted with snow, heavy winter snowpack in the Cascades could provide enough melt water to generate phreatomagmatic activity during early phases of mafic eruptions. Even a very limited phase of phreatomagmatic ash production could pose significant regional hazards. For this reason, seasonality should be an important consideration in hazard assessments for the central Oregon.

In order to fully address the hazards associated with mafic activity, tephra deposits from regional cinder cones need to be mapped and described. In this dissertation, I used detailed studies of tephra deposits, including isopach maps, volume estimates, grain size and sorting characteristics, juvenile componentry, and microtextural features, to make interpretations about eruption style. These studies reveal that not only were past cinder cone eruptions characterized by a wide range in eruption styles, but at least one eruption (Sand Mountain) produced a surprisingly large tephra deposit. Given the pattern of groundwater flux throughout the region, similar eruptions may have occurred at other recent vents. However, without mapping the tephra deposits and examining tephra clasts in detail, it is impossible to determine the extent to which phreatomagmatic activity contributed to explosive mafic eruptions at other Cascade vents.

In addition to mapping mafic tephra deposits, regional hazard assessments need to address the range of volcanic hazards posed to individual communities. Traditional hazard assessments typically focus on individual volcanoes rather than individual communities. Since central Oregon communities are at risk from multiple hazards posed by numerous vents, it would be better to address the range of hazards posed *to each community*, rather than *by each volcano*. This is especially important because future activity might not be limited to the summit or flanks of long-lived stratovolcanoes and calderas, but rather could occur anywhere in the region.

A community-based approach to assessing volcanic hazards and risks is described in Magill and Blong (2005) for Auckland, New Zealand. Communities in central Oregon are similar to Auckland in that they could be affected by a range of volcanic hazards, both proximal and distal, as well as mafic and silicic. Community based hazard

assessments would not only address the hazards and risks posed by multiple vents, they would also give local and regional agencies specific, community focused information to include in emergency operations plans. For all of these reasons, it is important that future hazard assessments in central Oregon focus on individual communities, rather than on individual volcanoes.

REFERENCES CITED

CHAPTER I

- Conrey, R.M., Sherrod, D.R., Donnelly-Nolan, J.M., Taylor, E.M. et al., 2000. The North-Central Oregon Cascade Margin: Exploring Petrologic and Tectonic Intimacy in a Propagating Intra-Arc Rift. MARGINS: Subduction Factory workshop. Eugene, Oregon.
- Erlund, E.J., Cashman, K.V., Wallace, P.J., Pioli, L., Rosi, M., Johnson, E.R., Delgado Granados, H., 2009. Compositional evolution of magma from Parícutin Volcano, Mexico: the tephra record. *Journal of Volcanology and Geothermal Research*, 197, 167–187.
- Hildreth, W., 2007. Quaternary Magmatism in the Cascades – Geologic Perspectives. U.S. Geological Survey, Professional Paper 1744.
- Johnson, E.R., Wallace, P.J., Cashman, K.V., Delgado Granados, H., Kent, A.J.R., 2008. Magmatic volatile contents and degassing-induced crystallization at Volcán Jorullo, Mexico: implications for melt evolution and the plumbing systems of monogenetic volcanoes. *Earth and Planetary Science Letters*, 269, 477–486.
- Priest, G.R., 1990. Volcanic and Tectonic Evolution of the Cascade Volcanic Arc, Central Oregon. *Journal of Geophysical Research*, 95(B12), 19583–19599.
- Ruscitto, D.M., Wallace, P.J., Johnson, E.R., Kent, A.J.R., Bindeman, I.N., 2010. Volatile contents of mafic magmas from cinder cones in the Central Oregon High Cascades: implications for magma formation and mantle conditions in a hot arc. *Earth and Planetary Science Letters*, 298, 153–161.
- Scott, W.E., Gardner, C.A., 1992. Geologic map of the Mount Bachelor volcanic chain and surrounding area, Cascade range, Oregon. U.S. Geological Survey, Miscellaneous Investigation Series Map I-1967.
- Sherrod, D.R., Smith, J.G., 1990. Quaternary extrusion rates of the Cascade Range, Northwestern United States and Southern British Columbia. *Journal of Geophysical Research*, 95(B12), 19465–19474.
- Sherrod, D.R., Taylor, E.M., Ferns, M.L., Scott, W.E., Conrey, R.M., Smith, G.A., 2004. Geologic map of the Bend 30- x 60-Minute Quadrangle, Central Oregon. U.S. Geological Survey, Geologic Investigations Series I-2683.
- Taylor, E.M., 1990. Volcanic History and Tectonic Development of the Central High Cascade Range, Oregon. *Journal of Geophysical Research*, 95(B12), 19611–19622.

Wells, R.E., 1990. Paleomagnetic Rotations and the Cenozoic Tectonics of the Cascade Arc, Washington, Oregon, and California. *Journal of Geophysical Research*, 95:B12, 19409–19417.

CHAPTER II

Achauer, U., Evans, J.R., Stauber, D.A., 1988. High-resolution seismic tomography of compressional wave velocity structure at Newberry Volcano, Oregon Cascade Range. *Journal of Geophysical Research*, 93:B9, 10135-10147.

Arrighi, S., Principe, C., Rosi, M., 2001. Violent strombolian and subplinian eruptions at Vesuvius during the post-1631 activity. *Bulletin of Volcanology*, 63, 126-150.

Asimow, P.D., Ghiorso, M.S., 1998. Algorithmic modifications extending MELTS to calculate subsolidus phase relations. *American Mineralogist*, 83, 1127–1131.

Beachly, M.W., 2011. The upper crustal P-wave velocity structure of Newberry volcano, Central Oregon. Masters Thesis, University of Oregon, Eugene, Oregon.

Brenna, M., Cronin, S.J., Nemeth, K., Smith I.E.M., Sohn, Y.K., 2011. The influence of magma plumbing complexity on monogenetic eruptions, Jeju Island, Korea. *Terra Nova*, 23, 70-75.

Carlson, R.W., Grove, T.L., Donnelly-Nolan, J.M., 2008. Concentrating the slab-fluid input to Newberry Volcano, Oregon. *Geochimica et Cosmochimica Acta*, 72:12S, 136.

Catchings, R.D., Mooney, W.D., 1988. Crustal structure of east central Oregon - Relation between Newberry Volcano and regional crustal structure. *Journal of Geophysical Research*, 93:B9, 10081-10094.

Cervantes, P., Wallace, P.J., 2003. Role of H₂O in subduction-zone magmatism: new insights from melt inclusions in high-Mg basalts from central Mexico. *Geology*, 31, 235-238.

Champion, D.E., Donnelly-Nolan, J.M., Lanphere, M.A., Ramsey, O.W., 2004. Magnetic excursion recorded in basalt at Newberry Volcano, central Oregon. *Eos Transactions, American Geophysical Union*, 85:47, abstract GP43B-086I.

Conrey, R.M., Sherrod, D.R., Donnelly-Nolan, J.M., Taylor, E.M. et al., 2000. The North-Central Oregon Cascade Margin: Exploring Petrologic and Tectonic Intimacy in a Propagating Intra-Arc Rift. MARGINS: Subduction Factory workshop. Eugene, OR.

- Donnelly-Nolan, J.M., 2008. Newberry and Medicine Lake: Two Large Rear-Arc Cascade Volcanoes. IAVCEI General Assembly, Reykjavik, Iceland, abstract 2-a P13.
- Donnelly-Nolan, J.M., 2009. Newberry Volcano, Oregon: No traveling hot spot is needed. *Eos Transactions, American Geophysical Union*, 90:52, abstract V41B-2180.
- Donnelly-Nolan, J.M., Champion, D.E., Grove, T.L., Baker, M.B., Taggart Jr., J.E., Bruggman, P.E., 1991. The Giant Crater lava field: Geology and geochemistry of a compositionally zoned, high-alumina basalt to basaltic andesite eruption at Medicine Lake volcano, California. *Journal of Geophysical Research*, 96:B13, 21843–21863.
- Donnelly-Nolan, J.M., Grove, T.L., Lanphere, M.A., Champion, D.E., Ramsey, D.W., 2008. Eruptive history and tectonic setting of Medicine Lake volcano, a large rear-arc volcano in the southern Cascades. *Journal of Volcanology and Geothermal Research*, 177, 313-328.
- Donnelly-Nolan, J.M., Ramsey, D.W., Jensen, R.A., Champion, D.E., Calvert, A.T., 2010. Preliminary Geologic Map of Newberry Volcano, Oregon. *Eos Transactions, American Geophysical Union*, abstract V11C-2293.
- Dzurisin, D., Lisowski, M., Wicks, C.W., 2009. Continuing inflation at Three Sisters volcanic center, central Oregon Cascade Range, USA, from GPS, leveling, and InSAR observations. *Bulletin of Volcanology*, 71:10, 1091-1110.
- Dzurisin, D., Lisowski, M., Wicks, C.W., Poland, M.P., Endo, E.T., 2006. Geodetic observations and modeling of magmatic inflation at the Three Sisters volcanic center, central Oregon Cascade Range, USA. *Journal of Volcanology and Geothermal Research*, 150:1-3, 35-54.
- Erlund, E.J., Cashman, K.V., Wallace, P.J., Pioli, L., Rosi, M., Johnson, E.R, Delgado Granados, H., 2009. Compositional evolution of magma from Parícutin Volcano, Mexico: the tephra record. *Journal of Volcanology and Geothermal Research*, 197, 167–187.
- Fitterman, D.V., 1988. Overview of the structure and geothermal potential of Newberry Volcano, Oregon. *Journal of Geophysical Research*, 93:B9, 10059-10066.
- Fitterman, D.V., Stanley, W.O., Bisdort, R.J., 1988. Electrical structure of Newberry Volcano, Oregon. *Journal of Geophysical Research*, 93:B9, 10119-10134.
- Francis, P., Oppenheimer, C., 2004. *Volcanoes*. Oxford University Press, New York, 135 p.

- Gettings, M.E., Griscom, A., 1988. Gravity model studies of Newberry Volcano, Oregon. *Journal of Geophysical Research*, 93:B9, 10109-10118.
- Ghiorso, M.S., Sack, R.O., 1995. Chemical mass transfer in magmatic processes. IV. A revised and internally consistent thermodynamic model for the interpolation and extrapolation of liquid–solid equilibria in magmatic systems at elevated temperatures and pressures. *Contributions to Mineralogy and Petrology*, 119, 197–212.
- Graham, D.W., Reid, M.R., Jordan, B.T., Grunder, A.L., Leeman, W.P., Lupton, J.E., 2009. Mantle source provinces beneath the northwestern USA delimited by helium isotopes in young basalts: *Journal of Volcanology and Geothermal Research*, 188, 128-140.
- Grove, T., Barr, J., Till, C., Donnelly-Nolan, J.M., Carlson, R., 2009. Shallow, hot, mantle melting in the High Lava Plains, Oregon. *Geological Society of America, Abstracts with Programs*, 41:7, 571.
- Hallett, D.J., Hills, L.V., Clague, J.J., 1997. New accelerator mass spectrometry radiocarbon ages for the Mazama tephra layer from Kootenay National Park, British Columbia, Canada. *Canadian Journal of Earth Sciences*, 34:9, 1202-1209.
- Heiken, G., 1978. Characteristics of Tephra from Cinder Cone, Lassen Volcanic National Park, California. *Bulletin of Volcanology*, 41-2, 119-130.
- Higgins, M.W., 1973. Petrology of Newberry Volcano, Central Oregon. *Geological Society of America Bulletin*, 84, 455-488
- Hildreth, W., 2007. Quaternary Magmatism in the Cascades – Geologic Perspectives. U.S. Geological Survey, Professional Paper 1744.
- Houghton, B.F., Gonnermann, H.M., 2008. Basaltic explosive volcanism: Constraints from deposits and models. *Chemie der Erde*, 68,117-140.
- Housh, T.B., Luhr, J.F., 1991. Plagioclase-melt equilibria in hydrous systems. *American Mineralogist*, 76, 477-492.
- Jensen, R.A., 2006. Roadside guide to the geology and history of Newberry Volcano. 4th edition. CenOreGeoPub, Bend, Oregon, 182 p.
- Jensen, R.A., Donnelly-Nolan, J.M., McKay, D., 2009. A field guide to Newberry Volcano, Oregon, *in* O'Conner, J.E., Dorsey, R.J., Madin. I.P., eds., *Volcanoes to Vineyards: Geologic Field Trips through the Dynamic Landscapes of the Pacific Northwest*. Geological Society of America Field Guide 15, 53-79.

- Johnson, E.R., Wallace, P.J., Cashman, K.V., Delgado Granados, H., Kent, A.J.R., 2008. Magmatic volatile contents and degassing-induced crystallization at Volcán Jorullo, Mexico: implications for melt evolution and the plumbing systems of monogenetic volcanoes. *Earth and Planetary Science Letters*, 269, 477–486.
- Jordan, B.T., Grunder, A.L., Duncan, R.A., Deino, A.L., 2004. Geochronology of age-progressive volcanism of the Oregon High Lava Plains: Implications for the plume interpretation of Yellowstone. *Journal of Geophysical Research*, 109, B10202.
- Kinzler, R.J., Donnelly-Nolan, J.M., Grove, T.L., 2000. Late Holocene hydrous mafic magmatism at the Paint Pot Crater and Callahan flows, Medicine Lake volcano, N. California and the influence of H₂O in the generation of silicic magmas. *Contributions to Mineralogy and Petrology*, 138, 1–16.
- Lange, R.A., Frey, H.M., Hector, J., 2009. A thermodynamic model for the plagioclase-liquid hygrometer/thermometer. *American Mineralogist*, 94, 494-506.
- Linneman, S.R., Myers, J.D., 1990. Magmatic Inclusions in the Holocene Rhyolites of Newberry Volcano, Central Oregon. *Journal of Geophysical Research*, 95:B11, 17677-17691.
- Luhr, J.F., 2001. Glass inclusions and melt volatile contents at Parícutin Volcano, Mexico. *Contributions to Mineralogy and Petrology*, 142, 261–283.
- MacLeod, N.S., Sherrod, D.R., 1988. Geologic evidence for a magma chamber beneath Newberry volcano, Oregon. *Journal of Geophysical Research*, 93:B9, 10067-10079.
- MacLeod, N.S., Sherrod, D.R., Chitwood, L.A., Jensen, R.A., 1995. Geologic Map of Newberry Volcano, Deschutes, Klamath, and Lake Counties, Oregon. U.S. Geological Survey, Miscellaneous Geologic Investigations Map I-2455.
- MacLeod, N.S., Walker, G.W., McKee, E.H., 1975. Geothermal significance of eastward increase in age of upper Cenozoic rhyolitic domes in southeast Oregon. Second United Nations Symposium on the Development and Use of Geothermal Resources, Proceedings, 1, 465-474.
- McBirney, A.R., Taylor Jr., H.P., Armstrong, R.L., 1987. Parícutin re-examined: a classic example of crustal assimilation in calc-alkaline magma. *Contributions to Mineralogy and Petrology*, 95, 4–20.
- McGetchin, T.R., Settle, M., Chouet, B.A., 1974. Cinder cone growth modeled after Northeast crater, Mount Etna, Sicily. *Journal of Geophysical Research*, 79:23, 3257-3272.

- McKay, D., Donnelly-Nolan, J.M., Jensen, R.A., Champion, D.E., 2009. The post-Mazama northwest rift zone eruption at Newberry Volcano, Oregon, *in* O'Connor J.E., Dorsey R.J., Madin I.P., eds., *Volcanoes to Vineyards: Geologic Field Trips through the Dynamic Landscape of the Pacific Northwest*. Geological Society of America Field Guide 15, 91-110.
- McKee, E.H., MacLeod, N.S., Walker, G.W., 1976. Potassium-argon ages of Late Cenozoic silicic volcanic rocks, southeast Oregon. *Isochron/West*, 15, 37-41.
- Moore, G., Carmichael, I.S.E., 1998. The hydrous phase equilibria (to 3 kbar) of an andesite and basaltic andesite from western Mexico: constraints on water content and conditions of phenocrysts growth. *Contributions to Mineralogy and Petrology*, 130, 304–319.
- Parfitt, E.A., 1998. A study of clast size distribution, ash deposition and fragmentation in Hawaiian-style volcanic eruptions. *Journal of Volcanology and Geothermal Research*, 84, 197-208.
- Parfitt, E.A., 2004. A discussion of the mechanisms of explosive basaltic eruptions. *Journal of Volcanology and Geothermal Research*, 134, 77-107.
- Peterson, N.V., Groh, E.A., eds., 1965. *Lunar Geological Field Conference Guide Book*, Oregon Department of Geology and Mineral Industries Bulletin, 51 p.
- Pioli, L., Erlund, E., Johnson, E., Cashman, K., Wallace, P., Rosi, M., Delgado Granados, H., 2008. Explosive dynamics of violent Strombolian eruptions: The eruption of Paricutin Volcano 1943-1952 (Mexico). *Earth and Planetary Science Letters*, 271, 359-368.
- Priest, G.R., 1990. Volcanic and Tectonic Evolution of the Cascade Volcanic Arc, Central Oregon. *Journal of Geophysical Research*, 95:B12, 19583–19599.
- Putirka K.D., 2005. Igneous thermometers and barometers based on plagioclase + liquid equilibria: Tests of some existing models and new calibrations. *American Mineralogist*, 90, 336–346.
- Riddick, S.N., 2011. *A Time Series Analysis of Volcanic Deformation near Three Sisters, Oregon, using InSAR*. Masters Thesis, University of Oregon, Eugene, Oregon.
- Roggensack, K., Hervig, R.L., McKnight, S.B., Williams, S.N., 1997. Explosive basaltic volcanism from Cerro Negro volcano: influence of volatiles on eruptive style. *Science*, 277, 1639–1642.
- Rowe, M.C., Kent, A.J.R., Nielsen, R.L., 2009. Subduction Influence on Oxygen Fugacity and Trace and Volatile Elements in Basalts Across the Cascade Volcanic Arc. *Journal of Petrology*, 50:1, 61-91.

- Ruscitto, D.M., Wallace, P.J., Johnson, E.R., Kent, A.J.R., Bindeman, I.N., 2010. Volatile contents of mafic magmas from cinder cones in the Central Oregon High Cascades: implications for magma formation and mantle conditions in a hot arc. *Earth and Planetary Science Letters*, 298, 153–161.
- Scott, W.E., Gardner, C.A., 1992. Geologic map of the Mount Bachelor volcanic chain and surrounding area, Cascade range, Oregon. U.S. Geological Survey, Miscellaneous Investigation Series Map I-1967.
- Sherrod, D.R., Mastin, L.G., Scott, W.E., Conrey, R.M., Schilling, S.P., 1997. Volcano Hazards at Newberry Volcano, Oregon. U.S. Geological Survey, Open File Report 97-513.
- Stovall, W.K., Houghton, B.F., Gonnermann, H., Fagents S.A., Swanson, D.A., 2010. Eruption dynamics of Hawaiian-style fountains: the case study of episode 1 of the Kilauea Iki 1959 eruption. *Bulletin of Volcanology*, 73:5, 511-529.
- Strong, M. Wolff, J., 2003. Compositional variations within scoria cones. *Geology*, 31, 143-146.
- Taylor, E.M., 1990. Volcanic History and Tectonic Development of the Central High Cascade Range, Oregon. *Journal of Geophysical Research*, 95:B12, 19611-19622.
- Valentine, G.A., Gregg, T.K.P., 2008. Continental basaltic volcanoes – Processes and problems. *Journal of Volcanology and Geothermal Research*, 177, 857-873.
- Valentine, G.A., Krier, D., Perry, F.V., Heiken, G., 2005. Scoria cone construction mechanisms, Lathrop Wells volcano, southern Nevada, USA. *Geology*, 33, 629-632.
- Walker, G.P.L., 1973. Explosive volcanic eruptions – A new classification scheme. *Geologische Rundschau*, 62, 431-446.
- Walker, G.P.L., Croasdale, R., 1972. Characteristics of some basaltic pyroclastics. *Bulletin of Volcanology*, 35, 303–317.
- Walker, G.W., 1974. Some implications of Late Cenozoic volcanism to geothermal potential in the High Lava Plains of south-central Oregon. *The Ore Bin*, 36:7, 109-119.
- Weldon, R.J. II, Fletcher, D.K., Weldon, E.M., Scharer, K.M., McCrory, P.M., 2003. An Update of Quaternary Faults of Central and Eastern Oregon. U.S. Geological Survey Open File Report 02-301.

Wells, R.E., 1990. Paleomagnetic Rotations and the Cenozoic Tectonics of the Cascade Arc, Washington, Oregon, and California. *Journal of Geophysical Research*, 95:B12, 19409–19417.

Wicks, C.W., Jr., Dzurisin, D., Ingebritsen, S., Thatcher, W., Lu, Z., Iverson, J., 2002. Magmatic activity beneath the quiescent Three Sisters volcanic center, central Oregon Cascade Range, USA. *Geophysical Research Letters*, 29:7, 1122.

Wilcox, R.E., 1954. Petrology of Parícutín volcano Mexico. U.S. Geological Survey Bulletin, 965:C, 281–353.

CHAPTER III

Abramoff, M.D., Magalhães, P.J., Ram, S.J., 2004. Image processing with ImageJ. *Biophotonics International*, 11:7, 36-42.

Bebbington, M.S., Cronin, S.J., 2011. Spatio-temporal hazard estimation in the Auckland Volcanic Field, New Zealand, with a new event-order model. *Bulletin of Volcanology*, 73, 55–72.

Büttner, R., Dellino, P., Zimanowski, B., 1999. Identifying magma–water interaction from the surface features of ash particles. *Nature*, 401, 688-690.

Chatters, R.M., 1968. Washington State University natural radiocarbon measurements, I. *Radiocarbon*, 10:2, 479-498.

Clynne, M.A., Muffler, L.J.P., 2010. Geologic map of Lassen Volcanic National Park and vicinity, California. U.S. Geological Survey, Scientific Investigations Map 2899.

Conrey, R.M., Sherrod, D.R., Donnelly-Nolan, J.M., Taylor, E.M. et al., 2000. The North-Central Oregon Cascade Margin: Exploring Petrologic and Tectonic Intimacy in a Propagating Inter-Arc Rift. MARGINS: Subduction Factory workshop. Eugene, OR.

Deardorff, N. D., 2011. Eruptive processes of mafic arc volcanoes - subaerial and submarine perspectives. Ph.D. Dissertation, University of Oregon, Eugene, Oregon.

Deligne, N.I., Conrey, R.M., Cashman, K.V., Champion, D.E., Amidon, W.H., Grant, G.E., 2012, submitted. Co-evolution of the Sand Mountain volcanic field and the upper McKenzie River, central Oregon Cascades, USA. *Geological Society of America Bulletin*.

Dellino, P., Kyriakopoulos, K., 2003. Phreatomagmatic ash from the ongoing eruption of Etna reaching the Greek island of Cefalonia. *Journal of Volcanology and Geothermal Research* 126, 341-345.

- Dzurisin, D., Lisowski, M., Wicks, C.W., 2009. Continuing inflation at Three Sisters volcanic center, central Oregon Cascade Range, USA, from GPS, leveling, and InSAR observations. *Bulletin of Volcanology*, 71:10, 1091-1110.
- Dzurisin, D., Lisowski, M., Wicks, C.W., Poland, M.P., Endo, E.T., 2006. Geodetic observations and modeling of magmatic inflation at the Three Sisters volcanic center, central Oregon Cascade Range, USA. *Journal of Volcanology and Geothermal Research*, 150:1-3, 35-54.
- Erlund, E.J., Cashman, K.V., Wallace, P.J., Pioli, L., Rosi, M., Johnson, E.R, Delgado Granados, H., 2009. Compositional evolution of magma from Parícutin Volcano, Mexico: the tephra record. *Journal of Volcanology and Geothermal Research*, 197, 167–187.
- Fierstein, J., Nathenson, M., 1992. Another look at the calculation of fallout tephra volumes. *Bulletin of Volcanology*, 54, 156-167.
- Francis, P., Oppenheimer, C., 2004. *Volcanoes*. Oxford University Press, New York, 135 p.
- Fries, C.J., 1953. Volumes and weights of pyroclastic material, lava, and water erupted by Parícutin volcano, Michoacán, Mexico. *Transactions, American Geophysical Union*, 34, 603–616.
- Hallett, D.J., Hills, L.V., Clague, J.J., 1997. New accelerator mass spectrometry radiocarbon ages for the Mazama tephra layer from Kootenay National Park, British Columbia, Canada. *Canadian Journal of Earth Sciences*, 34:9, 1202-1209.
- Heiken, G., 1978. Characteristics of Tephra from Cinder Cone, Lassen Volcanic National Park, California. *Bulletin of Volcanology*, 41-2, 119-130.
- Heiri, O., Lotter, A.F., Lemcke, G., 2001. Loss on ignition as a method for estimating organic and carbonate content in sediments: reproducibility and comparability of results. *Journal of Paleolimnology*, 25, 101-110.
- Hildreth, W., 2007. Quaternary magmatism in the Cascades—geologic perspectives. U.S. Geological Survey Professional Paper 1744.
- Hill, B.E., Connor C.B., Jarzempa, M.S., La Femina P., Navarro M., Strauch W., 1998. 1995 eruption of Cerro Negro volcano, Nicaragua, and risk assessment for future eruptions. *Geological Society of America Bulletin*, 110, 1231-1241.
- Houghton, B.F., Gonnermann, H.M., 2008. Basaltic explosive volcanism: Constraints from deposits and models. *Chemie der Erde*, 68,117-140.

- Luhr, J.F., Simkin, T., 1993. Parícutin: The Volcano Born in a Mexican Cornfield. Geoscience Press, 427 p.
- Macdonald, G.A., 1972. Volcanoes. Prentice-Hall, Englewood Cliffs, New Jersey, 510 p.
- Marcott, S.A., Fountain, A.G., O'Connor, J.E., Sniffen, P.J., Dethier, D.P., 2009. A Latest Pleistocene and Holocene glacial history and paleoclimate reconstruction at Three Sisters and Broken Top Volcanoes, Oregon, U.S.A. *Quaternary Research*, 71:2, 181–189.
- McGetchin, T.R., Settle, M., Chouet, B.A., 1974. Cinder cone growth modeled after Northeast crater, Mount Etna, Sicily. *Journal of Geophysical Research*, 79:23, 3257-3272.
- McKnight, S.B., Williams, S.N., 1997. Old cinder cone or young composite volcano?: the nature of Cerro Negro Nicaragua. *Geology* 25:4, 339–342.
- Ort, M.H., Elson, M.D., Anderson, K.C., Duffield, W.A., Hooten, J.A., Champion, D.E., Waring, G., 2008. Effects of scoria cone eruptions on nearby human communities. *Geological Society of America Bulletin*, 120:3-4, 476-486.
- Parfitt, E.A., 1998. A study of clast size distribution, ash deposition and fragmentation in Hawaiian-style volcanic eruptions. *Journal of Volcanology and Geothermal Research*, 84, 197-208.
- Parfitt, E.A., 2004. A discussion of the mechanisms of explosive basaltic eruptions. *Journal of Volcanology and Geothermal Research*, 134, 77-107.
- Pioli, L., Erlund, E., Johnson, E., Cashman, K., Wallace, P., Rosi, M., Delgado Granados, H., 2008. Explosive dynamics of violent Strombolian eruptions: The eruption of Parícutin Volcano 1943-1952 (Mexico). *Earth and Planetary Science Letters*, 271, 359-368.
- Priest, G.R., 1990. Volcanic and Tectonic Evolution of the Cascade Volcanic Arc, Central Oregon. *Journal of Geophysical Research*, 95:B12, 19583–19599.
- Pyle, D.M., 1989. The thickness, volume and grain size of tephra fall deposits. *Bulletin of Volcanology*, 51, 1–15.
- Riddick, S.N., 2011. A Time Series Analysis of Volcanic Deformation near Three Sisters, Oregon, using InSAR. Masters Thesis, University of Oregon, Eugene, Oregon.
- Ruscitto, D.M., Wallace, P.J., Johnson, E.R., Kent, A.J.R., Bindeman, I.N., 2010. Volatile contents of mafic magmas from cinder cones in the Central Oregon High Cascades: implications for magma formation and mantle conditions in a hot arc. *Earth and Planetary Science Letters*, 298, 153–161.

- Schick, J.D., 1994. Origin of the Compositional Variability of the Lavas at Collier Cone, High Cascades, Oregon. Masters Thesis, University of Oregon. Eugene, OR.
- Scott, W.E., 1990. Temporal relations between eruptions of the Mount Bachelor volcanic chain and fluctuations of late Quaternary glaciers. *Oregon Geology*, 52:5, 114-117.
- Scott, W.E., Gardner, C.A., 1992. Geologic map of the Mount Bachelor volcanic chain and surrounding area, Cascade range, Oregon. U.S. Geological Survey, Miscellaneous Investigation Series Map I-1967.
- Sherrod, D.R., Smith, J.G., 1990. Quaternary extrusion rates of the Cascade Range, Northwestern United States and Southern British Columbia. *Journal of Geophysical Research*, 95:B12, 19465–19474.
- Sherrod, D.R., Taylor, E.M., Ferns, M.L., Scott, W.E., Conrey, R.M., Smith, G.A., 2004. Geologic map of the Bend 30- x 60-Minute Quadrangle, Central Oregon. U.S. Geological Survey, Geologic Investigations Series I-2683.
- Stovall, W.K., Houghton, B.F., Gonnermann, H., Fagents S.A., Swanson, D.A., 2010. Eruption dynamics of Hawaiian-style fountains: the case study of episode 1 of the Kilauea Iki 1959 eruption. *Bulletin of Volcanology*, 73:5, 511-529.
- Taylor, E.M., 1965. Recent volcanism between Three Fingered Jack and North Sister, Oregon Cascade Range: Part I – History of volcanic activity. *Ore Bin*, 27:7, 121-147.
- Taylor, E.M., 1990. Volcanic History and Tectonic Development of the Central High Cascade Range, Oregon. *Journal of Geophysical Research*, 95:B12, 19611–19622.
- Valentine, G.A., Gregg, T.K.P., 2008. Continental basaltic volcanoes – Processes and problems. *Journal of Volcanology and Geothermal Research*, 177, 857-873.
- Valentine, G.A., Krier, D., Perry, F.V., Heiken, G., 2005. Scoria cone construction mechanisms, Lathrop Wells volcano, southern Nevada, USA. *Geology*, 33, 629-632.
- Walker, G.P.L., 1973. Explosive volcanic eruptions – A new classification scheme. *Geologische Rundschau*, 62, 431-446.
- Walker, G.P.L., Croasdale, R., 1972. Characteristics of some basaltic pyroclastics. *Bulletin of Volcanology*, 35, 303–317.

Wells, R.E., 1990. Paleomagnetic Rotations and the Cenozoic Tectonics of the Cascade Arc, Washington, Oregon, and California. *Journal of Geophysical Research*, 95:B12, 19409–19417.

Wicks, C.W., Jr., Dzurisin, D., Ingebritsen, S., Thatcher, W., Lu, Z., Iverson, J., 2002. Magmatic activity beneath the quiescent Three Sisters volcanic center, central Oregon Cascade Range, USA. *Geophysical Research Letters*, 29:7, 1122.

Wright Jr., H.E., Mann, D.H., Glaser, P.H., 1983. Piston cores for peat and lake sediments. *Ecology*, 65, 657–659.

CHAPTER IV

Aranda-Gomez, J.J., Luhr, J.F., 1996. Origin of the Joya Honda maar, San Luis Potosi, Mexico. *Journal of Volcanology and Geothermal Research*, 74, 1-18.

Arrighi, S., Principe, C., Rosi, M., 2001. Violent strombolian and subplinian eruptions at Vesuvius during the post-1631 activity. *Bulletin of Volcanology*, 63, 126-150.

Conrey, R.M., Sherrod, D.R., Donnelly-Nolan, J.M., Taylor, E.M. et al., 2000. The North-Central Oregon Cascade Margin: Exploring Petrologic and Tectonic Intimacy in a Propagating Inter-Arc Rift. MARGINS: Subduction Factory workshop. Eugene, OR.

Deligne, N.I., Conrey, R.M., Cashman, K.V., Champion, D.E., Amidon, W.H., Grant, G.E., 2012, submitted. Co-evolution of the Sand Mountain volcanic field and the upper McKenzie River, central Oregon Cascades, USA. *Geological Society of America Bulletin*.

P. Dellino, P., Gudmundsson, M.T., Larsen, G., Mele, D., Stevenson, J.A., Thordarson, T., Zimanowski, B., 2012. Ash from the Eyjafjallajökull eruption (Iceland): Fragmentation processes and aerodynamic behavior. *Journal of Geophysical Research*, 117:B00C04, 1-10.

Fisher, R.V., Schmincke, H.U., 1984. *Pyroclastic Rocks*, Springer-Verlag, Berlin, 472 p.

Gannett, M.W., Manga, M., Lite, K.E.J., 2003. Groundwater hydrology of the Upper Deschutes Basin and its influence on streamflow, *in* O'Connor, J.E., Grant, G.E., eds., *A Peculiar River: Geology, Geomorphology, and Hydrology of the Deschutes River, Oregon*. American Geophysical Union, Water Science and Application, 7, 39-49.

Gudmundsson, M.T., Pedersen, R., Vogfjörd, K., Thorbjarnardóttir, B., Jakobsdóttir, S., Roberts, M.J., 2010. Eruptions of Eyjafjallajökull Volcano, Iceland, *Eos*, 91:21, 190–191.

- Heiken, G.H., 1972. Morphology and petrography of volcanic ashes, Geological Society of America Bulletin. 83, 1961-1988.
- Houghton, B.F., Gonnermann, H.M., 2008. Basaltic explosive volcanism: Constraints from deposits and models. *Chemie der Erde*, 68, 117-140.
- James, E.R., Manga, M., Rose, T.P., Hudson, G.B., 2000. The use of temperature and isotopes of O, H, C and noble gases to determine the pattern and spatial extent of groundwater flow. *Journal of Hydrology*, 237:1-2, 100-112.
- Jefferson A., Grant, G.E., Rose, T.P., 2006. The influence of volcanic history on groundwater patterns on the west slope of the Oregon High Cascades. *Water Resources Research*, 42:W12411.
- Johnson, E.R., Wallace, P.J., Cashman, K.V., Delgado Granados, H., Kent, A.J.R., 2008. Magmatic volatile contents and degassing-induced crystallization at Volcán Jorullo, Mexico: implications for melt evolution and the plumbing systems of monogenetic volcanoes. *Earth and Planetary Science Letters*, 269, 477-486.
- Manga, M., 1997. A model for discharge in spring-dominated streams and implications for the transmissivity and recharge of quaternary volcanics in the Oregon Cascades. *Water Resources Research*, 33:8, 1813-1822.
- Németh, K., Martin, U., Harangi, Sz., 2001. Miocene phreatomagmatic volcanism at Tihany (Pannonian Basin, Hungary). *Journal of Volcanology and Geothermal Research* 111, 111-135.
- Parfitt, E.A., 1998. A study of clast size distribution, ash deposition and fragmentation in Hawaiian-style volcanic eruptions. *Journal of Volcanology and Geothermal Research*, 84, 197-208.
- Pioli, L., Erlund, E., Johnson, E., Cashman, K., Wallace, P., Rosi, M., Delgado Granados, H., 2008. Explosive dynamics of violent Strombolian eruptions: The eruption of Parícutin Volcano 1943-1952 (Mexico). *Earth and Planetary Science Letters*, 271, 359-368.
- Priest, G.R., 1990. Volcanic and Tectonic Evolution of the Cascade Volcanic Arc, Central Oregon. *Journal of Geophysical Research*, 95:B12, 19583-19599.
- Saar, M.O., Manga, M., 2004. Depth dependence of permeability in the Oregon Cascades inferred from hydrogeologic, thermal, seismic, and magmatic modeling constraints, *Journal of Geophysical Research*, 109:B4.
- Schipper, C.I., White, J.D.L., Zimanowski, B., Büttner, R., Sonder, I., 2011. Experimental interaction of magma and "dirty" coolants. *Earth and Planetary Science Letters*, 303, 326-336.

- Scott, W.E., Gardner, C.A., 1992. Geologic map of the Mount Bachelor volcanic chain and surrounding area, Cascade range, Oregon. U.S. Geological Survey, Miscellaneous Investigation Series Map I-1967.
- Sheridan, M.F., Wohletz, K.H., 1983. Hydrovolcanism: basic considerations, *in* Sheridan, M.F., Barberi, F., eds., Explosive Volcanism. *Journal of Volcanology and Geothermal Research* 17, 1-29.
- Sherrod, D.R., Taylor, E.M., Ferns, M.L., Scott, W.E., Conrey, R.M., Smith, G.A., 2004. Geologic map of the Bend 30- x 60-Minute Quadrangle, Central Oregon. U.S. Geological Survey, Geologic Investigations Series I-2683.
- SNOTEL Data Collection Network, National Water and Climate Center of the Natural Resources Conservation Service, U.S. Department of Agriculture, <http://www.wcc.nrcs.usda.gov/snow/> (December 2010).
- Taylor, E.M., 1990. Volcanic History and Tectonic Development of the Central High Cascade Range, Oregon. *Journal of Geophysical Research*, 95:B12, 19611–19622.
- Valentine, G.A., Gregg, T.K.P., 2008. Continental basaltic volcanoes – Processes and problems. *Journal of Volcanology and Geothermal Research*, 177, 857-873.
- Walker, G.P.L., Croasdale, R., 1972. Characteristics of some basaltic pyroclastics. *Bulletin of Volcanology*, 35, 303–317.
- Waters, A.C., Fisher, R.V., 1971. Base surges and their deposits, Capelinhos and Taal volcanoes. *Journal of Geophysical Research*, 76, 5496-5614.
- Wells, R.E., 1990. Paleomagnetic Rotations and the Cenozoic Tectonics of the Cascade Arc, Washington, Oregon, and California. *Journal of Geophysical Research*, 95:B12, 19409–19417.
- White, D.L., 1996. Impure coolants and interaction dynamics of phreatomagmatic eruptions. *Journal of Volcanology and Geothermal Research*, 74, 155-170.
- Wohletz, K.H., 1983. Mechanisms of hydrovolcanic pyroclast formation: grain-size, scanning electron microscopy, and experimental studies. *Journal of Volcanology and Geothermal Research*, 17, 31–64.
- Wohletz, K.H., McQueen, R.G., 1984. Experimental Studies of Hydromagmatic Volcanism. *Studies of Geophysics*, National Academic Press, Washington, 158–169.

CHAPTER IV

- Magill, C., Blong, R., 2005. Volcanic risk ranking for Auckland, New Zealand. I: Methodology and hazard investigation. *Bulletin of Volcanology*, 67:331-339.
- Magill, C., Blong, R., 2005. Volcanic risk ranking for Auckland, New Zealand. II: Hazard consequences and risk calculation. *Bulletin of Volcanology*, 67:340-349.